

**GAS HYDRATE EQUILIBRIUM MEASUREMENTS FOR MULTI-
COMPONENT GAS MIXTURES AND EFFECT OF IONIC LIQUID
INHIBITORS**

A Thesis

by

ENAS AZHAR OTHMAN

Submitted to the Office of Graduate and Professional Studies of
Texas A&M University
in partial fulfillment of the requirements for the degree of

MASTER OF SCIENCE

Chair of Committee,	Marcelo Castier
Co-Chair of Committee,	Mert Atilhan
Committee Member,	Mahmood Amani
Head of Department,	Nazmul Karim

May 2014

Major Subject: Chemical Engineering

Copyright 2014 Enas Azhar Othman

ABSTRACT

Qatar holds the world's third-largest proven reserves of natural gas at 885 trillion cubic feet according to a recent report. Because of its desert climate, gas hydrate formation may seem an unlikely event in Qatar. However, its natural gas reservoirs are located 80 km offshore, in the North Field, and the production of liquefied natural gas (LNG) depends on reliable flow from offshore wellheads to onshore processing facilities. Classical methods for inhibiting hydrate formation are used in order to prevent pipeline plugging but changing gas concentrations and operating conditions make flow assurance quite challenging in the North Field. Between 2008 and 2011, sudden temperature drops near gas pipelines caused various incidents of gas pipeline blockage by hydrates, with a loss of US\$ 10 million per day due to lost production for almost 4 weeks. Such unplanned shut downs jeopardize the reliable export of LNG to end users.

This work presents the recent investigation on synthetic multi-component gas mixtures whose compositions are typical of Qatari natural gases with initiatives aimed at helping producers minimize costs, optimize operations, and prevent interruption of gas flow in offshore drilling and production. In addition, it presents hydrate inhibition data from a newly commissioned micro bench top reactor, a high-pressure autoclave and a rocking cell. The conditions for hydrate formation for pure methane and carbon dioxide were also measured, for validation purposes. The measured data were compared with literature results and those of a commercial simulator, HydraFLASH®. Upon validation of the

calibration data and determination of the apparatus uncertainty, results for hydrate formation equilibrium points for Qatari natural gas sample were collected and compared to HydraFLASH® predictions. Different percentages of 2-hydroxy-N,N,N-trimethylethanaminium chloride, also known as choline chloride ionic liquid, were used as hydrate inhibitor for the same gas mixture. The ionic liquid's inhibition performance was compared to that of classical thermodynamic inhibitors (e.g. methanol). Ionic liquid inhibition showed (0.7 – 1.8) °C and (2 - 2.6) °C shift in the hydrate equilibrium curve with 1 wt. % and 5 wt. % of choline chloride respectively. While the inhibition performance of 1 wt. % and 5 wt. % of methanol, obtained using HydraFLASH® software, were 2.8 °C and 4.4 °C respectively.

DEDICATION

To my Parents

And

To my Husband

ACKNOWLEDGEMENTS

I would like to take the opportunity to thank all the individuals who helped and supported me during my study and research, ultimately leading to the successful completion of my Master of Science degree in chemical engineering.

Firstly, I would like to sincerely thank my committee chair, Prof. Marcelo Castier, and my co-chair Associate Prof. Mert Atilhan, and my other committee member, Associate Prof. Mahmood Amani, for their guidance and support throughout the course of this research.

Secondly, Thanks also go to my friends and colleagues and the department faculty and staff for making my time at Texas A&M University and Qatar University a great experience. I also want to extend my gratitude to postdoctoral Dr. Mohammad Tariq for his laboratory support and help with the experimental set-up.

Finally, yet importantly, I would like to express my heartfelt thanks to my beloved parents for their blessings, support, and encouragement and to my husband for his patience and love.

TABLE OF CONTENTS

	Page
ABSTRACT	ii
DEDICATION	iv
ACKNOWLEDGEMENTS	v
TABLE OF CONTENTS	vi
LIST OF FIGURES	viii
LIST OF TABLES	xii
1. INTRODUCTION.....	1
1.1. Introduction	1
1.2. Research Project Statement	4
2. LITERATURE REVIEW	8
2.1. Hydrate Overview	8
2.2. Background	14
2.3. Structure and Chemical Background	17
2.4. Hydrate Formation and Dissociation Mechanism	21
2.5. Hydrate Mitigation Remediation and Inhibition	26
2.6. Chemical Hydrate Inhibition	28
2.7. Hydrate Inhibition Selection Criteria	40
3. METHODOLOGY	41
3.1. Advanced Hydrate Experimental Methods	42
3.2. Hydrate Measurements via Instrumental Techniques	48
3.3. Temperature Control of Hydrate Experiments	50
3.4. Experimental Set-up	51
3.5. Materials	60
3.6. HydraFLASH® Software	62
3.7. Experimental Procedure	65
4. RESULTS AND DISCUSSION	83
4.1. Method to Obtain Thermodynamic (HLVE) Points	84

	Page
4.2. Method to Obtain Kinetic Induction Time	87
4.3. Micro Bench Top Reactor	89
4.4. High Pressure Autoclave	94
4.5. Rocking Cell	97
4.6. Discussion	106
5. CONCLUSION	108
REFERENCES	111

LIST OF FIGURES

		Page
Figure 1	Conceptual representation of hydrate formation in an oil-dominated system in pipeline	2
Figure 2	World proven gas reserves, source Oil & Gas Journal, Jan. 1, 2014..	5
Figure 3	Map of state Qatar showing the extent of the north field.....	6
Figure 4	Hydrate crystal unit structures: (a) cubic structure sI (b) cubic structure sII and (c) hexagonal structure sH	8
Figure 5	Formation of gas hydrate in a subsea pipeline (Petrobras - Brazil)...	9
Figure 6	Effect of gas gravity on hydrate formation	10
Figure 7	Hydrate equilibrium curve in ocean (temperature vs. depth).....	11
Figure 8	The three common hydrate unit crystal structure	19
Figure 9	Schematic model of labile cluster growth	22
Figure 10	Adsorption of gas molecules onto hydrate cavities at gas-water Interface.....	23
Figure 11	Methane hydrate equilibrium curve using micro bench top reactor....	24
Figure 12	Typical natural gas hydrate equilibrium curve	29
Figure 13	A schematic diagram showing the mechanism of absorbing KHIs on hydrate surface	31
Figure 14	A schematic diagram showing the effect of AAs inside the pipeline..	32
Figure 15	Sapphire cell high pressure test equipment	43
Figure 16	A schematic diagram of sapphire rocking cell set-up (left) and individual cell (right)	44
Figure 17	Rocking cells used by Shell Global Solutions International	45
Figure 18	Mini flow loop technique from inside (laboratory scale)	46

	Page
Figure 19	A wheel-shaped flow loop technique (laboratory scale) 47
Figure 20	Real plant large scale multiphase flow loop, France 47
Figure 21	Gas hydrate properties and associated characterization methods and instrument 48
Figure 22	Hydrate curves from micro DSC under variable methane pressure... 49
Figure 23	The top bench reactor test equipment consist of 1) reactor controller, 2) reactor cell, 3) heater aluminum block, 4) water bath.. 53
Figure 24	The head fitting of the reactor cell (Source: instrument manual)..... 54
Figure 25	High pressure autoclave cell main parts are 1) autoclave cell, 2) thermostat, 3) light source, 4) gas cylinder, and 5) control-PC..... 56
Figure 26	RC-5 experiment set-up are 1) base unit, 2) thermostat, 3) control PC..... 58
Figure 27	RC-5 base unit consist of 1) RC-5 bath, 2) temperature sensor, 3) gas supply, 4) test cell. Not illustrated: front panel..... 59
Figure 28	HydraFLASH® software main window expressing the main input for each run 63
Figure 29	Numerical result window for hydrate dissociation of QNG-S1 with 20% methanol inhibitor 64
Figure 30	Graphical representation for hydrate dissociation curve using QNG-S1 mixture with 20% methanol inhibitor of the aqueous mole fraction..... 65
Figure 31	A general schematic diagram of the whole experiment set-up 66
Figure 32	Temperature vs. time for leak test via micro bench top reactor 68
Figure 33	Pressure vs. time for leak test via micro bench top reactor 68
Figure 34	The relation between Parr thermocouple and pre-calibrated thermocouple wire for calibration purpose 70
Figure 35	The relation between Parr pressure sensor and pre-calibrated transducer for calibration purpose 71

	Page
Figure 36	SpacView – [Parr 4848] software main window 73
Figure 37	A complete program schedule in Hydrate software 76
Figure 38	Hydrate software main window and camera preview window 77
Figure 39	An assembling aid used to loosen and fasten the test cell 79
Figure 40	A complete program schedule in RC-5 software 80
Figure 41	RC-5 software main window showing measurements values and graphical representation for monitoring propose..... 81
Figure 42	Typical experimental hydrate liquid vapor equilibrium curve 85
Figure 43	A complete hydrate formation/dissociation loop zooming in the region where hydrate equilibrium point is found 86
Figure 44	Red line shows a complete hydrate equilibrium curve for the three hydrate formation/dissociation loops of gas mixture composition and experimental set-up 87
Figure 45	Schematic representation of the pressure changes with time during a typical kinetics hydrate formation 88
Figure 46	Pressure-temperature and pressure-time in the upper left corner used to obtain induction time 89
Figure 47	HLVE curve for pure CH ₄ using Micro rector compared with those obtained by Sloan (1998), specific gravity method and HydraFLASH®..... 91
Figure 48	HLVE curve for pure CO ₂ using Micro rector compared with those obtained by Sloan (1998), K-factor method and HydraFLASH®..... 92
Figure 49	HLVE curve for plain QNG-S1 system using micro rector compared with those obtained by specific gravity method and HydraFLASH®..... 93
Figure 50	Image of the hydrate formation/ dissociation process in high pressure autoclave..... 95

	Page
Figure 51	HLVE curve for plain QNG-S1 system using autoclave compared with those obtained by SG method and HydraFLASH® and the data obtained in micro reactor 96
Figure 52	HLVE curves for both plain and nitrogen rich QNG-S1 obtained by SG. method and HydraFLASH® for plain QNG-S1..... 98
Figure 53	Inhibition effect of 1 wt % and 5 wt% choline chloride on NR-QNG-S1 using RC-5 compared with that obtained using SG method..... 99
Figure 54	Inhibition effect of 1 wt % and 5 wt% choline chloride on plain QNG-S1 using RC-5 compared with those data obtained using autoclave, micro bench top reactor SG method and HydraFLASH..... 102
Figure 55	Comparing the inhibition effect of classical inhibitor and ionic liquid..... 104
Figure 56	Induction time measurement for 1 wt. % and 5 wt. % of choline chloride applied on plain QNG-S1 using RC-5 at starting pressure of 60 bar..... 105

LIST OF TABLES

		Page
Table 1	Experimental set-up used to study thermodynamic and kinetic behavior for hydrate formation/dissociation	15
Table 2	Characteristics for the three structures	20
Table 3	Chemical structure and authority for the common THIs, KHIs, AAs and ionic liquid inhibitors	33
Table 4	Application, benefits and limitation of chemical inhibitors	40
Table 5	Micro bench top reactor specifications	54
Table 6	High pressure autoclave cell specifications	57
Table 7	RC-5 main specifications	59
Table 8	QNG-S1 mixture composition used in this work	60
Table 9	NR-QNG-S1 mixture calculated composition used in this work	61
Table 10	Chemical structure and physical constants for ionic liquid inhibitor used in this work	62
Table 11	Inhibitor fraction on mass bases of aqueous phase	67
Table 12	The set conditions used in the three different devices utilized in this project	82
Table 13	Measured hydrate liquid vapor equilibrium points for pure methane using micro bench top reactor	90
Table 14	Measured hydrate liquid vapor equilibrium points for pure CO ₂ using the micro bench top reactor.....	92
Table 15	Measured hydrate liquid vapor equilibrium points for plain QNG-S1 system using micro bench top reactor	93
Table 16	Measured HLVE points for plain QNG-S1 system using autoclave..	95
Table 17	Measured HLVE points for NR-QNG-S1 system using rocking cell	99

Table 18 Measured HLVE points for plain-QNG-S1 system using rocking cell compared with autoclave 102

1. INTRODUCTION

1.1. INTRODUCTION

The State of Qatar has been economically booming since the late 1990's due to the exploration and utilization of gas fields. Oil and gas form about 60 % of gross domestic product, approximately 85% of the export earnings, and 70 % of government revenues. Industrial activities in both oil and gas sectors have resulted placing Qatar one of the wealthiest countries in the world with second highest per-capita income country. Yet Qatar is one of the world's fastest growing economy according to International Monetary Fund report [1]. With proved reserves of natural gas at approximately 885 trillion cubic feet, Qatar's natural gas production will continue to be a major income stream for the foreseeable future.

Natural gas processing has its own operational problems in both exploration and processing stages. One of the most widely known problems that natural gas industry suffers is formation of gas hydrate in gas distribution networks, pipelines, and exploration sites. Gas hydrates form wherever there are low enough temperatures, high enough pressures, and adequate amounts of free water in the environment (e.g., pipeline). As the gas hydrates are inevitably form in the confined areas in the process, they pose significant problems in two aspects: 1) health and safety risk and, 2) loss in production rate due to blockage and thus economic loss. Production problems from hydrates occur in a number

of critical areas, mainly in pipelines, where blockage can result in both gas and oil dominated systems as shown in Figure 1 [2; 3].

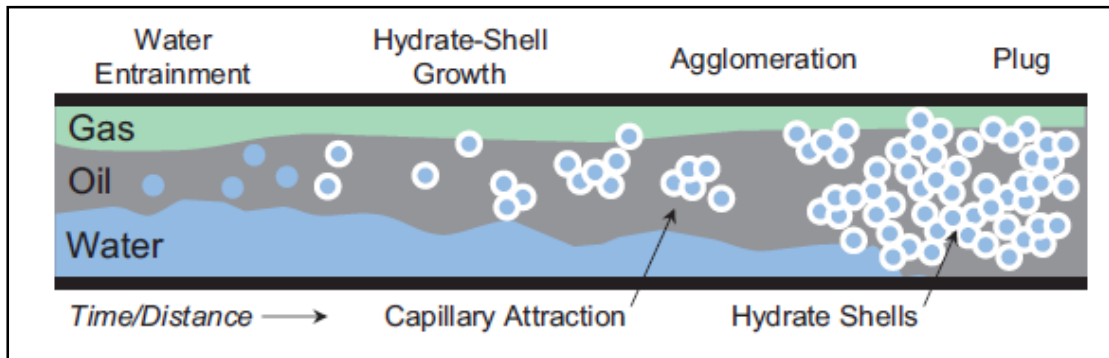


Figure 1: Conceptual representation of hydrate formation in an oil-dominated system in pipeline [3].

Similar problems can occur at valves and orifice plates due to the Joule-Thompson effect which lowers the temperatures as the gas expansion and thus causing water condensation, and eventually leading conditions that favor hydrate formation. Hydrates can build-up on control surfaces making the valve inoperable or cause damage to the valve seat. Such problems are especially apparent around the wellhead choke valves upon start up and could lead to catastrophic overpressure [4; 5; 6]. Thus, formation of hydrates within these units can cause plant shutdown due to blockages or can cause the gas to go beyond the desired production specifications.

More importantly, what concerns the industry the most are the safety issues related to hydrate plug motion. Hydrate density is analogous to that of ice and, if formed within

upstream pipes, the pressure can propel dense plugs at very high velocity. In such conditions the risk of occurrence of rupture in the pipeline through the downstream increases significantly. Similarly, hydrates can form single or multiple plugs which lead to problems when depressurizing lines for maintenance, particularly as hydrates contain around 164 volumes of hydrate former gas (e.g. methane) per volume of hydrate cage [7; 8; 9; 10].

As the exploration and production of natural gas moving to extreme conditions with unconventional drilling and exploration techniques, the problem of gas hydrate formation has become much more challenging in recent years. Typically, four techniques have been established to prevent gas hydrate formation in industry. These techniques are removing water prior to gas distribution to process (known as gas dehydration), keeping pressure below the hydrate equilibrium condition at the operating temperature, heating the gas to a temperature above the hydrate equilibrium condition at the operating pressure, or injecting a thermodynamic inhibitor [9].

Additionally, there are several commercial packages that are used to predict and determine the thermodynamics state of hydrate formation during the operation with specific gas mixtures in process facilities. Programs such as CSMHYD, CSMGem and HydraFLASH® have been used widely in recent years and they have shown appreciable accuracy for several hydrate phase equilibrium prediction for both single component and

multicomponent gas mixtures. In this project, HydraFLASH® is used to predict hydrate formation conditions to the best of its predefined limits.

This work addresses issues related to hydrate formation in Qatar natural gas systems, as discussed in section 1.2.

1.2. RESEARCH PROJECT STATEMENT

Between 2008 and 2011, Qatar oil and gas industry faced various incidents of gas pipeline blockage by hydrates because of a sudden temperature drop in the vicinity of gas pipelines. These incidents caused a loss of 10 million USD per day due to lost production from the pipelines for almost 4 weeks in the above mentioned industry [11]. Hydrate formation has a huge impact on gas industry, especially in Qatar, since it holds the world's third-largest reserves of natural gas at 885 trillion cubic feet according to proven reserves in the latest report of the Oil and Gas Journal, in 2014, as shown in Figure 2 [12].

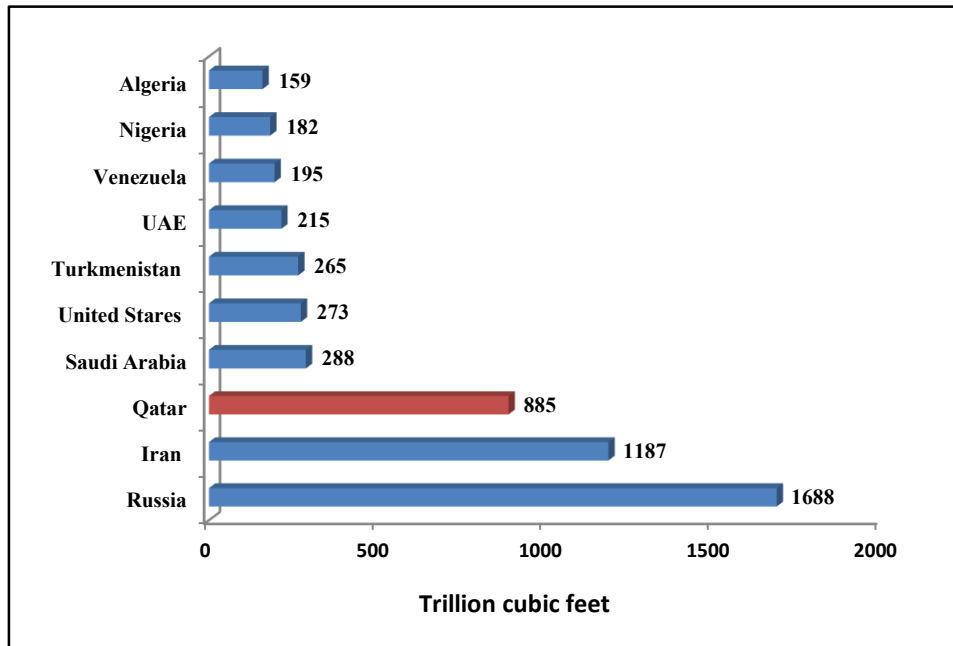


Figure 2: World proven gas reserves, source Oil & Gas Journal, Jan. 1, 2014.

This abundant natural resource makes Qatar one of the most important key players in LNG business around the globe. Qatar’s natural gas reservoirs are located 80 km off the shore in its North Field (Figure 3). Qatar’s LNG production is highly dependent on the reliable natural gas feed from the offshore wellheads to onshore processing facilities. Typical gas composition and pipeline operating conditions make flow assurance quite challenging in the North Field, causing unplanned shut downs and jeopardizing reliable LNG export to end users. Classical hydrate formation inhibition methods are used in order to prevent pipeline plugging.

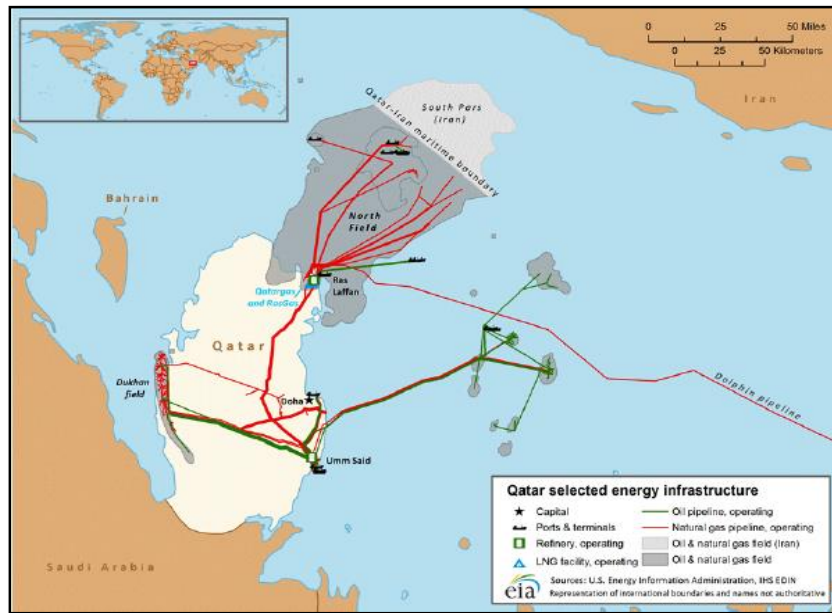


Figure 3: Map of state Qatar showing the extent of the north field [12].

Having mentioned all these facts about hydrate formation in pipelines and at wellheads, the primary objective of this study to establish academic know-how in gas hydrates in Qatar. Moreover, on the technical side, this study aims at obtaining hydrate equilibrium curves of Qatari natural gas mixtures and at evaluating the performance of classical and ionic liquid inhibitors using three different, newly commissioned high pressure hydrate cells. This goal has been achieved through the completion of the following phases:

1. Conducting a comprehensive research literature review.
2. Apparatus installation and validation.
3. Hydrate formation test using:
 - a. Micro bench top reactors (novelty)
 - b. Rocking cell (RC-5)
 - c. High pressure autoclave cell

4. Inhibition test with:
 - a. Classical inhibitor (HydraFLASH®)
 - b. Ionic liquid (Experimentally)
5. Hydrate curve determination (pressure and temperature conditions and induction time).
6. Comparing the collected hydrate formation equilibrium points of Qatar natural gas samples with theoretical predications of the HydraFLASH® software.

After this introductory chapter, chapter 2 presents a literature review that discusses the fundamentals of gas hydrates, their formation mechanism and the role of inhibitions. Chapter 3 describes briefly hydrate experimental methods and instrumental techniques used in different laboratories to study hydrate thermodynamic and kinetic behaviors. Additionally, it presents a detailed description of the experimental set-up used in this project, the way of administrating them and analyzing their data. Chapter 4 shows and investigates the data aimed to be studied in this project. Chapter 5 lists the main outcomes, recommendations and future work.

2. LITERATURE REVIEW

2.1. HYDRATE OVERVIEW

Clathrates of nature gas, commonly called gas hydrates, are ice-like compounds and have crystalline structures, which are formed with the proper combination of small guest molecules, like methane, and carbon dioxide, which are trapped in cavities of a hydrogen-bonded water framework. They are available in nature in three forms: cubic structures (sI) and (sII) as well as the hexagonal structure (sH), as shown in Figure 4. Geographically, gas hydrate can be formed at continental boundaries and permafrost regions or areas of similar environment, such as Gulf of Mexico, Black Sea and Caspian Sea.

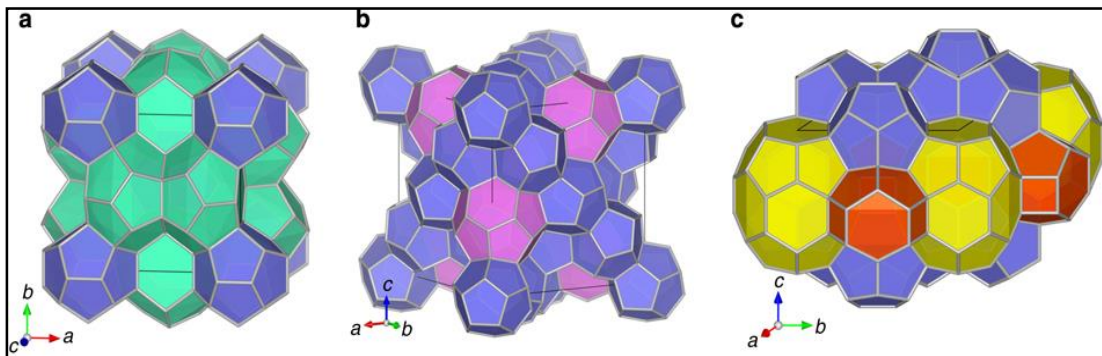


Figure 4: Hydrate crystal unit structures: (a) cubic structure sI (b) cubic structure sII and (c) hexagonal structure sH [13].

Natural gas hydrates can be formed at the gas-liquid interface over the whole pipeline length. This can generate small amount of gas hydrate over a long period of time, but it is often insufficient to clog the pipeline. Yet, upon pipeline restart, flow regimen and the mixing of the phases enhances gas-water contact and favors hydrates formation, increasing the amount and accumulation of hydrates that eventually can plug the pipeline as shown in the very famous picture in Figure 5. Small amounts of hydrates are typically formed and cannot be avoided in pipelines; in specific conditions, small hydrate agglomerates are detected as well in the bulk fluid phase. Hydrate formation does not become a hazard to pipeline flow unless hydrate agglomerates accumulate in large amounts. In such cases, blockage occurs as hydrates accumulate on the pipe walls, narrowing of the flow area very rapidly. This growing amount of hydrates can eventually shut-in the entire pipeline or field till hydrates can be completely dissociated [14].

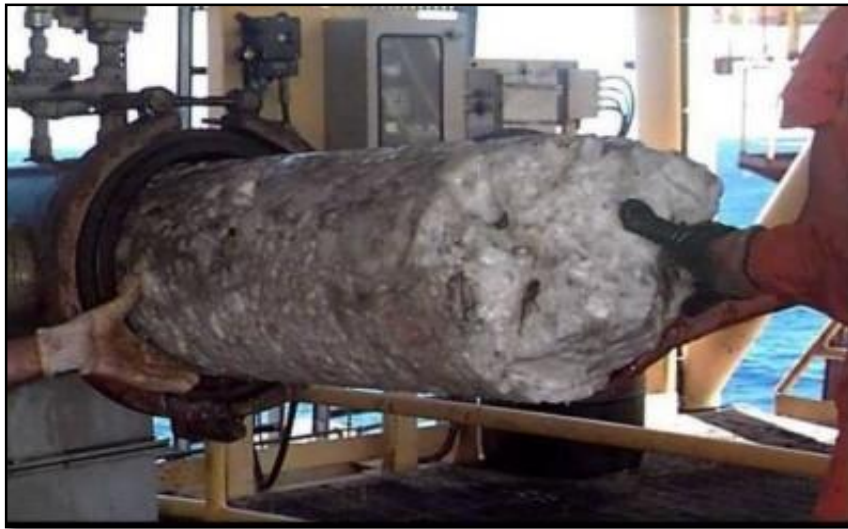


Figure 5: Formation of gas hydrate in a subsea pipeline (Petrobras - Brazil) [10].

The temperature and pressure conditions for hydrate formation are based on gas composition. Typically, high molar mass (molecular weight) natural gas such as those rich in CO₂ and/or H₂S will more easily form hydrates at high temperature and low pressure compared with low molar mass gases as shown in Figure 6, reported by Katz [15]. However, in the absence of additional information, the formation condition of natural gas hydrate is usually taken to be equal to that of the methane hydrate, which is about 38 bar and 277 K. At the high pressure conditions that natural gas pipelines are operated, hydrates will typically form as a result of fluid cooling, because of heat exchange with the external environment or induced by flow line processes, such as depressurization across valves or turbo expanders.

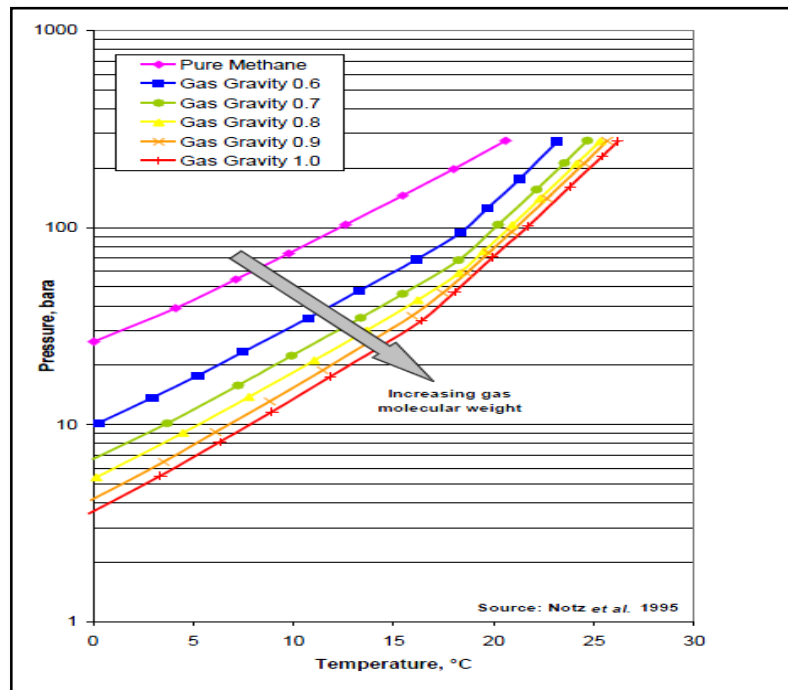


Figure 6: Effect of gas gravity on hydrate formation (Notz *et al.* 1995).

The source of water for hydrate formation is either free water from reservoir or condensed water from cooling the hydrocarbon fluid. During the cold winter months, when the outside temperature is low, onshore pipelines are usually at risk of hydrate formation. Offshore, at water depths below 900 m, the temperature is usually uniform around 3.8°C; pipeline temperature drops to this value within a few miles of the wellhead, setting the fluid conditions in the pipeline within the hydrate stability zone as presented in Figure 7 [10; 16].

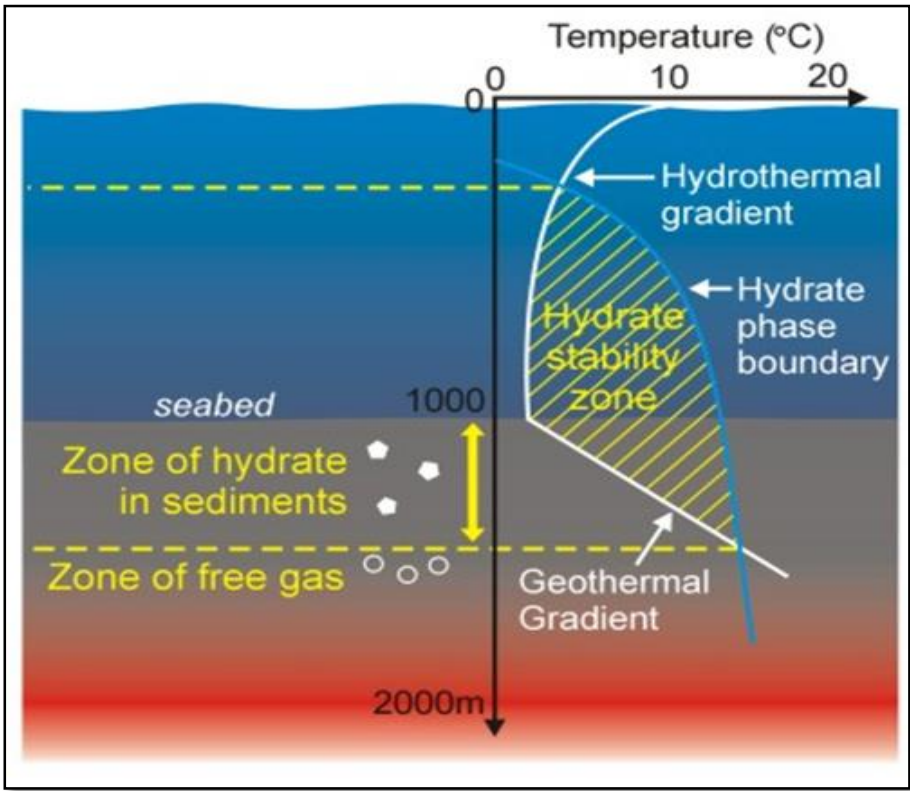


Figure 7: Hydrate equilibrium curve in ocean (temperature vs. depth) [17].

Besides economic losses associated with lost production caused by hydrate plugs, gas hydrates also pose serious safety concerns as hydrate formation divides the pipe into two segments of different pressure: the upstream region with high pressure and the downstream with low pressure. This difference in pressure can result in severe pipe rupture, ejecting a solid projectile which is dangerous for people nearby. This is a serious concern not only during construction stages but also during operation of process facilities, mainly within pipelines, and platforms, as hydrates can easily form there and agglomerate into large masses. As such, the prevention of hydrates in pipelines requires substantial investments, as much as 10 to 15% of the production cost [18].

Despite the significant problems experienced by industry due to hydrates formation, they play an important role in some industrial applications such as gas mixture separation, storage and transportation as reported by Changyu *et al* (2011). Once gas hydrates are formed, the water-free composition of each species in the hydrate phase will be different from that in the residual vapor phase. The faster hydrate forming compound will be present largely in the hydrate phase. According to this phenomenon, gas mixture separation processes, using hydrate-based separation, have been widely implemented. The main industrial processes that apply this principle are: (1) the recovery of CO₂ and H₂S from flue gas and other global warming gases; (2) the recovery of methane from low-concentration coal mine methane; (3) the recovery of organic contaminants from gaseous or aqueous mixtures; (4) the recovery of hydrogen from hydrogen-containing light hydrocarbon gas mixtures; and (5) the separation of methane and ethane in natural gas, oil

processing, and ethylene production. Furthermore, hydrate-based gas separation is much more efficient and has various advantages over traditional separation methods, such as gas absorption, selective adsorption, membrane process, and cryogenic fractionation [19].

Thus, despite being a problem-causing substance in industry, natural gas hydrates have great potential in storage and transport as they can capture a large amount of methane in the cage structure. As estimation, natural gas volume at standard condition can be shrunk up to 164 times when it is in the form of hydrate [10; 20]. This reduction in volume varies according to the structure of hydrate crystal. Consequently, avoiding extra cooling and compression of natural gas will dramatically decrease the operational cost during transportation. Natural gas in the hydrate form is very stable especially in cold climates such as Russia and Norway [20].

2.2. BACKGROUND

Hydrates were discovered in 1810 when Sir Humphrey Davy observed the first crystallization of chlorine hydrate during his research on the synthesis of newly discovered elements and compounds [21]. However, it remained somewhat of a scientific curiosity until Hammerschmidt reported in 1934 that natural gas hydrates were identified to be an irritant for gas industry [22]. Hydrate significance increased in the 1970s when they plugged large offshore pipelines, arctic fields, and wells of high-pressure facilities. Studies over the past two decades indicated that gas hydrates form in large masses after shutdown and restart of the process pipelines facilities.

A review of literature and past researches showed that hydrates can be studied from two different perspectives; thermodynamic conditions (hydrate liquid vapor equilibrium points) and kinetic behavior (induction time). To do so, there are several methods and techniques that can be implemented in laboratories and industry. The most common methods used to study thermodynamic and kinetic behaviors were high-pressure cells and reactors. Experimental set-ups applied by different groups to study thermodynamic and kinetic behavior of hydrate formation/dissociation are summarized in Table 1.

Table 1: Experimental set-up used to study thermodynamic and kinetic behavior for hydrate formation/dissociation.

Research group	Experimental set-up	Research investigation	Ref.
Gayet <i>et al.</i>	Isochoric high pressure stainless steel cell, no agitation	Investigate hydrate formation of methane–water system via monitoring pressure variation using constant cooling rate.	[23]
Kim <i>et al.</i>	Stainless steel high-pressure cell with large observation window.	Investigate hydrate dissociation curve of methane/ethane–water system via monitoring temperature variation using constant heating rate.	[24]
Sakaguchi <i>et al.</i>	Pyrex cell equipped with charge coupled device camera (CCD).	Investigate hydrate formation and growth at atmospheric conditions.	[25]
Kang <i>et al.</i> & Fleyfel <i>et al.</i>	Visual rocking cell, attached with nuclear magnetic resonance (NMR)	Investigate hydrate formation by visual observation and NMR peak monitoring.	[26; 27]
Koh <i>et al.</i>	Differential scanning calorimetry (DSC).	Quantify and compare the effect of different kinetic hydrate inhibitors on hydrate mitigation	[3; 7]
Gaillard <i>et al.</i>	Mini flow loop with pressure up to 75 bar.	Investigate methane hydrate formation, administrate kinetic modeling and test the inhibitor performance	[28]
Lee <i>et al.</i>	Visual mini flow loop with pressure up to 80 bar	Investigate hydrate plugging mechanism and inspect inhibitor performance	[29]
Del Villano & Kelland	Stainless steel-sapphire high pressure autoclave	Investigate hydrate kinetic behavior via studying the rate of crystal growth.	[30]

This research attempts to study hydrate formation and mitigation for Qatar natural gas (QNG-S1) from the viewpoints of thermodynamics and kinetics. From a thermodynamic point of view, three different apparatus were used to obtain Hydrate liquid Vapor Equilibrium (HLVE) points and curves, to determine the hydrate stability zone (hydrate hazard region) and to examine the effect of ionic liquid inhibitors with different concentration. Such equipment are micro bench top reactor, high pressure autoclave and rocking cell available at Qatar University. Commissioning a micro bench reactor as a typical hydrate cell is considered a novelty of this project. This study proves that this piece of equipment can be used as an economical hydrate cell for preliminary studies. From a kinetic point of view, the rate of hydrate crystal growth (induction time) was inspected using two different investigations: first, the hydrate was examined to see if the memory-effect phenomenon influences the induction time. Secondly, the effect of the presences of hydrate inhibitors at different concentrations, on the induction time, was studied.

2.3. STRUCTURE AND CHEMICAL BACKGROUND

Gas Hydrates, are solid crystalline composed of water and gas molecules, formed when the small guest molecule (< 0.9 nm) such as methane or carbon dioxide is entrapped in a cage of host, which is hydrogen bond water molecules, under optimum temperature and pressure [2; 10]. There is no bonding between host and guest molecule which makes the latter free to rotate within the cavity of water molecules [10].

In the 19th century, hydrate was classified by Humphry Davy depending on the captured guest molecule: (1) simple hydrates, where each cavity contains a single guest molecule; (2) mixed hydrates, in which the same kind of cavities contain two or more gas species; (3) double hydrates, which have two different types of cavity containing unlike gas species [31; 32]. In the middle of the 20th century, a group of scientists (von Stackelberg & Muller) came with a new classification based on polyhedral with twelve or more vertices. The main types are cubic structures I (sI), cubic structures II (sII) and the hexagonal structure H (sH) formed by different types of cavities as illustrated in Figure 8 [13; 33; 34].

2.3.1. Cubic Structure I

Cubic Structure I (sI), which is called Type I, contains small guest molecules (0.4-0.55 nm). It has 46 water molecules per 8 gas molecules. The water molecules form two small pentagonal dodecahedrons (5^{12}) and six tetrakaidecahedrons ($5^{12}6^2$). The pentagonal

dodecahedron, which is a basic part in all hydrate structures, has a 12-sided cavity of equal sided pentagonal faces formed by 20 water molecules. On the other hand, 12 pentagons and 2 hexagons are combined to form tetrakaidecahedron leading to a slightly larger cavity than the previous one [2].

2.3.2. Cubic Structure II

Cubic Structure II, called Type II, holds guest gas molecule larger than sI (0.6-0.7nm). This structure contains the highest number of water molecules (136 water molecules per 24 gas molecules). The water molecules form 16 pentagonal dodecahedrons (5^{12}) and 8 hexakaidecahedrons ($5^{12}6^4$), which consists of 12 pentagonal faces and 4 hexagonal faces [2].

2.3.3. Hexagonal Structure H

Hexagonal Structure H (sH), which is called Type H, is much more complex than the sI and sII. It is formed only when large and small guest molecules are mixed together (0.8-0.9 nm) [1]. Structure H has the lowest number of water molecules (i.e., 34 water molecules per 6 gas molecules) and three different cavity sizes. Moreover, it is the only structure in nature that has a cavity with three square faces together with six pentagonal and three hexagonal faces ($4^35^66^3$). Accordingly, structure H unit cell consists of three

pentagonal dodecahedrons (5^{12}) with two irregular dodecahedrons ($4^35^66^3$) and one icosahedron ($5^{12}6^8$), which is the largest cavity [2].

The basic building block of each hydrate structure is presented in Figure 8. It is clearly shown that there is at least one non-polar guest molecule within each cage in all of the three structures. The guest molecule size should not be too large to fill the whole cavity; however, it has to be big enough to stabilize in cavity [2]. Nevertheless, under unusual conditions such as at low temperature and very high pressure, they can have multiple cage occupancy with unusually small guest molecules e.g. hydrogen and noble gasses [2; 35]. Table 2 shows the main unit cell's characteristics for the three structures discussed above.

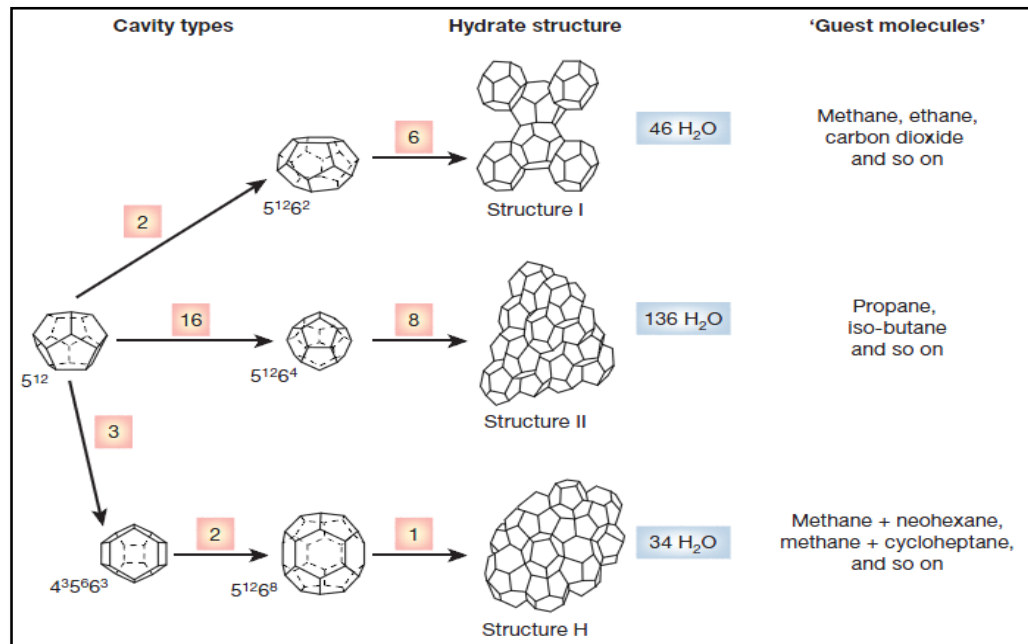


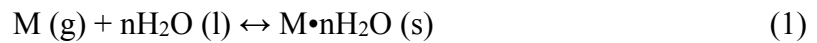
Figure 8: The three common hydrate unit crystal structure [2].

Table 2: Characteristics for the three structures [2].

Hydrate crystal structure	(sI)		(sII)		(sH)		
	Small	Large	Small	Large	Small	Medium	Large
Description	5 ¹²	5 ¹² 6 ²	5 ¹²	5 ¹² 6 ⁴	5 ¹²	4 ³ 5 ⁶ 6 ³	5 ¹² 6 ⁸
Number of cavities per unit cell	2	6	16	8	3	2	1
Average cavity radius (°A)	3.95	4.33	3.91	4.73	3.91	4.06	5.71
Coordination number *	20	24	20	28	20	20	36
Number of water per unit cell	46		136		34		
Resources	Earth's Natural environment (ocean depth)		Human made environment (industry)		Both environments		
Formers examples	Methane, ethane, carbon dioxide		Propane, iso-butane,		Methane + neohexane, Methane + cycloheptane		

2.4. HYDRATE FORMATION AND DISSOCIATION MECHANISM

The understanding of the hydrate formation/dissociation kinetics is important for predicting the amount of hydrate formed at certain times and conditions. The general reaction for gas hydrate formation can be expressed as:



where M denotes natural gas molecules, n is number of water molecules required to form a gas hydrate per one molecule of gas, and $M \cdot nH_2O$ is the gas hydrate [36; 37].

Gas hydrate formation is a time-dependent process that can be divided into hydrate nucleation, hydrate growth, and dissociation as illustrated in Figure 9 [16; 35].

2.4.1. Hydrate formation

The hydrate formation process is divided into two main steps: hydrate nucleation and hydrate growth. Hydrate nucleation is basically defined as a microscopic process in which tens of thousands molecules form small clusters that build up to hydrate nuclei, and then the growth step follows [16]. These steps will be presented briefly.

2.4.1.1. Hydrate nucleation

There are two main hypothesized mechanisms for hydrate formation, namely, labile cluster nucleation and nucleation at interface/local structuring. In the first mechanism, the nucleation is driven by gas molecules dissolved in the aqueous phase at the interface; here, the dissolved molecules cause a local structuring of the surrounding water molecules into clusters. These clusters tend to face share stress/force and agglomerate due to a reduction in free energy. If these agglomerated clusters reach a critical value, a nucleus is formed onto which further hydrate formation agglomerates [35]. This mechanism is clearly displayed in Figure 9.

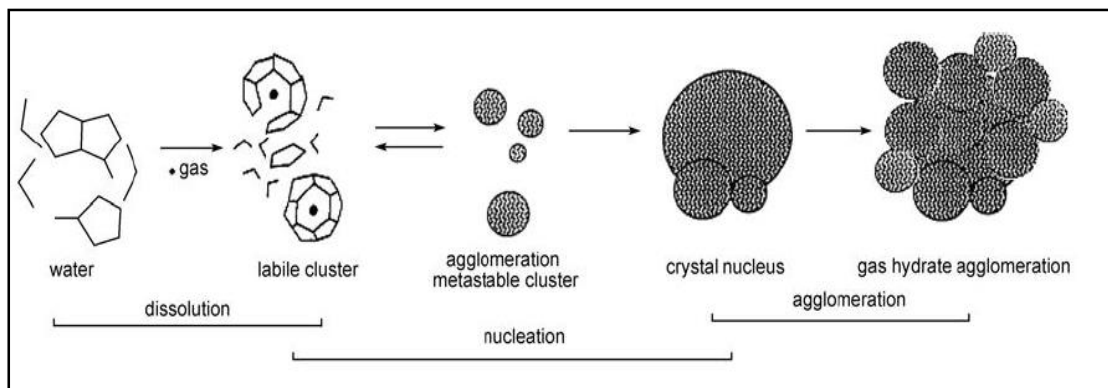


Figure 9: Schematic model of labile cluster growth [35].

In the second mechanism, the gas gets adsorbed onto the liquid surface rather than dissolving in the bulk phase. Here, gas adsorption causes a local structuring of the water to create half a clathrate cage, the gas migrates via surface diffusion into the cage, and

then a full cage is formed around it. This process continues with one clathrate cage forming on the face of another until a critical mass of nucleus is formed causing further rapid growth. Molecular simulations have provided support for this model as shown in Figure 10 [38].

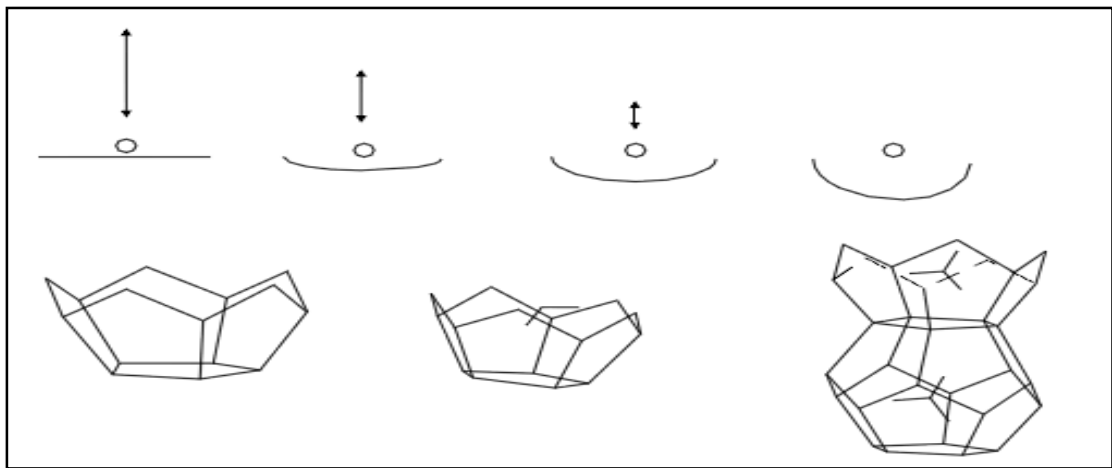


Figure 10: Adsorption of gas molecules onto hydrate cavities at gas-water interface [38].

2.4.1.2. Hydrate growth

Hydrate growth is an exothermic process and can be defined as the growth of stable hydrate nuclei into gas hydrate agglomeration. Mass transfer, heat transfer, and kinetics of crystal growth such as gas composition, agitation, surface area, and displacement from equilibrium conditions play significant roles in the process of agglomeration. The effect of the first two parameters has been evaluated in an isochoric system with varying

temperature throughout this experimental project, as present in Figure 11. Linear pressure drop between point 1 and 2 indicates the formation of labile cluster which is structured because of meta-stability [16; 39]. In contrast, sharp pressure drop, which starts at point 2, indicates the start of hydrate formation. The dramatic fall continues till point 3 where rapid hydrate agglomeration is finalized. Then, a slow heating process starts to dissociate the beginning formed hydrate through point 3 to A, causing a little pressure rise in the followed by a significant increase till point A, which represents the temperature and pressure of the hydrate equilibrium point [16].

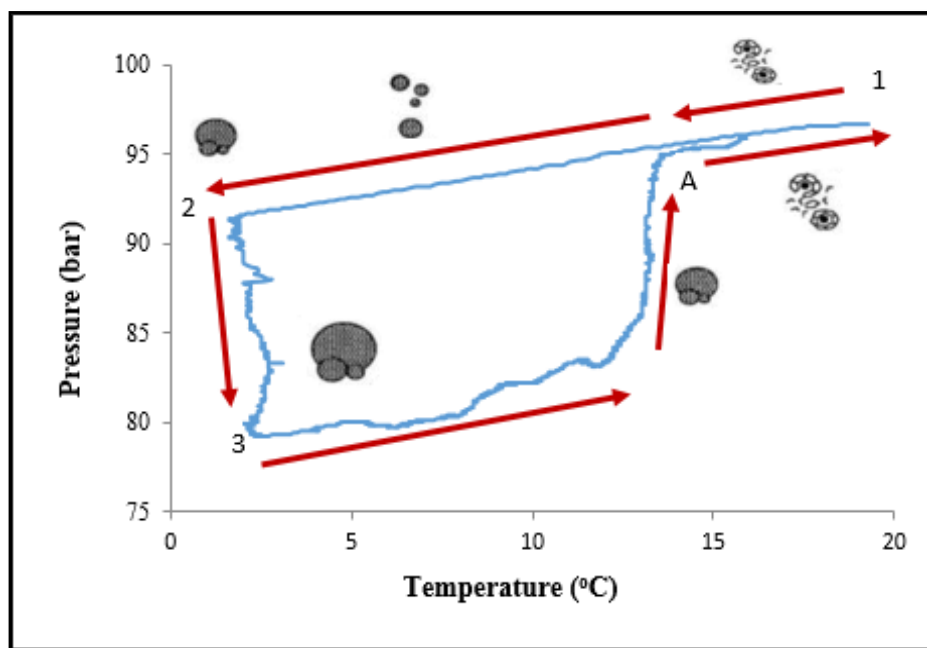


Figure 11: Methane hydrate equilibrium curve using micro bench top reactor.

2.4.2. Hydrate Dissociation

Hydrate dissociation is an endothermic process. This means that external heat must be supplied to decompose gas hydrate into gas molecule and water by breaking the hydrogen bonds between water molecules and the van der Waals interaction forces between the guest and host molecules of the hydrate lattice [16]. The former one is a stronger bond than the latter due to polar bonding between hydrogen and oxygen atoms.

Typically, in the oil and gas industry, there are various techniques to delay and change the conditions of hydrate formation that blocks pipelines. These methods are depressurization, thermal dissociation, dehydration, and inhibitor injection as it will be discussed in detail in the next section.

2.5. HYDRATE MITIGATION REMEDIATION AND INHIBITION

Much attention is still given to ways of preventing hydrate formation in pipelines. Based on the three conditions mentioned for hydrate formation, availability of gas and water under low temperature and/or high pressure, various methods are typically used to prevent hydrates [14]:

- **Gas dehydration methods:** In gas dehydration, water condensation from the gas phase is prevented by drying the gas using either triethylene glycol or molecular sieves.
- **Thermal methods (temperature control):** the system can be prevented from entering hydrate formation zone by controlling the temperature through passive insulation or active heating. Passive insulation functions well in preventing hydrate formation during normal operation as hot production fluid is continuously heating the system. The role of active heating becomes important once the system is shutdown, when no more hot fluid is produced.
- **Hydraulic method (pressure control):** The system should be designed and operated at low pressure to eliminate and mitigate hydrate formation in the pipeline. However, keeping the system pressure outside the hydrate envelop is not practical at ambient temperature as fluid transportation usually takes place at pressure higher than that needed for hydrate formation.

- **Chemical methods (injection chemical inhibitors):** The most practical way of preventing gas hydrate is by injecting chemical inhibitors such as methanol and monoethylene glycol. This approach has a significant effect on the hydrate morphology kinetics and phase diagram.

All these methods have drawbacks associated with the nature of the application. Gas dehydration or removing water may not be feasible or practical between the wellhead and the platform, so it is not widely used. Heating or insulating the pipeline is another alternative; however, it is costly and impractical to install over long distances. Maintaining low pressures in the pipeline is another option; however, it is inefficient and not cost effective, as high production rates require higher pressures. The most common method for hydrate prevention is injection of a chemical hydrate inhibitor into the pipeline.

2.6. CHEMICAL HYDRATE INHIBITION

In industry, chemical inhibitors are classified as thermodynamic inhibitors (THIs) and low dosage hydrate inhibitors (LDHIs) beside the newly discovered ionic liquid inhibitors. The description of these inhibitors is summarized below [40].

2.6.1. Thermodynamic inhibitors

Thermodynamic hydrate inhibitors are the most common chemicals for preventing hydrate formation. They work by decreasing water activity and changing bulk thermodynamic properties as they make hydrogen bonds with water molecules and prevent them from forming ordered cages to entrap gas molecules. Consequently, the equilibrium curve for hydrate formation is shifted to higher pressure and lower temperature; hence, the hydrate stability zone is compressed as illustrated in Figure 12 [40]. Nevertheless, THIs are very expensive because of the high concentration, up to 60%, needed for complete prevention [41]. Additionally, they are environmentally prohibited in deeper seas and oceans due to their huge impact on marine life.

The most common chemicals that act as THIs are alcohols, glycols, and salts. For instance, methanol (CH_3OH) and monoethylene glycol (MEG, $\text{HOCH}_2\text{CH}_2\text{OH}$) are extensively used in inhibiting gas hydrate formation, removing and melting gas hydrate blockage. In industry, the use of diethylene glycol (DEG) and triethylene glycol (TEG) is limited as

THIs due to their poor efficiency; however, they are widely used in the dehydration process [40; 42].

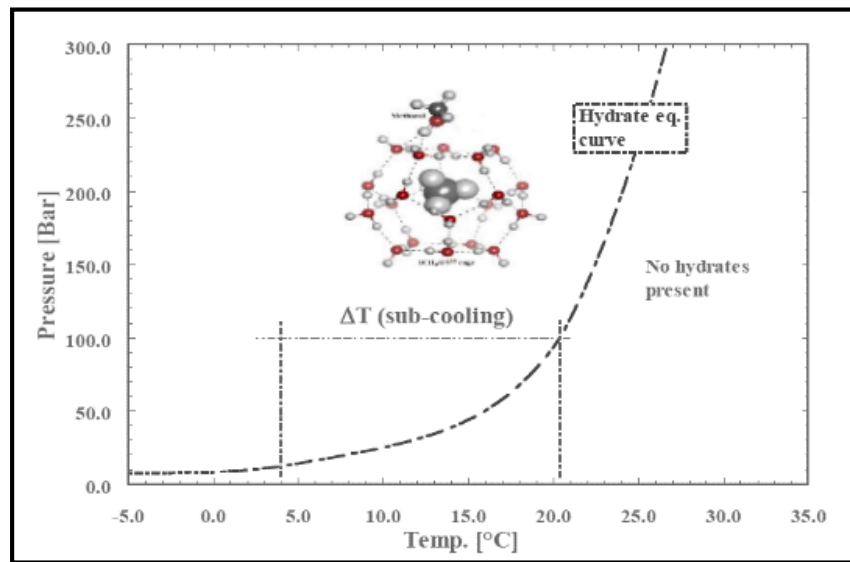


Figure 12: Typical natural gas hydrate equilibrium curve [40].

2.6.2. Low dosage hydrate inhibitors

Low dosage hydrate inhibitors (LDHI) have caught the attention of the researchers in academia and industry in hydrates research. Furthermore, they have been developed as an effective alternative to THIs depending on the field and fluid conditions. The name of LDHIs is derived from their efficient performance at low concentration compared with THIs (typically less than 1 wt % in the liquid phase). There are two main subdivisions of LDHIs: kinetic inhibitor (KHIs) and anti-agglomeration (AAs) [43].

2.6.2.1. Kinetic hydrate inhibitors

Kinetic hydrate inhibitors (KHIs) are polymer and co-polymers, such as Poly-vinylpyrrolidone (PVP), that are added to retard the formation of clathrate hydrate, and they contain small cyclic amide groups (active unit) [40; 43; 44]. Unlike THIs, KHIs limit or delay the formation of hydrate (i.e., nucleation and growth) by reducing the nucleation rate of hydrate, suppressing hydrate formation for time longer than the residence time of the water in the hydrate formation region, and preventing the formation of critical nucleus as shown in Figure 13 [6; 10]. In other words, hydrate crystal growth is controlled with KHIs; accordingly, their effect is time dependent, and eventually hydrate will form and block the pipeline if the traveling process is significantly long through the pipeline [40; 42]. However, this problem can be overcome by combining KHIs with THIs as their hybrid results in longer induction time and higher sub-cooling temperature, which is the difference between the hydrate equilibrium temperature and the operating temperature at a given pressure as illustrated in Figure 12 [44; 45]. Generally, KHIs are more preferable than THIs since they have higher efficiency in preventing hydrate formation with low concentration (< 1 wt. %) [46]. However, the only concern in using this method is the large molar volume or size of the molecule used. As it was observed recently that hydrate inhibition performance is less for high molecular weight inhibitors for both KHIs and THIs.

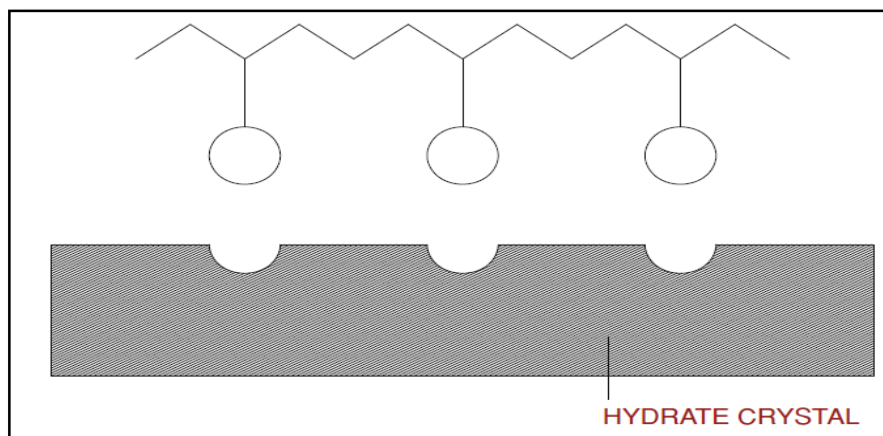


Figure 13: A schematic diagram showing the mechanism of absorbing KHIs on hydrate surface [10]. Reprinted with permission from Gas Hydrates Immense Energy Potential and Environmental Challenges, by Carlo Giavarini and Keith Hester, 2011, Springer, London. Copyright [2011] by Springer.

2.6.2.2. Anti-agglomeration (AAs)

Another class of LDHIs widely used in the prevention of hydrate blockage is anti-agglomerants (AAs), which work by keeping hydrate crystals dispersed and nonstick, thus preventing their agglomeration into large masses and plugging the pipelines as per Figure 14 [10]. Furthermore, they are typically used with surface-active agents, which provides emulsification that occurs between the gas/condensate phases and free water within the pipeline. This prevents the agglomeration of hydrate crystal, keeps the fluid viscosity low, and allows the hydrates to be transported along with the produced fluids [47]. Typically, anti-agglomerants are less dependent of time and the degree of sub-cooling of the system compared to KHIs. In deep and ultra-deep water cases, where very extreme conditions prevail as in the Gulf of Mexico, North Sea and West Africa-Nigeria, anti-agglomerant are observed to perform better than KHIs [48; 49].

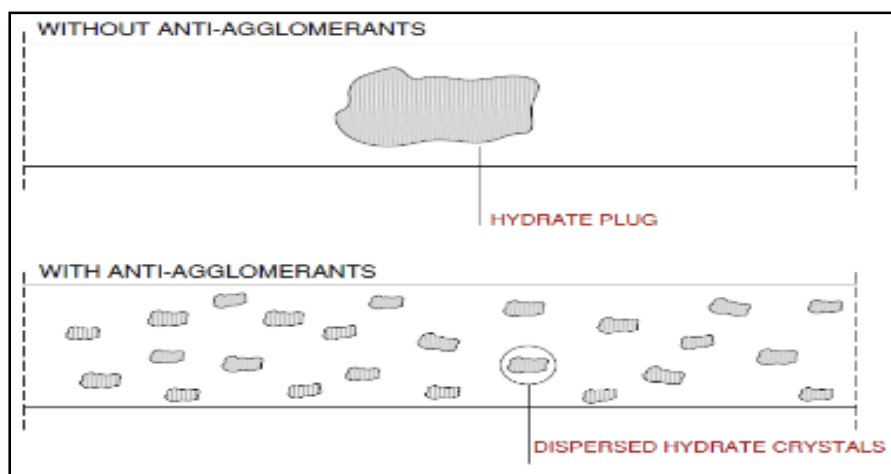


Figure 14: A schematic diagram showing the effect of AAs inside the pipeline [10]. Reprinted with permission from Gas Hydrates Immense Energy Potential and Environmental Challenges, by Carlo Giavarini and Keith Hester, 2011, Springer, London. Copyright [2011] by Springer.

2.6.2.3. Ionic liquid (ILs)

Ionic liquid inhibitors are a newly discovered type of inhibitors, firstly described by Xiao *et al.* in the first decennium of the 21st century [50]. It has a dual function inhibition-effect as a thermodynamic and kinetic inhibitor for methane hydrate and carbon dioxide hydrate as well. These inhibitors not only shift the HLVE curve to a lower temperature and higher pressure but also have the ability to prolong the induction time by delaying hydrate nucleation and growth. This type of inhibitor gained popularity due to their green and safe character, inflammability, stability in high temperature, and liquidity in a wide temperature range. Furthermore, it allows the choice between numerous cations and anions, making it tunable agents [50; 51; 52; 53].

Table 3 lists chemical components along with their chemical structures and issuing authority for the most common THIs, both kind of LDHIs and ionic liquids.

Table 3: Chemical structure and authority for the common THIs, KHIs AAs and ionic liquid inhibitors [41]

Chemical Name	Chemical Structure	Issuing Authority
Thermodynamic Hydrate Inhibitors		
Methanol	$\text{H}_3\text{C}-\text{OH}$	-
Ethylene Glycol	$\text{HO}-\text{CH}_2-\text{CH}_2-\text{OH}$	-
Diethylene Glycol	$\text{HO}-\text{CH}_2-\text{CH}_2-\text{O}-\text{CH}_2-\text{CH}_2-\text{OH}$	-
Triethylene Glycol	$\text{HO}-\text{CH}_2-\text{CH}_2-\text{O}-\text{CH}_2-\text{CH}_2-\text{O}-\text{CH}_2-\text{CH}_2-\text{OH}$	-
Kinetic Hydrate Inhibitors		
Polyvinylpyrrolidone (PVP)	$\left[\begin{array}{c} \text{CH}-\text{CH}_2 \\ \\ \text{N} \\ \\ \text{C=O} \end{array} \right]_n$	CSM
Polyvinylcaprolactam (PVCap)	$\left[\begin{array}{c} \text{CH}-\text{CH}_2 \\ \\ \text{N} \\ \\ \text{C=O} \end{array} \right]_n$	CSM
Terpolymer Gaffix (VC-713)	$\left[\begin{array}{c} \text{CH}-\text{CH}_2 \\ \\ \text{N} \\ \\ \text{C=O} \end{array} \right]_a \left[\begin{array}{c} \text{CH}-\text{CH}_2 \\ \\ \text{N} \\ \\ \text{C=O} \end{array} \right]_b \left[\begin{array}{c} \text{CH}-\text{CH}_2 \\ \\ \text{C=O} \\ \\ \text{O} \\ \\ \text{CH}_2 \\ \\ \text{CH}_2 \\ \\ \text{NMe}_2 \end{array} \right]$	CSM

Table 3: Continued

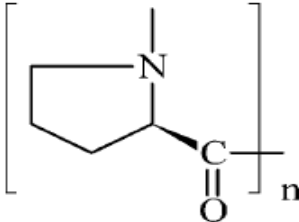
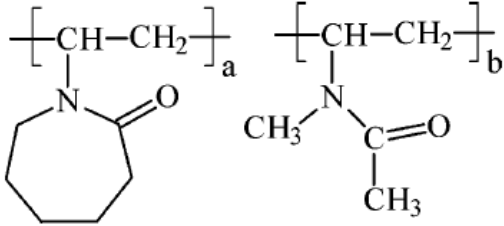
Chemical Name	Chemical Structure	Issuing Authority
Kinetic Hydrate Inhibitors		
Polyethyacrylamide	$\left[\begin{array}{c} \text{CH}-\text{CH}_2 \\ \\ \text{O}=\text{C} \\ \\ \text{NH} \\ \\ \text{C}_2\text{H}_5 \end{array} \right]_n$	CSM
Polyvinyl-Nmethyl acetamide	$\left[\begin{array}{c} \text{CH}-\text{CH}_2 \\ \\ \text{N} \\ / \quad \backslash \\ \text{CH}_3 \quad \text{C}=\text{O} \\ \quad \quad \\ \quad \quad \text{CH}_3 \end{array} \right]_n$	CSM
Polyethyloxazoline	$\left[\begin{array}{c} \text{N}-\text{CH}_2-\text{CH}_2 \\ \\ \text{C}=\text{O} \\ \\ \text{C}_2\text{H}_5 \end{array} \right]_n$	CSM
Poly-L-proline		RF/ ExxonMobil/ total
<p><i>N</i>-methyl-<i>N</i>-vinylacetamide:vinyl caprolactam 1:1 copolymer (VIMA:VCap) where a = b.</p>		RF/ ExxonMobil/ total

Table 3: Continued

Chemical Name	Chemical Structure	Issuing Authority
Kinetic Hydrate Inhibitors		
Polyacryloylpyrrolidine	$\left[\begin{array}{c} \text{CH}-\text{CH}_2 \\ \\ \text{O}=\text{C} \\ \\ \text{N} \\ \\ \text{C}_4\text{H}_7 \end{array} \right]_n$	EPR
Polydiethylacrylamide,	$\left[\begin{array}{c} \text{CH}-\text{CH}_2 \\ \\ \text{O}=\text{C} \\ \\ \text{N} \\ / \quad \backslash \\ \text{C}_2\text{H}_5 \quad \text{C}_2\text{H}_5 \end{array} \right]_n$	EPR
Polyisopropylacrylamide	$\left[\begin{array}{c} \text{CH}-\text{CH}_2 \\ \\ \text{O}=\text{C} \\ \\ \text{NH} \\ \\ \text{CH} \\ / \quad \backslash \\ \text{CH}_3 \quad \text{CH}_3 \end{array} \right]_n$	EPR
Polyethylmaleimide	$\left[\begin{array}{c} \text{CH}-\text{CH} \\ \quad \\ \text{N} \\ \\ \text{C}_2\text{H}_5 \end{array} \right]_n$	EPR

Table 3: Continued

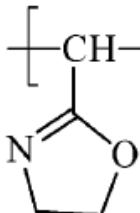
Chemical Name	Chemical Structure	Issuing Authority
Kinetic Hydrate Inhibitors		
Opened ring polyethyloxazoline,	$\left[\begin{array}{c} \text{N}-\text{CH}_2-\text{CH}_2 \\ \\ \text{O}=\text{C} \\ \\ \text{C}_2\text{H}_5 \end{array} \right]_n$	EPR
Closed ring polyethyloxazoline	$\left[\begin{array}{c} \text{CH}-\text{CH}_2 \\ \\ \text{N} \quad \text{O} \end{array} \right]_n$ 	EPR
Polyisobutylacrylamide	$\left[\begin{array}{c} \text{CH}-\text{CH}_2 \\ \\ \text{O}=\text{C} \\ \\ \text{NH} \\ \\ \text{CH}_2-\text{CH}-\text{CH}_3 \\ \\ \text{CH}_3 \end{array} \right]_n$	EPR
Polyisopropylmethacrylamide	$\left[\begin{array}{c} \text{CH}_3 \\ \\ \text{C}-\text{CH}_2 \\ \\ \text{O}=\text{C} \\ \\ \text{NH} \\ \\ \text{CH} \\ / \quad \backslash \\ \text{CH}_3 \quad \text{CH}_3 \end{array} \right]_n$	EPR

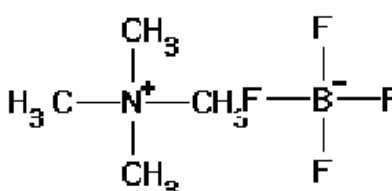
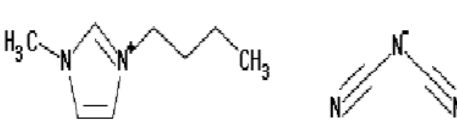
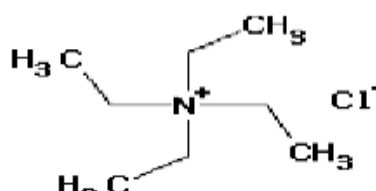
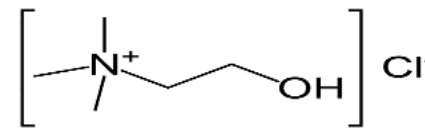
Table 3: Continued

Chemical Name	Chemical Structure	Issuing Authority
Kinetic Hydrate Inhibitors		
Polyisopropylmethacrylamide: <i>N</i> -vinyl- <i>N</i> -methyl acetamide copolymer (VIMA:iPMA)	$\left[\begin{array}{c} \text{CH}_3 \\ \\ \text{C} - \text{CH}_2 \\ \\ \text{O}=\text{C} \\ \\ \text{N} \\ \\ \text{CH} \\ / \quad \backslash \\ \text{CH}_3 \quad \text{CH}_3 \end{array} \right]_m \quad \left[\begin{array}{c} \text{CH} - \text{CH}_2 \\ \\ \text{N} \\ / \quad \backslash \\ \text{CH}_3 \quad \text{C}=\text{O} \\ \\ \text{CH}_3 \end{array} \right]_n$	EPR
Anti-agglomeration (AAs)		
Polyetherdiamine	$\text{H}_2\text{N} \left[\begin{array}{c} \text{CH}_3 \\ \\ \text{CH}_2 - \text{CH} - \text{O} \end{array} \right]_n \text{CH}_2 - \begin{array}{c} \text{CH}_3 \\ \\ \text{CH} - \text{NH}_2 \end{array}$	BJ Unichem Chemical Services
Dodecyl-2-(2-caprolactamyl) ethanamide	$\text{C}_{10}\text{H}_{21} - \text{NH} - \text{C}(=\text{O}) - \text{CH}_2 - \text{CH}_2 - \text{N} \begin{array}{c} \diagup \\ \diagdown \end{array} \begin{array}{c} \text{O} \\ \diagdown \\ \diagup \end{array}$	CSM
Amine oxide surfactant (dodecylbutylmethylamine oxide)	$\text{C}_{12}\text{H}_{25} - \text{N}(\text{CH}_2\text{CH}_2\text{CH}_2\text{CH}_3)(\text{CH}_3) - \text{O}$	RF

Table 3: Continued

Chemical Name	Chemical Structure	Issuing Authority
Anti-agglomeration (AAs)		
Carbonylpyrrolidine surfactant (R = C ₈₋₁₄)		RF
Isopropylamide carboxylic acid surfactants (R = C ₈₋₁₄)		RF
Betaine surfactants. R is a long alkyl chain with various spacer groups.		RF
Alkyl ether tributylammonium bromide (R = C ₁₂₋₁₄).		Goldschmidt.

Table 3: Continued

Chemical Name	Chemical Structure	Issuing Authority
Ionic Liquid		
1-Butyl-3-methylimidazolium tetrafluoroborate		-
1-Butyl-3-methylimidazolium dicyanamide		-
Tetraethyl ammonium chloride		-
2-hydroxy-N,N,N-trimethylethanaminium chloride, also known as choline chloride		-

* CSM: Colorado School of Mines

* EPR: Exxon Production Research

* RF: RF- RF-Rogaland Research

2.7. HYDRATE INHIBITION SELECTION CRITERIA

The selection criteria of hydrate inhibition mainly depends on technical and economic considerations. The applications, benefits, and limitations of THIs, KHIs, and AAs are shown in Table 4.

Table 4: Application, benefits and limitation of chemical inhibitors [44].

Thermodynamic Hydrate inhibitors	Kinetic hydrate Inhibitors	Anti-Agglomerant Inhibitors
Application		
1. Multiphase 2. Gas & condensate 3. Crude oil	1. Multiphase 2. Gas & condensate 3. Crude oil	1. Multiphase 2. Gas & condensate 3. Crude oil
Benefits		
1. Robust & effective 2. Well understood 3. Predictable 4. Proven track-record	1. Lower OPEX/CAPEX 2. Low volumes (<1 wt. %) 3. Environmentally friendly 4. Non-toxic 5. Tested in gas systems	1. Lower OPEX/CAPEX 2. Low volumes (<1 wt %) 3. Environmentally friendly 4. Non-toxic 5. Wide range of subcooling
Limitations		
1. Higher OPEX/CAPEX 2. High volume (10-60 wt. %) 3. Toxic / hazardous 4. Environmentally harmful 5. Volatile-losses to vapor 6. Salting out	1. Limited subcooling (<10°C) 2. Time dependency 3. Shutdowns 4. System specific-testing 5. Compatibility 6. Precipitation at higher temps 7. Limited exp. in oil system 8. No predictive models	1. Time dependency 2. Shutdowns 3. Restricted to lower water-cuts 4. System specific-testing 5. Compatibility 6. Limited experience 7. No predictive models

3. METHODOLOGY

This section sheds light on four main things. It first provides a brief background on the experimental methods and techniques used in the field of gas hydrates. Secondly, it gives a short description of equipment and materials utilized in this work. In addition, it includes a brief description of the HydraFLASH® software, which is used to obtain theoretical data to compare with the experimental data. Lastly, detailed description of the procedure for the three apparatus used in this work is provided towards the end of this section. These pieces of equipment are: micro bench top reactor, high pressure autoclave, and rocking cell.

As by the time the project was started, the micro reactor was commissioned to test materials, execute the designed experimental plan, and develop the certain backbone know-how of dealing with hydrate studies as it was required to execute the experimental project. Moreover, using this high-pressure reactor at the initial stages of the proposed project was necessary. It provided the team with the necessary experience dealing with high-pressure cells as it was fully recalibrated - including pressure and temperature controlling and monitoring systems. After being able to work within +/- 1° C accuracy level, newer cells arrived to the laboratory, which are designed as the typical hydrate experimental set-up (i.e., rocking cell and high pressure autoclave). These cells are designed for more accurate hydrate studies and have programmable temperature ramping options, better heat transfer, temperature/pressure monitoring systems.

3.1. ADVANCED HYDRATE EXPERIMENTAL METHODS

Natural Gas hydrate equilibrium curves and inhibitor performances can be studied via various techniques that can be categorized in to real field fluid and gas flow simulation. There are various equipment that can be used for this propose and they are discussed in the following subsection.

3.1.1. High-pressure autoclave cell

A high-pressure autoclave cell is commonly used to examine gas hydrate formation and to test the effectiveness and efficiency of mostly THIs and as well as LDHIs. The main feature of this device is that long term experiments, of up to 30 days or longer, are possible. This piece of equipment is designed to: 1) study gas hydrate formation and dissociations, 2) measure the induction time for formation of hydrates by monitoring the temperature increase and pressure drop as a function of time during the process of hydrate formation, and 3) detect transition visually [45].

The autoclave cell can be either a sapphire cell or a stainless steel cell, as shown in Figure 15 [54]. A sapphire cell is placed in a water bath in which the two stainless steel holders fix the sapphire cylinder. This cell is supported with by a magnetic stirrer mechanism at the bottom to create a magnetic rotating field [41]. Moreover, this cell is connected to a temperature control unit.

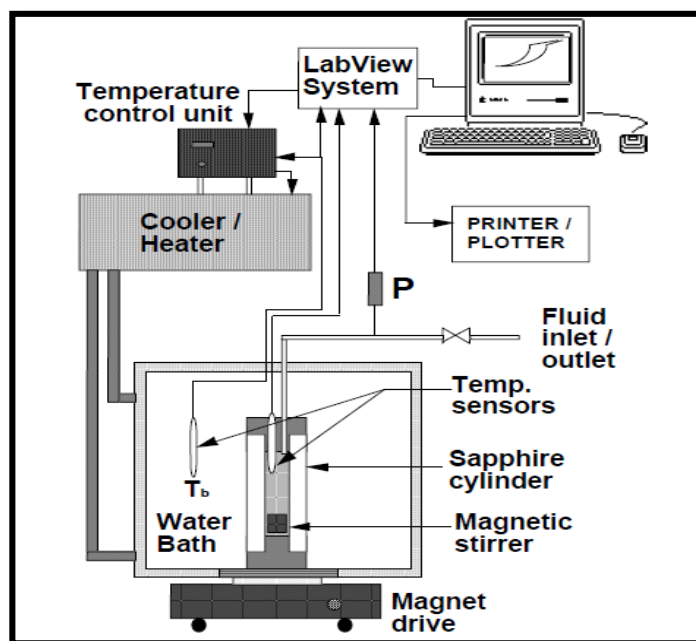


Figure 15: Sapphire cell high pressure test equipment [54].

3.1.2. Rocking cell

Another technique for testing mostly the performance of LDHIs uses a rocking cell, which can be a rocker rig, or ball stop rig. There are two types of such cells: stainless steel rocking cell (RC-5) and sapphire rocking cell (RC-S) as shown in Figures 16 and 17 respectively. The RC-5 is well engineered, user friendly, and allows long-time runs, of up to 30 days [55]. It was reported as such that this technique is used by Shell to analyze the anti-hydrate activity of KHLs [56].

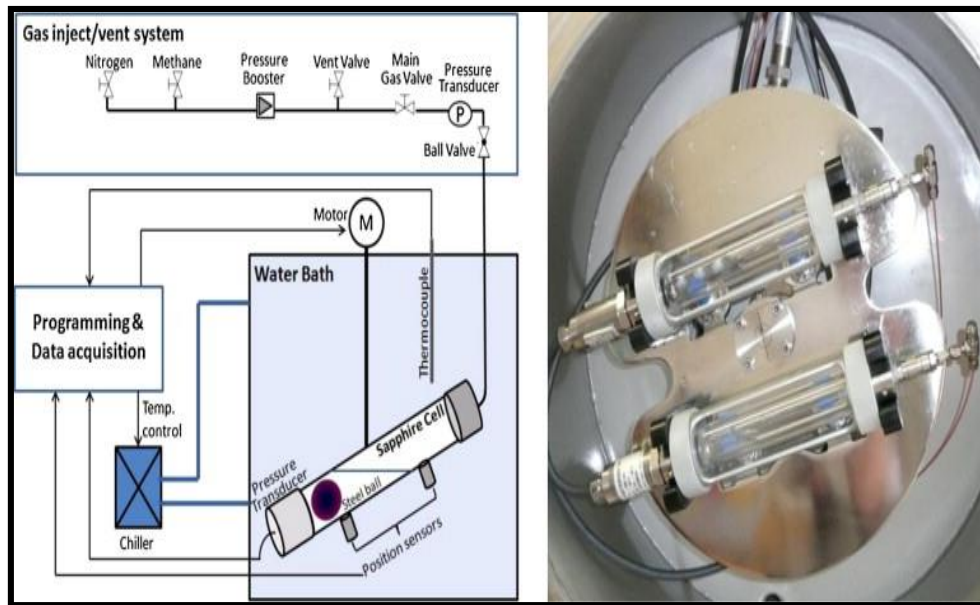


Figure 16: A schematic diagram of sapphire rocking cell set-up (left) and individual cell (right) [55].

On the other hand, sapphire rocking cell saves considerable development and measuring time and, accordingly, the project cost is reduced. Sapphire rocking cells are entirely transparent and the whole measurement environment is visible for better visual observation of the samples behavior and the development of the gas hydrates [55]. The measuring principle of the rocking cell is based on the constant rocking of temperature-controlled, pressurized test cells [55]. Sapphire rocking cells work by moving a steel ball in motion (forward and backward), which remarkably enhances the mixing effect of the enclosed mixture and leads to strong shear forces and turbulence, simulating pipeline condition [55]. This rocking cell only allows spread and limited size of hydrate to form in order not to impact the movement of the steel ball. This is a simple but effective for testing natural gas hydrate with AAs [41].

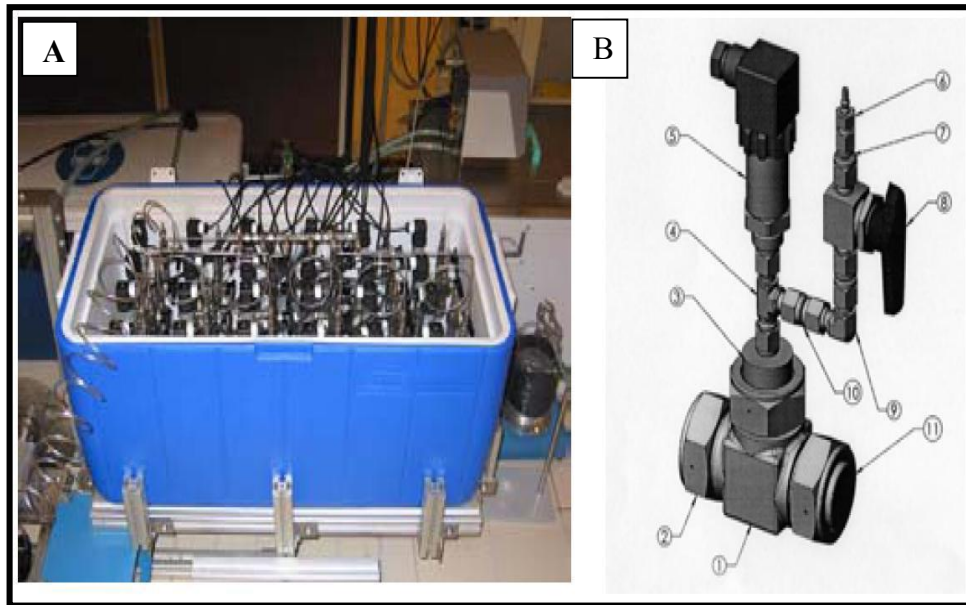


Figure 17: Rocking cells used by Shell Global Solutions International. Picture A shows the whole cell which contains 24 cells. Picture B shows an individual cell with its main parts: the 1'' tee (1), the end-nuts (2), the pressure transducer (5), a HP quick-connect gas inlet (6), a ball valve (8), and O-ring tightened blind flanges (11)[56].

3.1.3. Mini flow loop

The mini flow loop, vertical placed pipe-wheel or loop-wheel is a complicated technique that simulates real field flow conditions, as shown in Figure 18 [57]. The pipe has a window allowing visual observation, with diameters of $\frac{1}{4}$ " to 3" or even bigger sizes if desired. This equipment consist of a pipe, a pump, and a mixing tank to circulate a mixture of water and liquid hydrocarbon through the loop [41]. Each part of the loop has its own thermometer and pressure meter that is used to monitor the pressure drop due to hydrate formation [58]. Micro flow loop, recently developed, are smaller in size, simpler to

operate, and easier to maintain and clean than conventional loops that is explained in details elsewhere [57].



Figure 18: Mini flow loop technique from inside (laboratory scale) [57].

The main restriction to using flow loops is that the pump might get damaged due to the reason of the crushed hydrates at the suction side of the pump that also leads to some difficulties in interpreting the experimental data [41]. Figures 19 and 20 show examples of wheel shaped a flow loop and a real flow loop respectively [10].



Figure 19: A wheel-shaped flow loop technique (laboratory scale) [57].



Figure 20: Real plant large scale multiphase flow loop, France [10].

3.2. HYDRATE MEASUREMENTS VIA INSTRUMENTAL TECHNIQUES

There is a broad range of molecular studies and analytical techniques applicable to natural gas hydrate characterization, including hydrate crystal structure, composition, and cage occupancy determination. For these purposes, several analyses are required such as thermal analysis, crystallographic analysis, topographic analysis, size and size distribution analysis, spectroscopic analysis, interfacial tension and intermolecular particle force analysis, and methods involving gas hydrates inhibition [59]. For each of them, different testing instruments are used depending on the states of matter as per Figure 21.

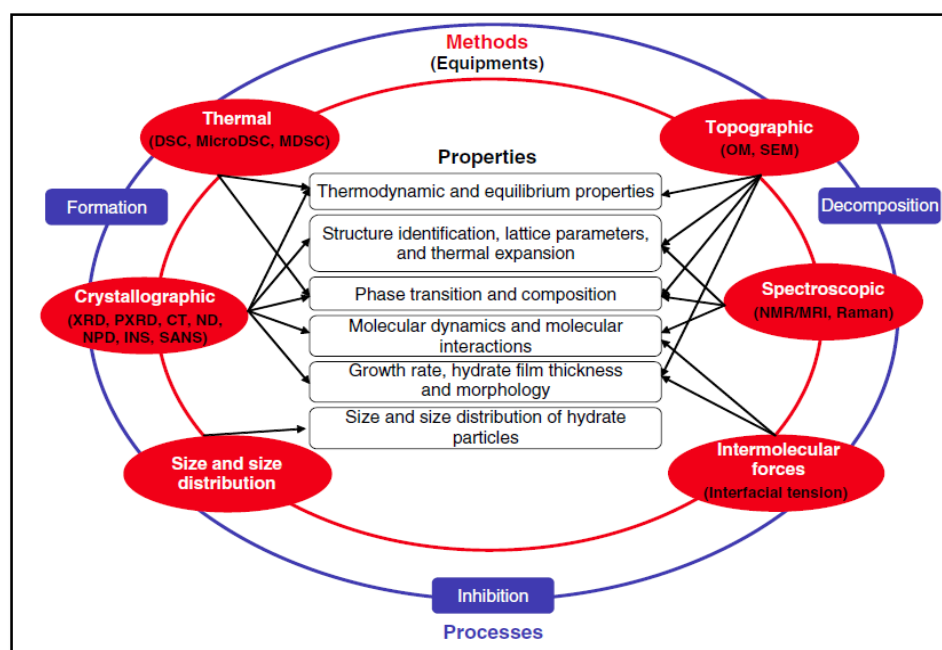


Figure 21: Gas hydrate properties and associated characterization methods and instrument [59]. Reprinted with permission from “Instrumental Analysis of Gas Hydrates Properties” by Y. Rojas and X. Lou, 2009. *Journal of Chemical Engineering*, 5, 310-323, Copyright [2009] by John Wiley and Sons.

3.2.1. Differential scanning calorimetry (DSC) Method

One of the most common methods of thermal analysis is differential scanning calorimetry (DSC), which can be defined as “the measurement of the change of the difference of heat flux to the sample and to a reference sample while they are subjected to a controlled temperature program” [60]. This technique can be used in several fields such as material characterization, measurements comparison, kinetic, stability and safety examination. Furthermore, it can be used to study hydrate dissociation in different aqueous media such as extremely concentrated salt solutions and water/oil emulsions at pressures up to 12 MPa [60; 61; 62; 63]. Another use of this technique is measuring the inhibition effect (low dosage level) on the formation and dissolution of natural gas hydrates [3]. Examples of hydrate dissociation curves using variable methane pressure are shown Figure 22.

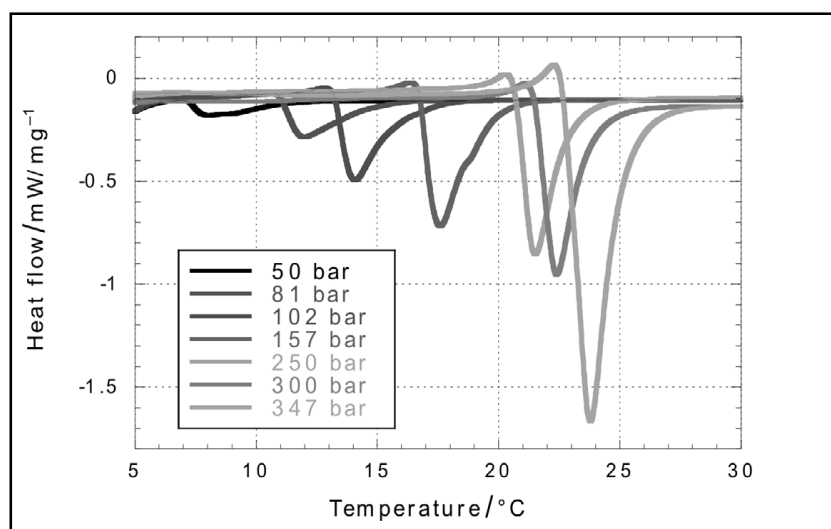


Figure 22: Hydrate curves from micro DSC under variable methane pressure [64].

3.3. TEMPERATURE CONTROL OF HYDRATE EXPERIMENTS

Various methods are used to evaluate inhibition performance on gas hydrate formation. The most commonly used ways are: 1) constant temperature or isothermal method, 2) constant cooling method, and 3) ramping method. A brief description of each of them follows.

3.3.1. Constant temperature

In this method, the fluid temperature is reduced to a specific sub-cooling point and kept at this condition for a sufficient time until hydrate is formed. This can be performed with or without stirring. Most of thermodynamic and kinetic studies prefer using this method due to the simplicity in indicating induction time [65; 66].

3.3.2. Constant cooling

The constant cooling method is achieved by cooling the system to an extremely low temperature (high sub-cooling) with stirring [54]. The drawback of this method is the difficulty in determining induction time, especially in a closed system under rapid cooling. This is because pressure drop usually occurred with fluid cooling [54]. The sudden pressure drop and temperature rise indicate hydrate formation. This is mainly due to gas uptake and heat release (exothermic reaction) during hydrate formation [54; 67].

3.3.3. Ramping

Ramping method is preferred in determining induction time as the pressure is maintained constant for a sufficient period of time [54]. This method typically needs longer time than others since the cooling process is done in a stepwise manner. This means that the fluids are cooled to a specific sub-cooling temperature and then kept at this temperature for a few hours, followed by another cooling step and kept again. Ramping process can be repeated until the hydrate crystals are formed [54].

3.4. EXPERIMENTAL SET-UP

Natural gas hydrate equilibrium curves and inhibition performances can be studied via various techniques that are applied to simulate real field fluid/gas flow conditions. This section presents the equipment used in this thesis.

3.4.1. Micro bench top reactor (Parr Instrument Company)

A micro bench top reactor is an isochoric system (i.e., constant volume) normally used to carry out reactions on a micro level scale in order to minimize the costs of expensive gases and chemicals. The reactor used was a micro bench top reactor 4590 (Parr Instrument Company). The novelty of this work was to modify it into a hydrate cell. The modifications were:

1. Exchanging movable heater down to heater aluminum block.

2. Heating and cooling the vessel using temperature water bath instead of internal heating.
3. Redesigning the connection between vessel and cylinder such as fittings and tubing (i.e. replacing all rubber tubing by metal).
4. Calibrating both of thermocouple and pressure gage by comparing their reading with pre-calibrated thermocouple wire (Omega) and pressure transducers (Paroscientific, Inc. model 735) respectively and finding a correlation between their data that applied for whole results obtained using this device.

The set-up of this cell after the above mentioned modification is shown in Figure 23 and consists of:

1. Cell to carry out the reaction.
2. Controller to turn on and control the stirrer motor, and monitor temperature ($^{\circ}\text{C}$), pressure (bar) and stirrer speed (RPM).
3. Rough vacuum pump to remove air by depressurizing the cell to around zero bar.
4. Water bath “thermostat” for heating and cooling purpose.
5. Heater aluminum block to isolate the vessel from surrounding conditions.
6. Gas booster with control panel to increase the pressure inside the vessel.
7. Gas cylinder.
8. PC with SpecView – [Parr4848] software to control temperature variables and stirrer rate. Also, it is used to collect and record temperature, pressure and stir rate as a function of time.

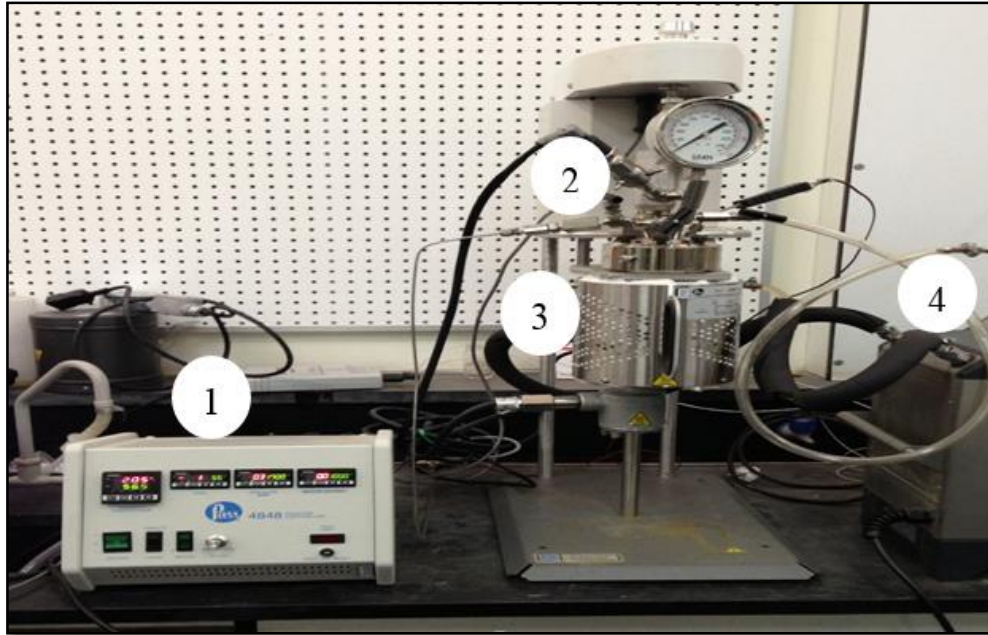


Figure 23: The top bench reactor test equipment consist of 1) reactor controller, 2) reactor cell, 3) heater aluminum block, 4) water bath. The remaining for parts are not shown in this figure due to positioning issue.

The vessel is made of stainless steel with a volume of 100 ml. The head fitting of this vessel consists of a magnetic drive, pressure gage, and thermocouple. The specifications of this vessel are shown in Table 5, followed by a photograph of the individual cell in Figure 24. The magnetic drive is important for speeding up hydrate formation by simulating the fluid flow condition in the pipeline. Pressure gage and thermocouple are used for reading the pressure and temperature within the vessel.

Table 5: Micro bench top reactor specifications.

Micro bench top reactor specifications	
Material	Stainless steel
Sizes (mL)	100 ml
Maximum temperature	225 °C
Temperature accuracy	+/-2°C
Maximum pressure	2900 psi (200 bar)
Pressure accuracy	0.01% up to max. 10000 psi
Stirring speed range	1-1999 RPM

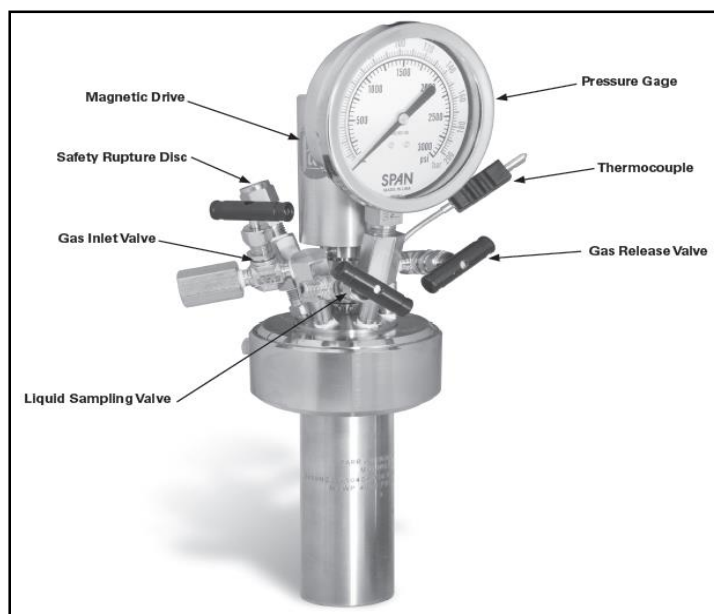


Figure 24: The head fitting of the reactor cell (Source: instrument manual).

3.4.2. High-pressure autoclave cell (PSL Systemtechnik GmbH)

A high-pressure autoclave cell is a device frequently used to test gas hydrate formation because of its ability to simulate pipeline conditions. The apparatus used in this project was a gas hydrate autoclave GHA 200 - PSL Systemtechnik GmbH. This cell is made of stainless steel with a pressure-resistant sapphire glass window to enable capturing the whole process of hydrate formation inside the autoclave using a boroscope-camera. The set-up of this cell is shown in Figure 25 and consists of:

1. Autoclave with integrated stirrer to carry out the reaction.
2. Thermostat to monitor and regulate the temperature inside the autoclave.
3. Light source to supply the camera with the light needed to film hydrate formation process.
4. Gas cylinders of the test sample.
5. Control-PC with software (Hydrate V4) to program the whole experiment and record time, temperature, and pressure data.

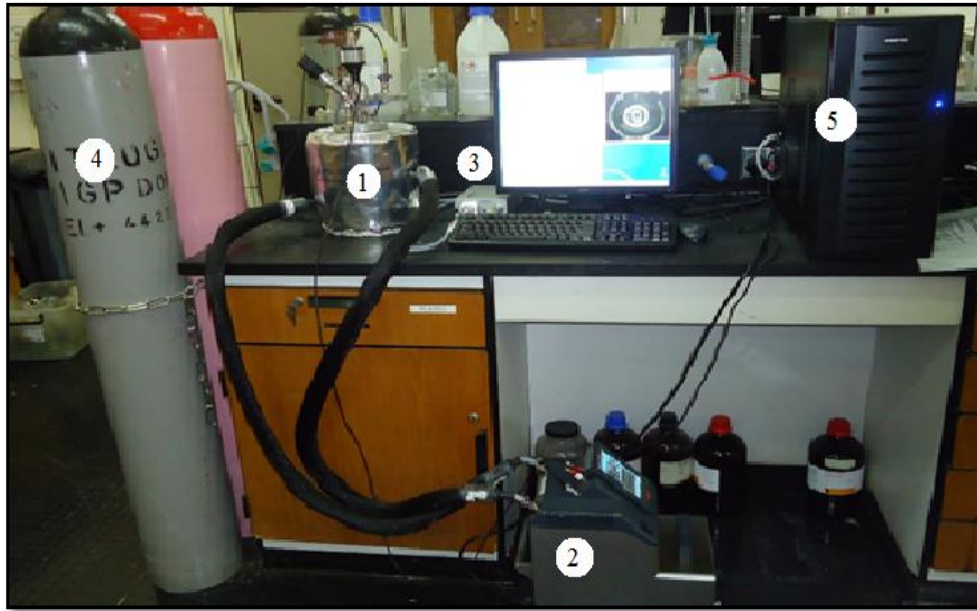


Figure 25: High pressure autoclave cell main parts are 1) autoclave cell, 2) thermostat, 3) light source, 4) gas cylinder, and 5) control-PC.

The autoclave body volume is 450 mL in total; however, it was recommended by the supplier to fill it up to 200 mL with fluid. The autoclave body consists of a joined magnetic stirrer which is placed at the bottom of the vessel. This stirrer is intended to simulate real life pipeline situations via high-mixing turbulence, which in turn enhances hydrate formation. It is also fitted with pressure and temperature sensors. The former is connected to the control-PC, while the latter is connected to the sensor socket of the thermostat to control the target temperature set by the control-PC. Furthermore, it is equipped with a boroscope-camera and a light source to allow the capturing hydrate formation within the autoclave. The specifications of the autoclave are shown Table 6.

Table 6: High pressure autoclave cell specifications

High pressure autoclave cell specifications	
Material	Stainless steel
Sizes	450 mL, 200 mL fluid (recommended)
Temperature range	-10 up to 60 °C
Temperature accuracy	0.1 °C
Maximum pressure	2900 psi (200 bar)
Pressure accuracy	0.5 % full scale
Stirring speed range	12-2000 RPM

3.4.3. Rocking cell (PSL Systemtechnik GmbH)

Rocking cell is a well-known technique for testing the performance of LDHIs on hydrate formation. There are two types: rocking cell (RC-5) and sapphire rocking cell (RC-S). The former was used in this project. It contains five test cells that can be run simultaneously for different mixtures and at different conditions. This equipment was also bought from PSL Systemtechnik GmbH. The whole experimental set-up is shown in Figure 26 and consists of:

1. RC-5 base unit, where hydrate formation process takes place.
2. Thermostat to monitor and regulate the temperature in the RC-5 bath.
3. Gas cylinders of the test sample.

- Control-PC with WinRCS V1.4 software to program the whole experiment and record time, temperature and pressure data.



Figure 26: RC-5 experiment set-up are 1) base unit, 2) thermostat, 3) control-PC.

The RC-5 base unit consists of three main parts as per Figure 27, 1) RC-5 bath, 2) test cells, 3) front panel. The RC-5 bath, also called an integrated bath, is filled with water-glycol mixture as a coolant and it is where the test cells are mounted on a movable axis controlled by an integrated stepper-motor. Each test cell is made of stainless steel and has a volume of 40 ml. A gas supply is built on the top of every cell while the connection for the temperature sensor is attached to its side. Each cell contains a stainless steel mixing ball with a diameter of 10 mm in order to create strong shear forces and turbulences within the cell, intended to simulate realistic pipeline situation. The front panel is mainly used for controlling the cell inlet and outlet. The specifications of RC-5 are shown in Table 7.

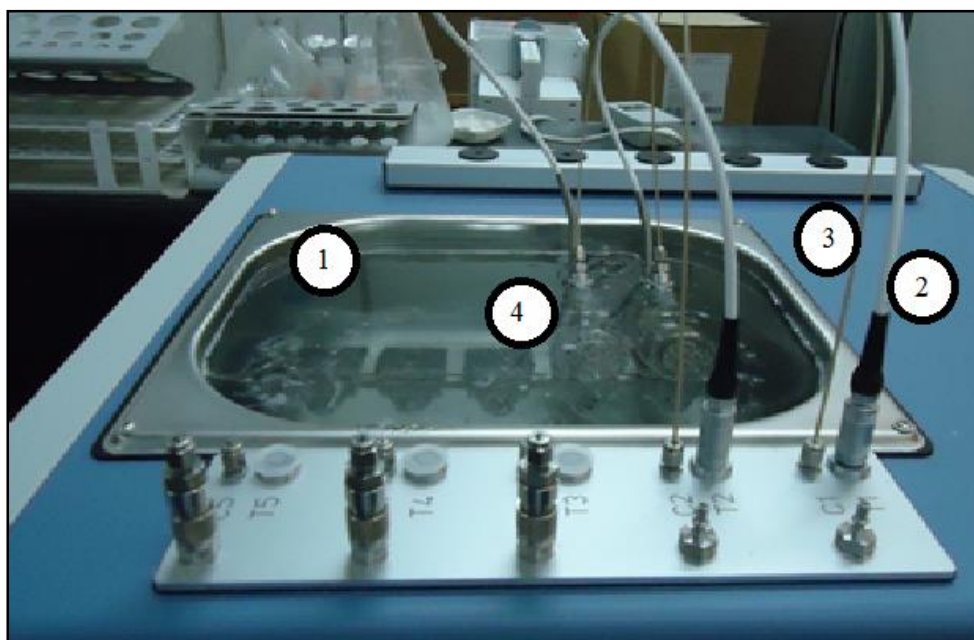


Figure 27: RC-5 base unit consist of 1) RC-5 bath, 2) temperature sensor, 3) gas supply, 4) test cell. Not illustrated: front panel.

Table 7: RC-5 main specifications.

RC-5 specifications	
Material	Stainless steel
Sizes	Test chamber 40 mL
Temperature range	-10 up to 60 °C
Maximum pressure	2900 psi (200 bar)
Accuracy	+/- 0.5%
Rocking rate	1-20 / min

3.5. MATERIALS

The following mentioned were used:

- Pure methane (99.995%) and carbon dioxide (99.999%), both purchased from Buzwair and used for calibration of the micro bench top reactor.
- Synthetic Qatar natural gas mixtures (Plain-QNG-S1), representing north field of Qatar natural gas, purchased from National Industrial Gas Plants (NIGP). However due to laboratory safety concerns, this natural gas mixture contains no hydrogen sulfide (H₂S). The composition of this gas mixture on mole basis is shown in Table 8. It was supplied in cylinders with a maximum pressure of 68 bar.

Table 8: Plain QNG-S1 mixture composition used in this work.

No.	Component	MW (g/mole)	QNG-S1* mole fraction
1	Methane	16.043	0.84990
2	Ethane	30.070	0.05529
3	Propane	44.097	0.02008
4	2-methylpropane	58.123	0.00401
5	Butane	58.123	0.00585
6	2-methylbutane	72.150	0.00169
7	Pentane	72.150	0.00147
8	Octane	114.231	0.00152
9	Toluene	92.140	0.00090
10	Methylcyclopentane	84.160	0.00102
11	Nitrogen	28.013	0.03496
12	Carbon Dioxide	44.010	0.02331

* Relative uncertainty for samples: CH₄ 0.2%, C₂ to C₄ 2.0%, C₅ plus higher 5%, N₂ and CO₂ 2%.

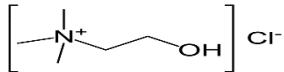
- The second type of natural gas mixture used in this study is Nitrogen Rich Qatar Natural Gas mixture 1 (NR-QNG-S1). This mixture is prepared by adding about 50% of N₂ into the QNG-S1 mixture. The calculated compositions are shown in Table 9.

Table 9: NR-QNG-S1 mixture calculated composition used in this work.

No.	Component	MW (g/mole)	NR-QNG-S1 mole fraction
1	Methane	16.043	0.42495
2	Ethane	30.070	0.02765
3	Propane	44.097	0.01004
4	2-methylpropane	58.123	0.00200
5	Butane	58.123	0.00293
6	2-methylbutane	72.150	0.00085
7	Pentane	72.150	0.00074
8	Octane	114.231	0.00076
9	Toluene	92.140	0.00045
10	Methylcyclopentane	84.160	0.00051
11	Nitrogen	28.013	0.51748
12	Carbon Dioxide	44.010	0.01166

- One type of ionic liquid inhibitor called 2-hydroxy-N,N,N-trimethylethanaminium chloride, also known as choline chloride, was used as hydrate inhibitor as shown in Table 10.

Table 10: Chemical structure and physical constants for ionic liquid inhibitor used in this work.

Component	Formula	Molar mass (g/mol)	Chemical Structure	Supplier
Choline Chloride	C ₅ H ₁₄ ClNO	139.62		IOLITCE

3.6. HydraFLASH® SOFTWARE

There are several user friendly predictive programs such as CSMHYD, CSMGem and HydraFLASH® that can be used to determine the thermodynamics of hydrate formation, and these have been shown to give accurate phase equilibria data for gas hydrates of simple and multicomponent gas mixtures within about 2 K and 10% in pressure [68]. In this project, the HydraFLASH® software (version 2.2.21) was utilized. This software was originally developed in 1986 and has proven to predict hydrate formation equilibrium points accurately (i.e., temperature and pressure). This can be achieved using different equations of state: (Soave-Redlich-Kwong (SRK), Peng-Robinson (PR) and Valderrama-Patel-Teja (VPT)), cubic plus association equation of state (CPA), and perturbed chain statistical associating fluid theory equation of state (PC-SAFT). In this work, CPA was applied because it consistently good performance in systems having components that can form hydrogen bonds such as water and methanol. The van der Waals and Platteuw model is applied to describe the hydrate phase. The main window of this program is shown in Figure 28.

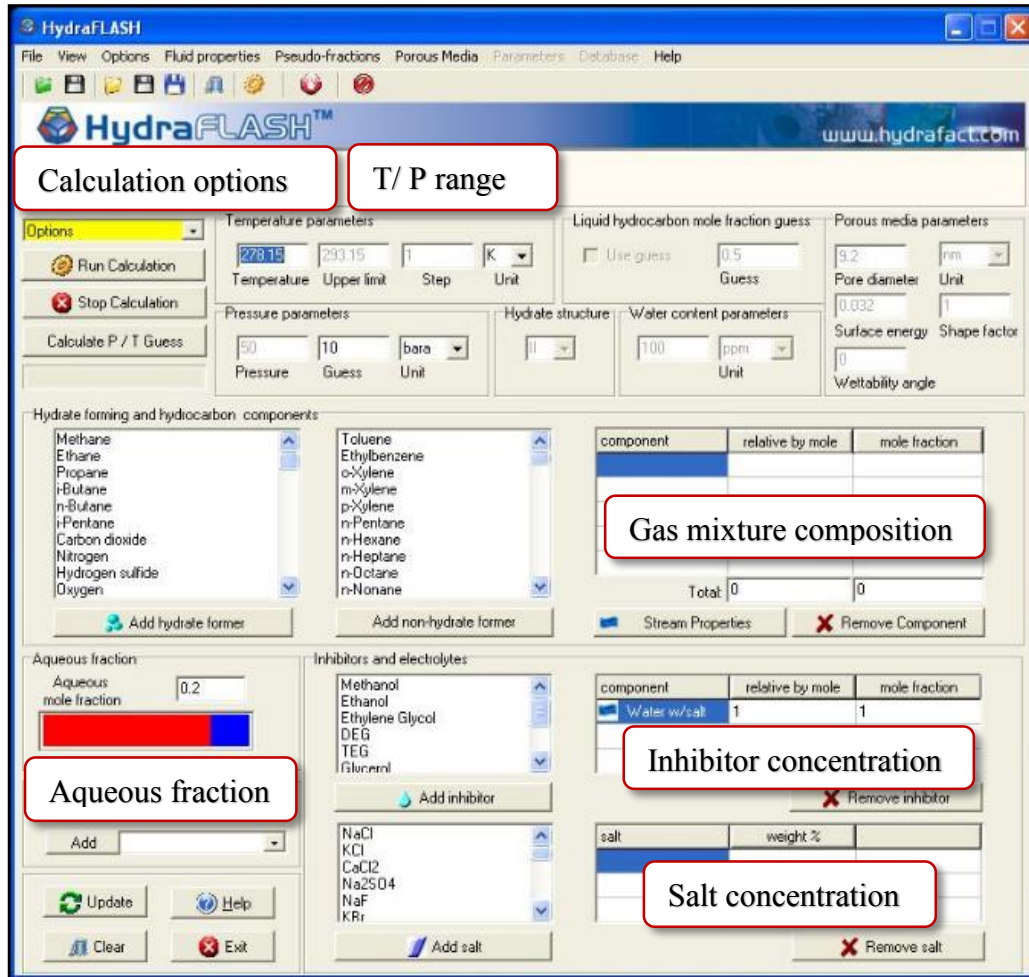


Figure 28: HydraFLASH® software main window expressing the main input for each run.

An example of use of this software in this project is shown in Figure 29, which was prepared for QNG-S1 with aqueous mole fraction of 30% of which 20% methanol (as a classic THIs) and the remaining is water.

Results

File Edit

HydraFLASH® www.hydract.com

Type of calculation: Hydrate line
Hydrate structure: II

Nitrogen	0.024472				
Met.Cyc.Pentane	7.14E-04				
Toluene	6.3E-04				
n-Pentane	0.001029				
n-Octane	0.001064				
Methanol	0.06				
WATER	0.24				
No salts chosen					
Temperature (K):	Pressure (bara):	Vapour/ LHC fraction:	Polar liquid fraction:	Liquid HC fraction:	Hydrate structure:
278.15	148.599	0.697349	0.302651	-	II
279.15	191.84	0.697098	0.302902	-	II
280.15	239.101	0.696884	0.303116	-	II
281.15	290.236	0.696694	0.303306	-	II
282.15	345.317	0.696519	0.303481	-	II
283.15	404.436	0.696357	0.303643	-	II
284.15	467.555	0.696205	0.303795	-	II

Figure 29: Numerical result window for hydrate dissociation of QNG-S1 with 20% methanol inhibitor.

HydraFLASH's results can be presented numerically, graphically or exported into an Excel sheet. A screenshot of the graphical output is illustrated in Figure 30.

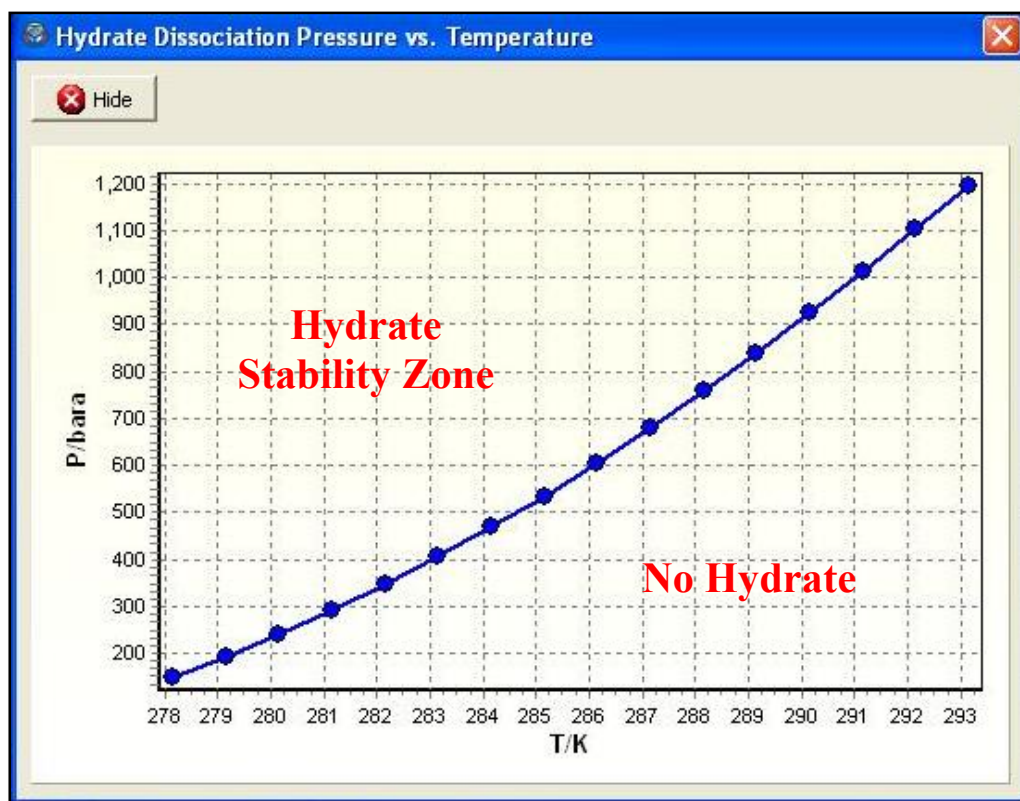


Figure 30: Graphical representation for hydrate dissociation curve using QNG-S1 mixture with 20% methanol inhibitor of the aqueous mole fraction.

3.7. EXPERIMENTAL PROCEDURE

In general, the same procedure for preparing the chemicals and filling the test cells was followed in all high pressure equipment; however, there are some minor difference from the technical point of view for each equipment that was used. This section discusses the main steps implemented in this project, which are chemical preparation, leaking test, and apparatus calibration with CH_4 , and CO_2 before starting the experimenting with QNG-S1.

In addition, it shows details of how to use the three different high pressure cells. A general schematic diagram of this experiment set-up is shown in Figure 31.

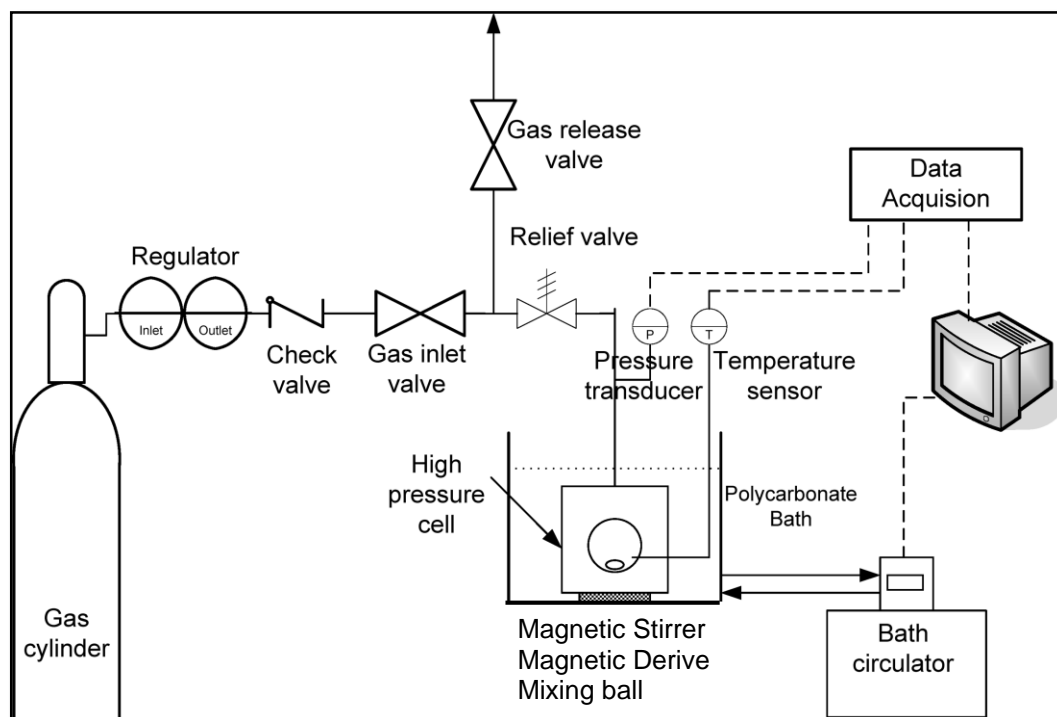


Figure 31: A general schematic diagram of the whole experiment set-up [69]. Reprinted with permission from “Hydrate Equilibrium Data of the CH₄ + C₃H₈ Gas Mixture and Simulated Natural Gas in the Presence of 2,2-Dimethylbutane and Methylcyclohexane ” by Yutaek Seo, Seong-Pil Kang, Jonghyub Lee, Jiwoong Seol and Huen Lee, 2011. Journal of Chemical and Engineering Data, 56, 2316-2321, Copyright [2011] by American Chemical Society.

3.7.1. Preparation of chemicals

The inhibitors to be evaluated were dissolved in ultrapure water before starting the test up to the target concentrations choline chloride shown in Table 11.

Table 11: Inhibitor fraction on mass bases of aqueous phase.

Inhibitor name	Case 1	Case 2
Choline chloride in aqueous phase/ mass %	1	5

3.7.2. Leak test

One of the major problems that high-pressure laboratory work includes is the gas leak. Therefore, a leak test is the first step to start working with any high-pressure cell. Water free leak test main steps are:

1. Set water bath “thermostat” at 24 °C.
2. Run the bath for three hours and ensure that the temperature profile is stable.
3. Charge the used CO₂ at 86 bar or any other available gases and close all valves.

At this stage, the observed temperature increases slightly.

4. Record temperature/pressure equilibrium for 12 hours. If there is a leak, pressure drop will be observed; otherwise, all readings should remain stable.

Examples of the expected relation between temperature/pressure vs. time are shown in Figures 32 and 33 respectively. These graphs show no pressure drop after the temperature was equilibrated, which equilibrate earlier than pressure due to the fact that pressure react slower to fluctuations than temperature. These graphs state clearly means that there is no leak in this experimental set-up.

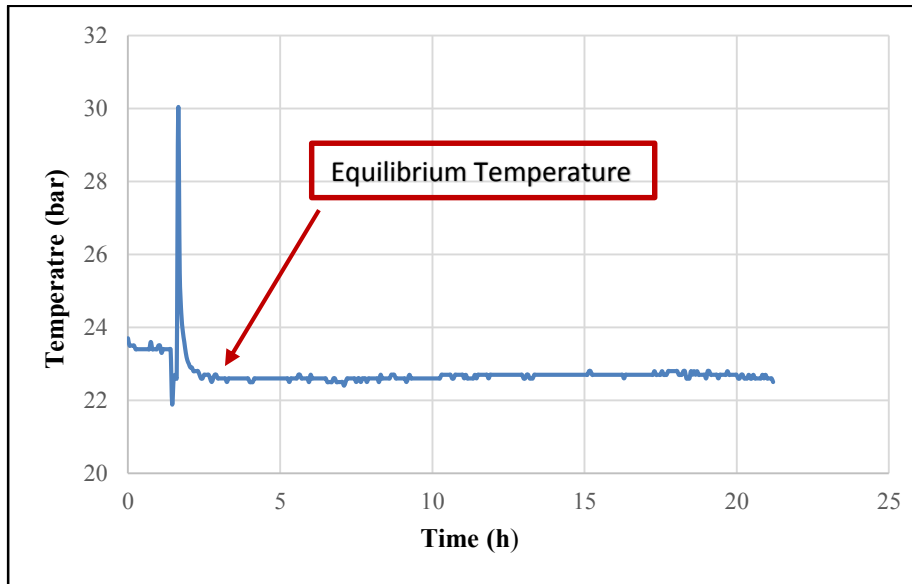


Figure 32: Temperature vs. time for leak test via micro bench top reactor.

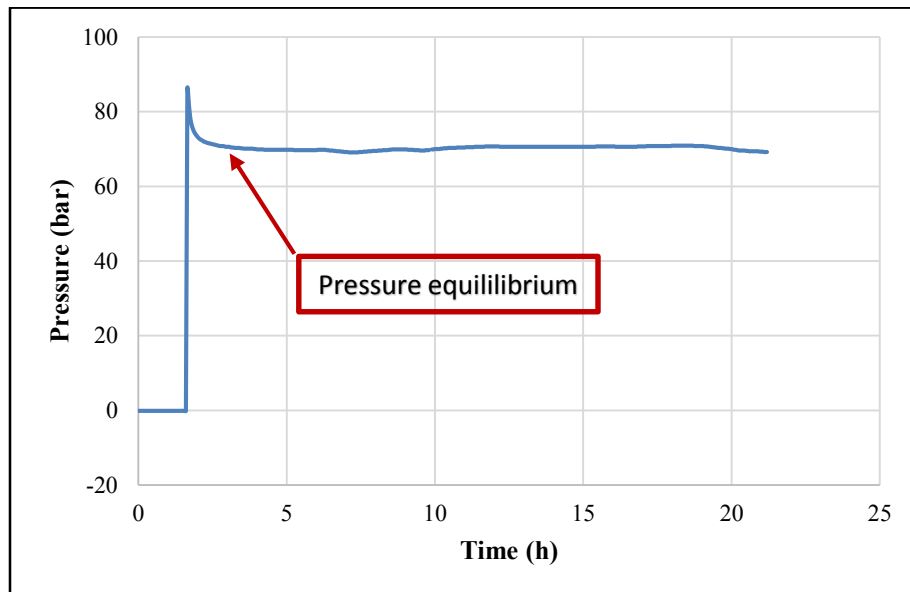


Figure 33: Pressure vs. time for leak test via micro bench top reactor.

3.7.3. Calibration of the equipment

Calibration was performed for micro bench top reactor while the other two apparatus (i.e., RC-5 and Autoclave cell) were pre-calibrated by the manufactures. Pure methane and carbon dioxide were used to achieve this purpose. Micro reactor calibration was performed using the same method applied for the main target, QNG-S1, which is explained below.

3.7.4. Apparatus usage mechanism

The semi-batch reactor, RC-5, and autoclave differ mainly in 1) opening, closing, and fixing the vessel, 2) creating agitation for a realistic simulation of fluid flow, similar to that in pipeline, 3) data acquisition software. These are minor operability differences, yet, the method for each of the used devices is explained separately.

3.7.5. Micro bench top reactor

The first was to calibrate the temperature and pressure sensors. They were standardized by comparing their readings with pre-calibrated sensors in an open system. Temperature sensor is manufactured by Minco Inc. brand 4 wire PRT which shows values as good as 0.05 K level, this was used to calibrate the thermometer in Parr. Pressure sensor is Paroscientific brand and valid for maximum 10000 psi with accuracy of 0.05 in full scale and it is calibrated against dead weight gauge in Houston in 2011. The obtained data were

drawn and correlated as shown in Figures 34 and 35. This correlation was applied to all experimental results obtained in this isochoric reactor according to the following relations:

$$\text{Corrected temperature (}^{\circ}\text{C)}: T_C = 0.9923T_m - 1.143 \quad [1]$$

$$\text{Corrected pressure (bar)}: P_C = 1.0002P_m + 1.5937 \quad [2]$$

Where;

T_C : corrected temperature

T_m : measured temperature, obtained using Parr thermocouple

P_C : corrected pressure

P_m : measured pressure, obtained using Parr sensor

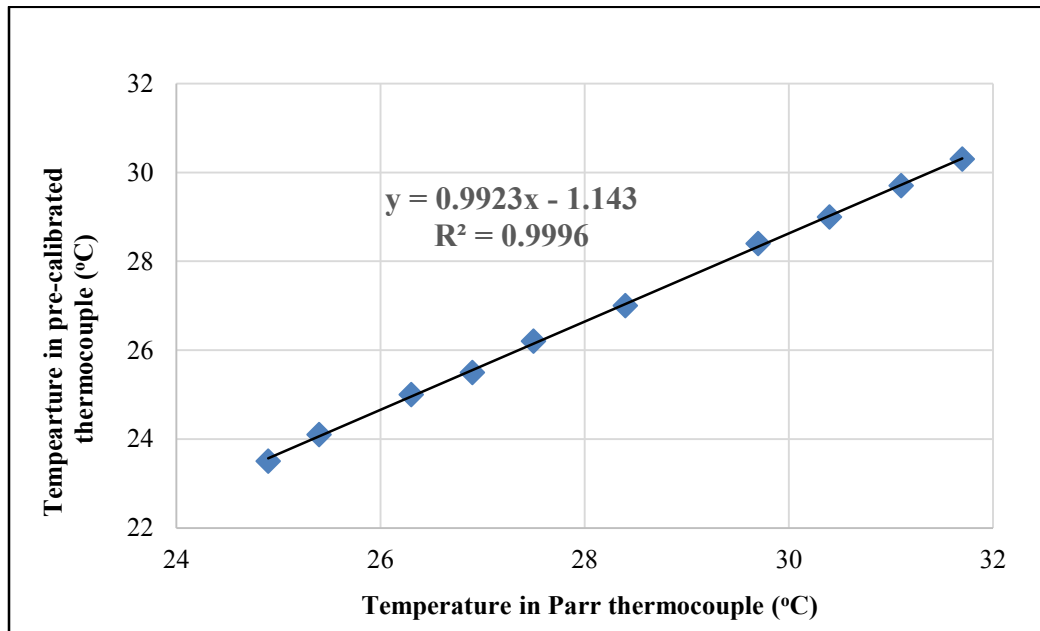


Figure 34: The relation between Parr thermocouple and pre-calibrated thermocouple wire for calibration purpose.

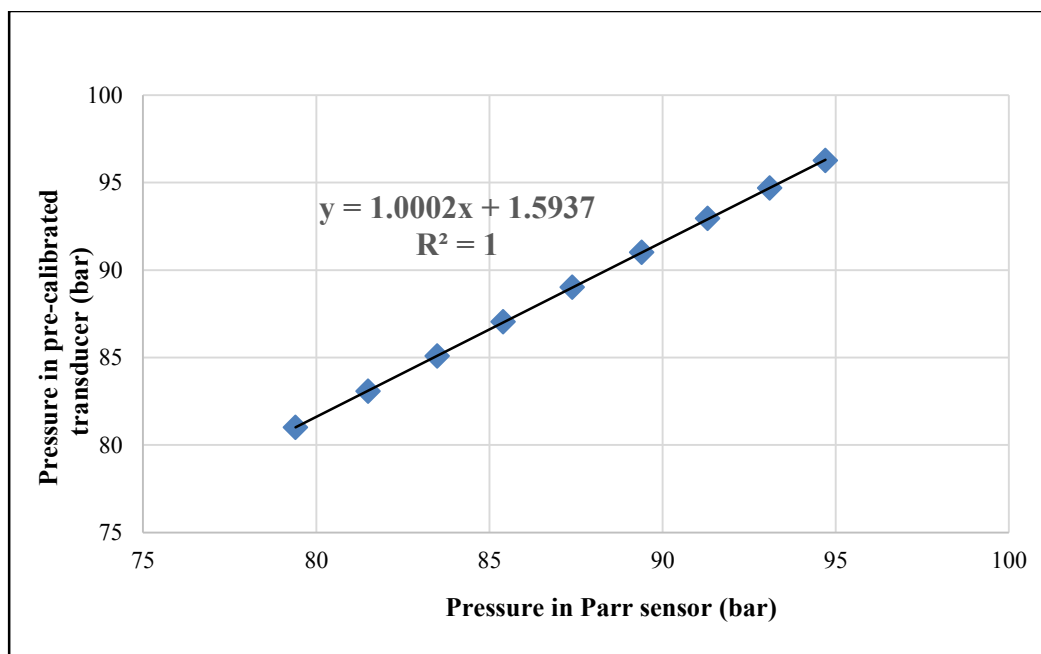


Figure 35: The relation between Parr pressure sensor and pre-calibrated transducer for calibration purpose.

The experiment was started by loading the cell with 30 ml of ultrapure water; then it was pressurized with CH₄, CO₂ or QNG-S1 to the target pressure, for each set of experiments, according to the following routine:

1. The removable vessel was removed from the support stand and the gas release valve was opened to discharge any internal pressure before opening or closing the cell.
2. The magnet housing of the vessel was washed carefully several times from inside with distilled water and filled with the aqueous solution enclosing the chemical to be studied (i.e., ultrapure water and inhibitors). Then the magnet housing was closed and sealed properly by mounting the head fittings and fixing the six cap

screws and the O-Ring closure. Thereafter, the whole cell was attached to the support stand again.

3. The vessel with its aqueous content was flushed to remove any gas impurities. This process was achieved via two stages:
 - a. The vessel was vacuumed by a rough vacuum pump for 4 hours to depressurize thy system up to zero bar.
 - b. The vessel was purged with the gas that attempted to be used for three to four times to confirm that the vessel contained no impurities.
4. The vessel was charged with the tested natural gas, and in order to reach the desired/started pressure (outside hydrate formation region) the boosting process was applied using the booster with its control panel. The booster is used whenever the supplied pressure is less than operational pressure. Then, the hydrate cell was left for an hour with agitation to saturate and stabilize (i.e., reach its temperature and pressure equilibrium condition).
5. The experimental control software (Parr 4848 controller) was launched, logging, and recording the data for temperature, pressure, and time. The software's main window is shown in Figure 36. The data were saved in a CSV format file which can be exported into an Excel file.

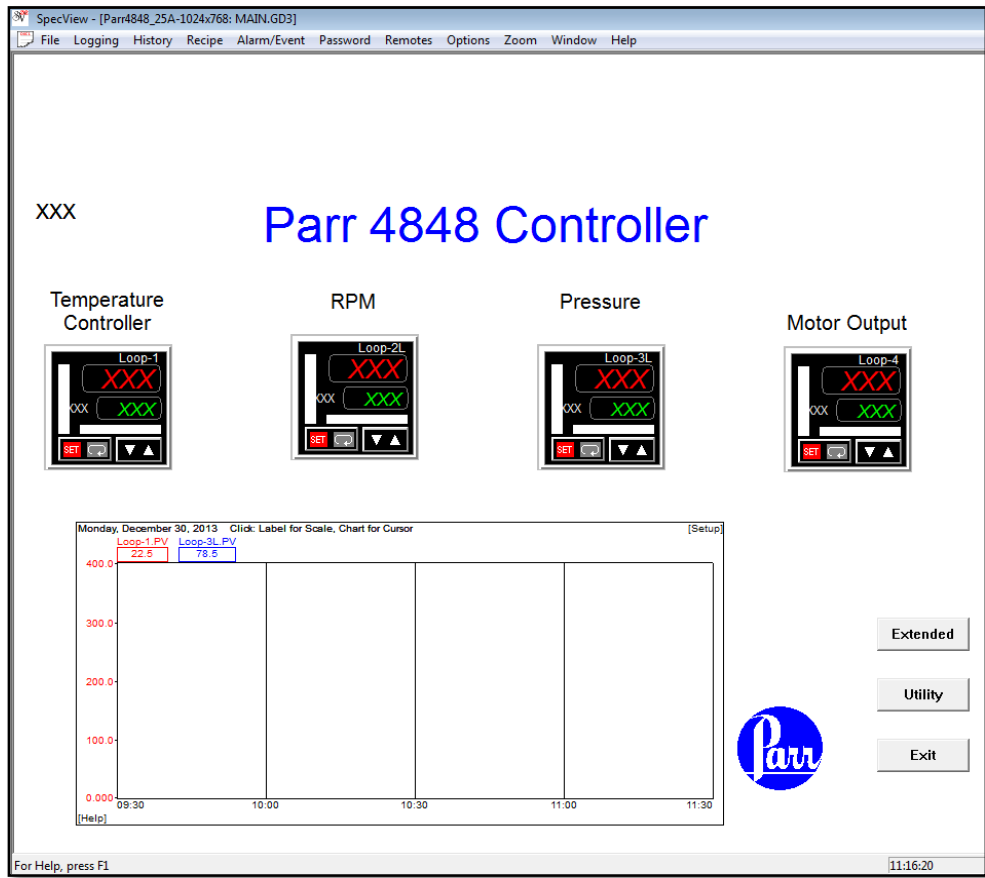


Figure 36: SpecView – [Parr 4848] software main window.

6. Fluid inside the vessel was cooled rapidly at a rate of $2\text{ }^{\circ}\text{C/h}$ from room temperature to $2\text{ }^{\circ}\text{C}$ with agitation. Then, the system was left overnight at this temperature to form hydrate. By the time hydrate was formed, the stirrer was stopped as the hydrated plugged the whole cell.
7. After hydrate was formed, a heating process was started back to the initial temperature with a tremendously slow rate ($0.05\text{ }^{\circ}\text{C/h}$) for complete hydrate melting.

8. Step 7 was repeated several times for the same fluid until a complete loop was obtained. This repeatability of the process was required because the water bath could be ramped for 50 hours maximum.

3.7.5.1. High pressure autoclave cell

The operation of the high pressure autoclave began by loading 30% of the cell volume (450 ml) with ultrapure water (135 ml), then pressuring it directly with the tested gas QNG-S1 to the target pressure, as desired by each set of the experiments, according to the following steps:

1. Autoclave lid and all mounted head connections such as borescope-camera, temperature/pressure sensors, and inlet/outlet gas valves were detached from the vessel after discharging any internal pressure via opening the gas release valve.
2. The magnet housing of the autoclave was washed carefully several times from inside with distilled water and filled with the aqueous solution enclosing the chemical to be studied (i.e., ultrapure water and inhibitors). Lid thread was also cleaned from foreign particles and well-greased with the lubricant. Then the magnet housing was sealed properly by mounting the head connections and carefully closing the lid by hand.

3. The aqueous content within the vessel was flushed twice by purging it with the tested gas up to the full bottle pressure (68 bar) to ensure that the vessel did not have any gas impurities.
4. The vessel was charged with the tested sample of QNG-S1 up to 68 bar (bottle maximum pressure) and, in order to reach the desired/started pressure, the system was connected to a high pressure generator which is a manually operated piston screw pump used to compress the tested gas within a small volume to develop high pressure (i.e., up to 688 bar). Temperature/pressure conditions within the cell were monitored via pressure display of autoclave-software until they were stabilized.
5. Autoclave-software main window was opened to design the whole experiment program Figure 37. The script was edited depending on isothermal cooling method according to the following steps:
 - a. Initialization phase of the experiment was started to adjust autoclave temperature to 20 °C (start temperature) and to make an overall check for experiment cell. This was completed with fast stirring (500 RPM) in order to equilibrate and saturate the liquid/gas mixture.
 - b. The experimental phase of the experiment was then started by cooling the fluid inside the vessel rapidly at a rate of 1.8 °C/h from 20°C to 2°C with agitation (150 RPM). Then, the system was left for two days at this temperature to form hydrate. By the time hydrate was formed, the stirrer was stopped as the hydrate completely plugged the cell. In the autoclave,

it took longer to form hydrate plug, because of its large volume (400 mL) compared to the isochoric reactor (100 mL).

- c. After hydrate was formed, a heating process was started back to the initial temperature with very slow rate (0.01 °C/h) for complete hydrate melting. Furthermore, and an additional isothermal heating step was applied in order to close HLVE loop and heating stage up to 30 °C to destroy any residual hydrate crystal.

Line	Command	Start Time	Duration	Start Temperature	Stop Temperature	Speed	Absolute Pressure Loss			
1	Constant Temperature (Start Time, Duration, Temperature)	00:00:00	01:00:00	20.0 °C						
2	Stirrer (Start Time, Duration, RPM)	00:00:00	01:00:00			500 RPM				
3	Wait for Start Button, then start logging									
4	Ramp (Start Time, Duration, Start Temp., Stop Temp.)	00:00:00	10:00:00	20.0 °C	2.0 °C					
5	Stirrer (Start Time, Duration, RPM)	00:00:00	10:00:00			150 RPM				
6	Photo every (Time interval)	00:30:00								
7	Constant Temperature (Start Time, Duration, Temperature)	10:00:00	48:00:00	2.0 °C						
8	Stirrer (Start Time, Duration, RPM)	10:00:00	166:00:00			150 RPM				
9	Ramp (Start Time, Duration, Start Temp., Stop Temp.)	58:00:00	166:00:00	2.0 °C	20.0 °C					
10	End logging									
11										

First part: Initialization. Will be active as soon as the experiment is started.
 Second part: Experiment. Will be active after the START button was pressed.
 Third part: Completion. Will automatically be entered when the END statement was encountered.
 Please remember that each of these parts does have its own timeline which starts at 00:00:00.

Buttons: Load..., Save As..., Sort & Validate Script, OK, Cancel

Figure 37: A complete program schedule in Hydrate software

The pressure, temperature, and time data can be monitored in Hydrate data acquiring software main window (Figure 38). These data were recorded and saved in a dat format file which can be exported into an Excel file.

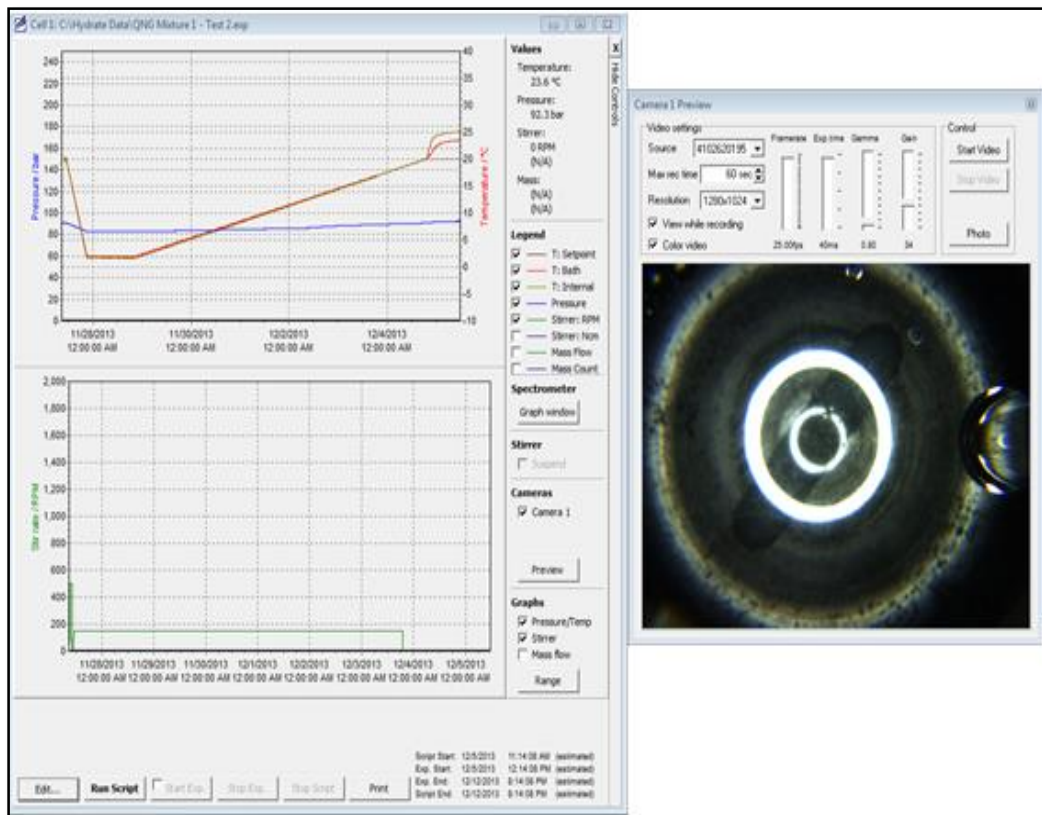


Figure 38: Hydrate software main window and camera preview window.

3.7.5.2. Rocking cell

The rocking rig used in this experiment was delivered by PSL Systemtechnik with two test cells, which can be upgraded later up to five cells. This means that two runs can be

performed simultaneously. However, the only variables possible, for these simultaneous runs, can be the composition of the sample and pressure. The test procedure with this experimental set-up was started by filling each cell (40 mL) with 15 mL of ultrapure water (30% of cell volume), then pressuring it directly with the sample gas QNG-S1 to the target pressure, as desired by each set of the experiments, according to the following approach:

1. The test cell was removed from its platform axis after it was depressurized, and the temperature sensor, and pressure supply tube were disconnected. Then it was mounted on the assembling aid and the screw lid was opened with a jaw wrench as per Figure 39.
2. The ball casing of the test cell and the mixing ball were washed carefully for several times with distilled water and filled with the prepared test mixture (i.e., ultrapure water and inhibitors) according to the experiment requirement. Then, the test cell was sealed properly in the same way it was opened, reinstalled to its corresponding place on the platform axis in RC-5 bath, and reconnected to the temperature sensor and pressure supply.

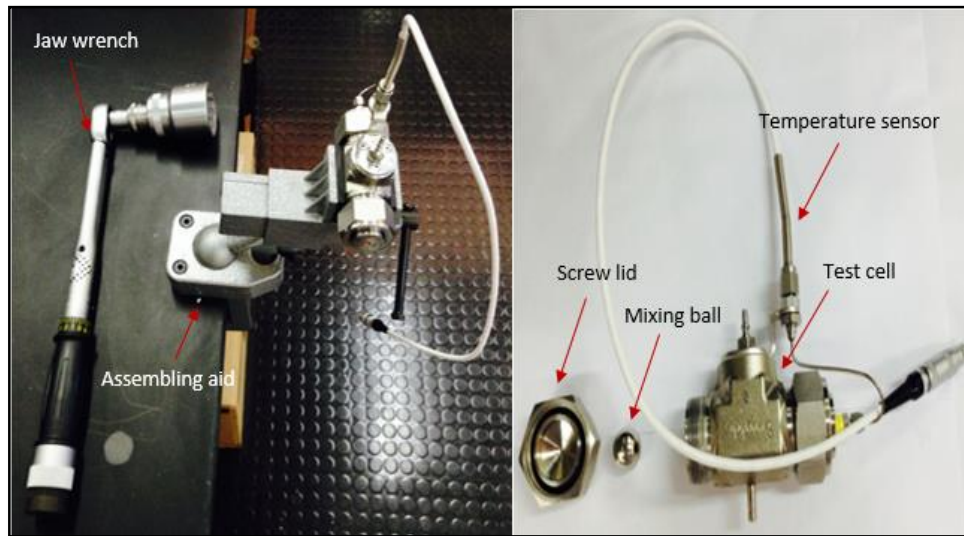


Figure 39: An assembling aid used to loosen and fasten the test cell.

3. Each test cell with its aqueous content was flushed, filled with tested sample of QNG-S1, and pressurized up to the desired/started pressure following the same manner applied in high pressure autoclave vessel (step 3 and step 4).
4. After temperature/pressure conditions within each test cell were stabilized, the RC-5 software was started to design the whole experiment program (Figure 40). The script was edited depending on isothermal cooling method following the same initialization and experimental phases applied in the autoclave except for the hold time required to form hydrate plug and the way of creating turbulence and agitation. The liquid vapor mixture within each cell was left for 24 hour at 2 °C after it was cooled from 20 °C, which was half the time required for the same mixture within autoclave. This is because its volume (40 mL) is small compared to autoclave (450 mL). In addition, the mixing ball was programmed according to the following parameters: 1) rocking rate: 10 rocks/min, and 2) rocking angle: 30°.

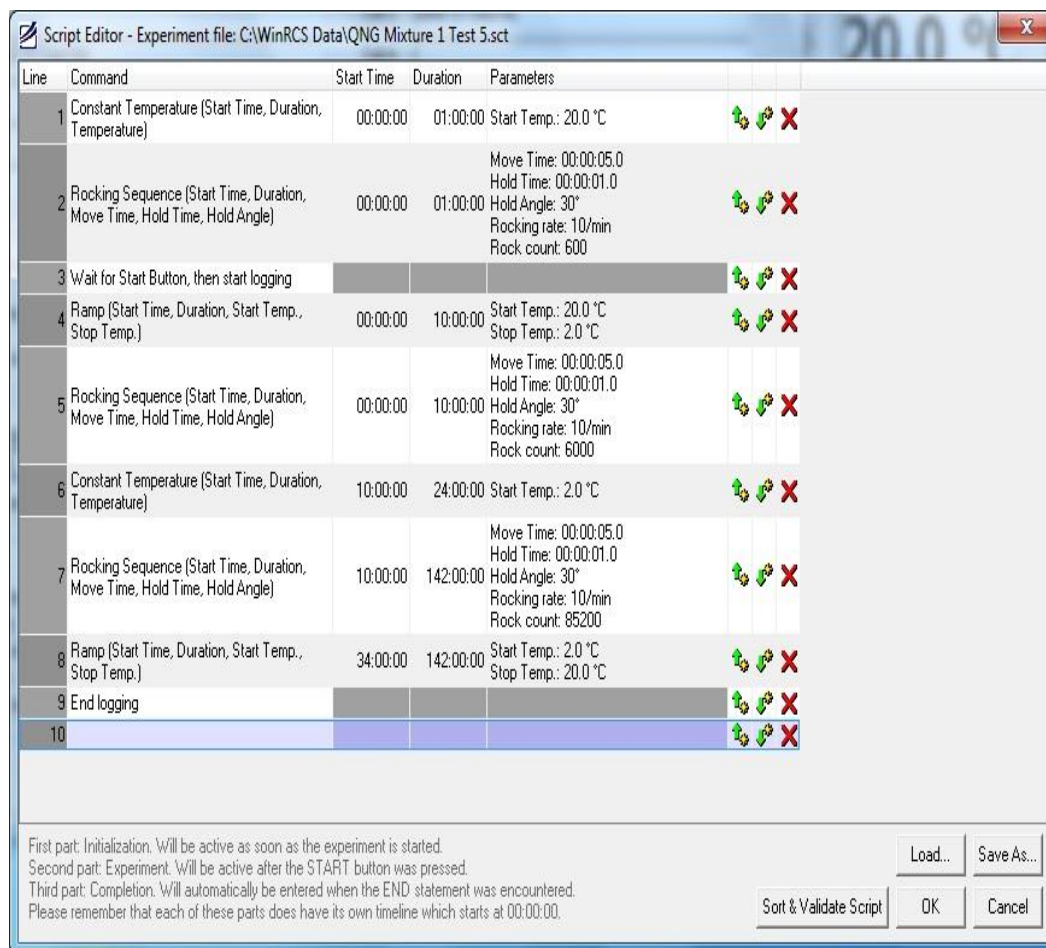


Figure 40: A complete program schedule in RC-5 software

The pressure, temperature, and time data can be monitored in the RC-5 main window (Figure 41). These data were recorded and saved in a dat format file which can be easily exported into an Excel file.

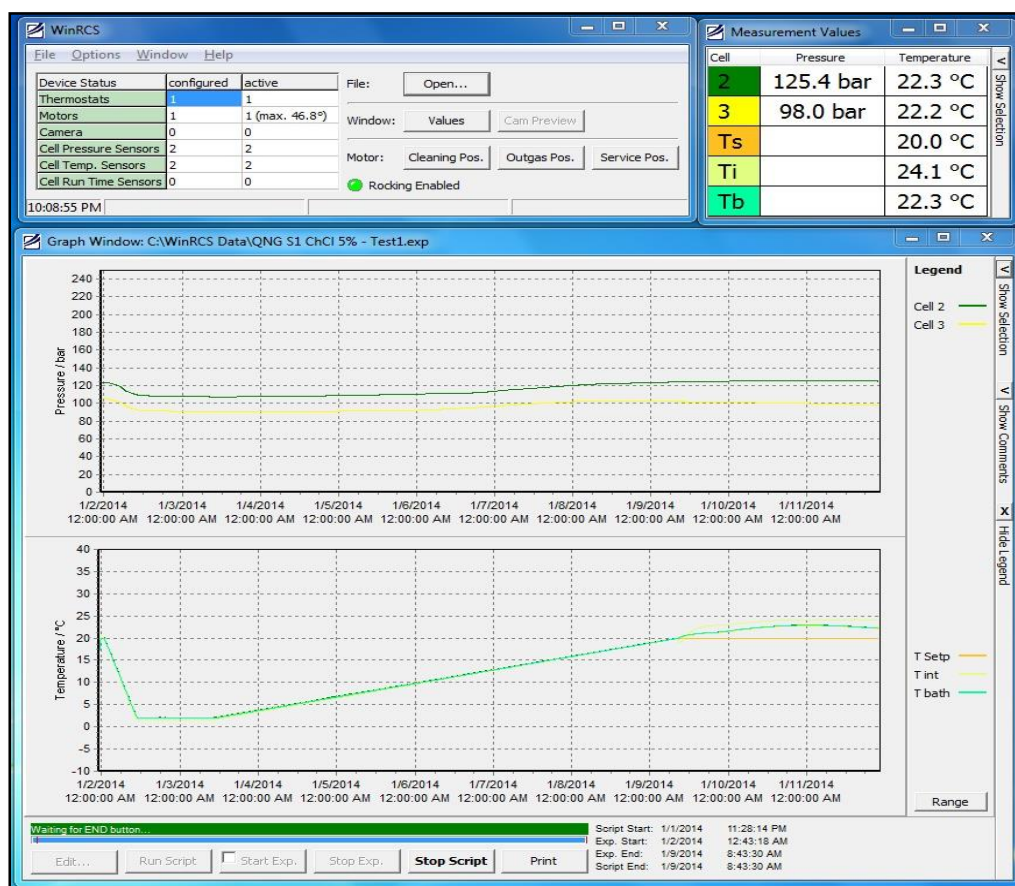


Figure 41: RC-5 software main window showing measurements values and graphical representation for monitoring propose.

The main parameters applied in the isochoric reactor, autoclave, and rocking cell experiments in order to find the hydrate equilibrium curve, are summarized in Table 12.

Table 12: The set conditions used in the three different devices utilized in this project

Parameter	Micro bench top reactor	High pressure autoclave	Rocking cell
Aqueous Sample volume (mL)	30	135	15
Agitation source	Magnetic derive	Magnetic stirrer	Mixing ball
Cooling rate (°C/h)	2	1.8	1.8
Heating rate (°C/h)	0.05	0.1	0.1
Tested samples	CH ₄ , CO ₂ and QNG-S1	QNG-S1 with C ₅ H ₁₄ CINO	QNG-S1 with C ₅ H ₁₄ CINO

4. RESULTS AND DISCUSSION

Preliminary studies on hydrate equilibrium curve measurements started at Qatar University's Chemical Engineering laboratory in late 2011. A basic hydrate equilibrium cell was commissioned along with its pressure and temperature monitoring/control systems. The initial work on this thesis started in late 2012 with the intention of micro bench top reactor, which is a reaction cell, redesigned to become a hydrate cell. It was calibrated using pure methane and carbon dioxide to verify its performance and efficiency before it was used for measuring plain QNG-S1 hydrate equilibrium points. In the calibration phase, some deviation in HLVE point (around 2 °C) for the hydrate equilibrium cell was observed because of its poor heat transfer characteristics. However, the initial experiments with the micro bench top reactor helped in understanding the hydrate making process, sub-cooling effect, memory effect, induction time requirement, and dehydration temperature ramping effect, as well as the last isothermal step followed by heating stage up to 30 °C at the dissociation side. In a sense, the initial hydrate micro bench top reactor that was constructed and commissioned served for training purposes. Later on, the measurements were started using commercial hydrate cells: autoclave, and rocking cell.

This section presents the experimental results using three different experimental set-ups at different temperature/pressure conditions. This study was performed to determine QNG-S1 hydrate equilibrium points using the micro bench top reactor and the autoclave.

In addition, the rocking cell was used to study the effect of injecting ionic liquid inhibitors on hydrate equilibrium points, induction time, and memory effect.

4.1. METHOD TO OBTAIN THERMODYNAMIC (HLVE) POINTS

Thermodynamic HLVE data for gas hydrate is usually obtained using the isochoric/high pressure method. In this method, 30% of the vessel volume is loaded with the aqueous phase (water with or without inhibitors) as required by each set of experiments. Thereafter, the cell is pressurized with the tested gas sample to the desired pressure, below the expected hydrate forming region, and left with agitation for an hour to saturate and equilibrate. As the temperature and pressure of the system stabilize, the gas/ liquid mixture is cooled rapidly (2 °C/h) to a temperature just above pure water freezing point to ensure hydrate formation. This mixture should be kept at that temperature for sufficient time (24 hour) to allow system equilibration and hydrate agglomeration. Hydrate formation in the vessel can be detected by a sharp pressure drop and/or confirmed by visual observation when the cell is equipped with a boroscope-camera. The temperature should then be increased in very small steps of around (0.1 °C/h). A P-T diagram is obtained for each experimental run as shown in Figure 42, from which the equilibrium point can be obtained.

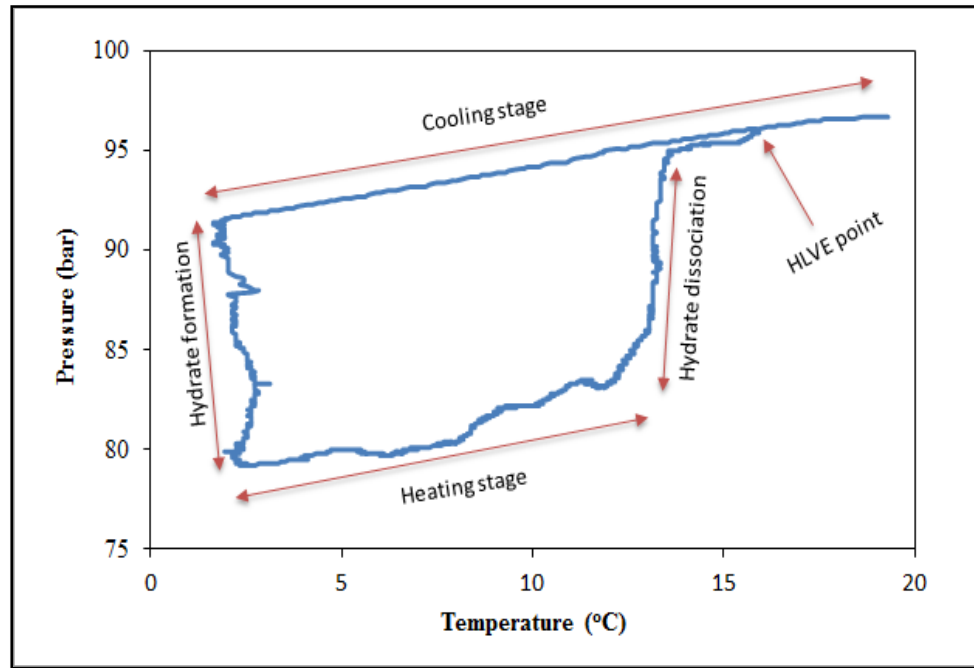


Figure 42: Typical experimental hydrate liquid vapor equilibrium curve

Obtaining hydrate equilibrium points is the most critical concern in thermodynamic study as it should be selected carefully from hundreds of points. Typically, studying hydrate thermodynamic behavior means finding hydrate equilibrium points rather than developing a complete HLVE loop as per Figure 43.

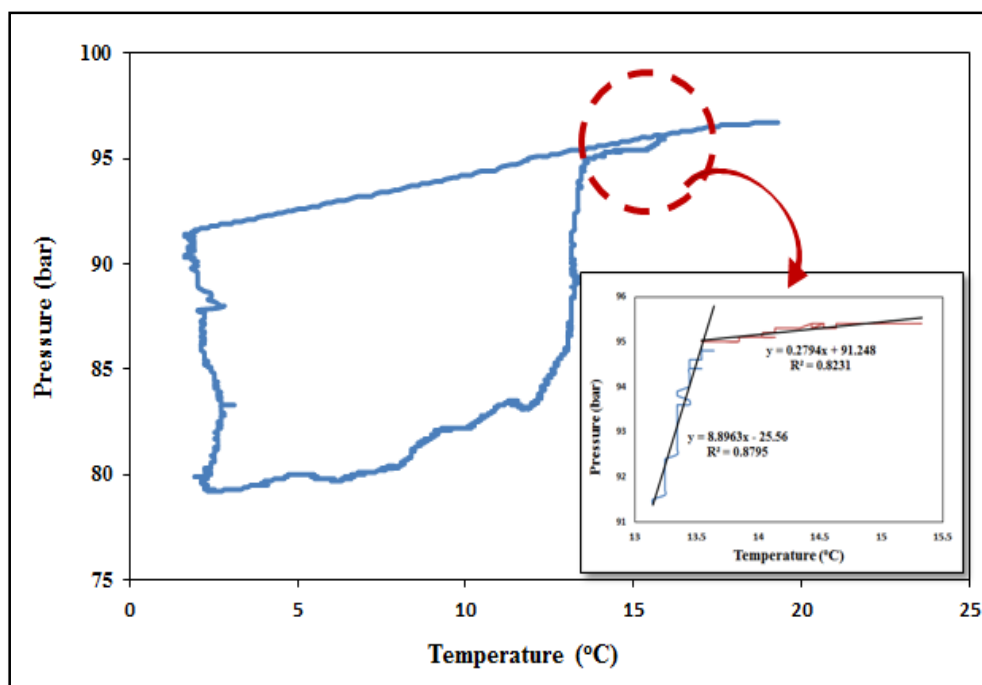


Figure 43: A complete hydrate formation/dissociation loop zooming in the region where hydrate equilibrium point is found.

These points can be obtained through zooming in the shaded region, splitting them into two segment lines and trying to fit them into two different trend-lines with linear regression almost equal to 1. Then, by solving their algebraic equations simultaneously, the first hydrate equilibrium point is obtained. The same procedure is repeated for all loops belonging to the same gas mixture composition and experimental set-up, obtained at different starting pressure, to build a complete hydrate equilibrium curve, represented by the red line in Figure 44.

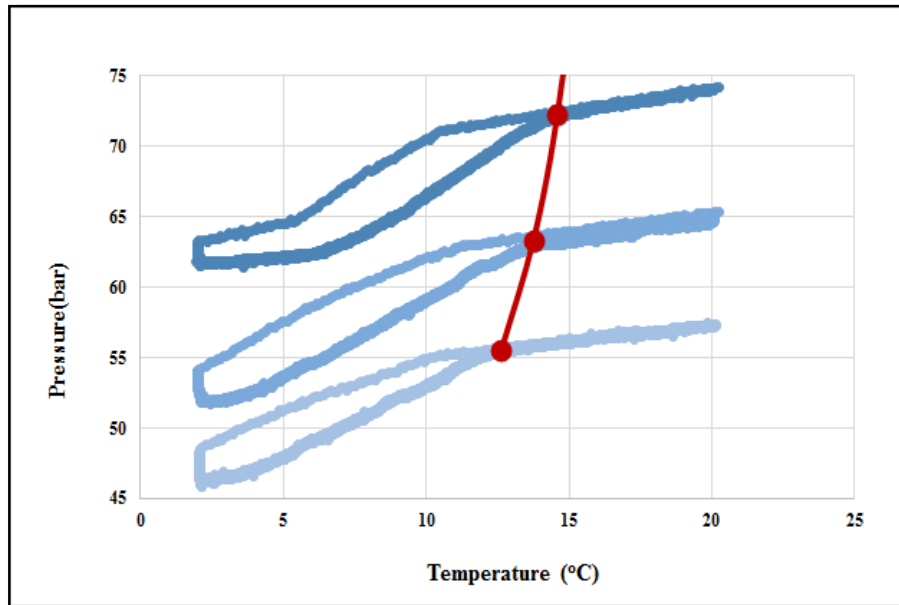


Figure 44: Red line shows a complete hydrate equilibrium curve for the three hydrate formation/dissociation loops of gas mixture composition and experimental set-up.

4.2. METHOD TO OBTAIN KINETIC INDUCTION TIME

Induction time is one of the vital parameters used to characterize hydrate formation, because a longer induction time allows transport of the fluids through pipelines without hydrate crystallization. It can be defined as the time between the complete dissolution and the initiation of hydrate formation [70]. The induction time can be obtained from pressure-time relationship for a hydrate forming system as shown in Figure 45. Usually, this measurements should be repeated several times to get the most accurate data.

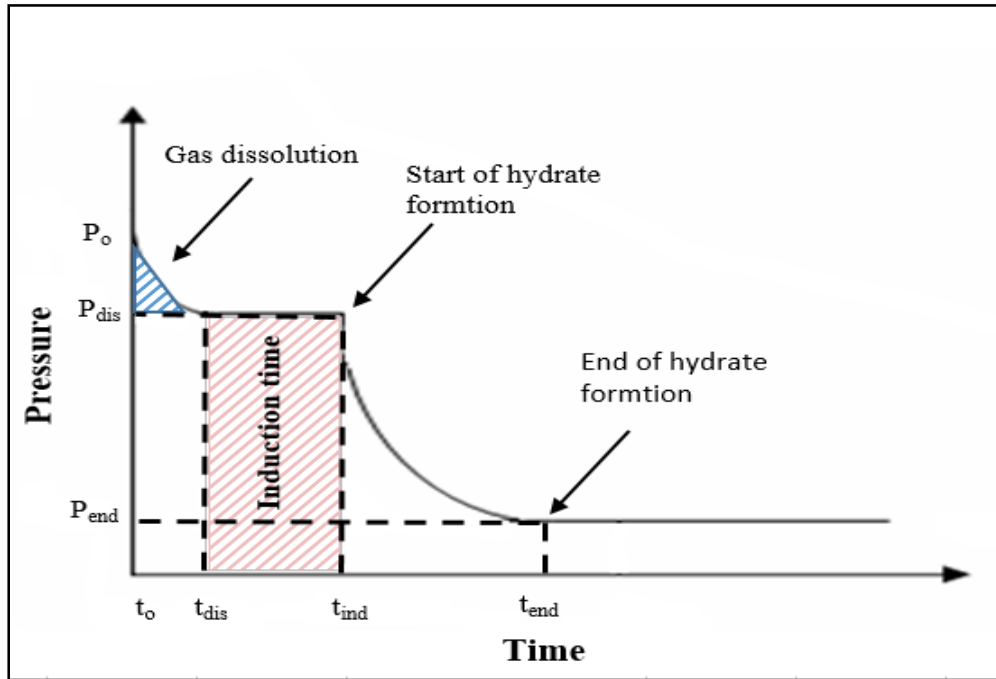


Figure 45: Schematic representation of the pressure changes with time during a typical kinetics hydrate formation.

In Figure 45, the dissolution of gas in the aqueous phase is represented by a little pressure drop between P_0 to P_{dis} . This, followed by steady-state condition where the pressure is stabilized till t_{ind} at which a sharp pressure drop, is obtained due to the beginning of hydrate formation. The pressure keeps falling due to gas consumption till P_{end} where no more hydrate forms [70].

In this work, induction time was measured as the difference between the time at which HLVE-temperature occurs, and the time at which catastrophic pressure drop occurs in a pressure-time diagram, as illustrated in Figure 46. Induction time measurements will be

presented for the data obtained using RC-5 to show the effect of varying experimental conditions and inhibitions.

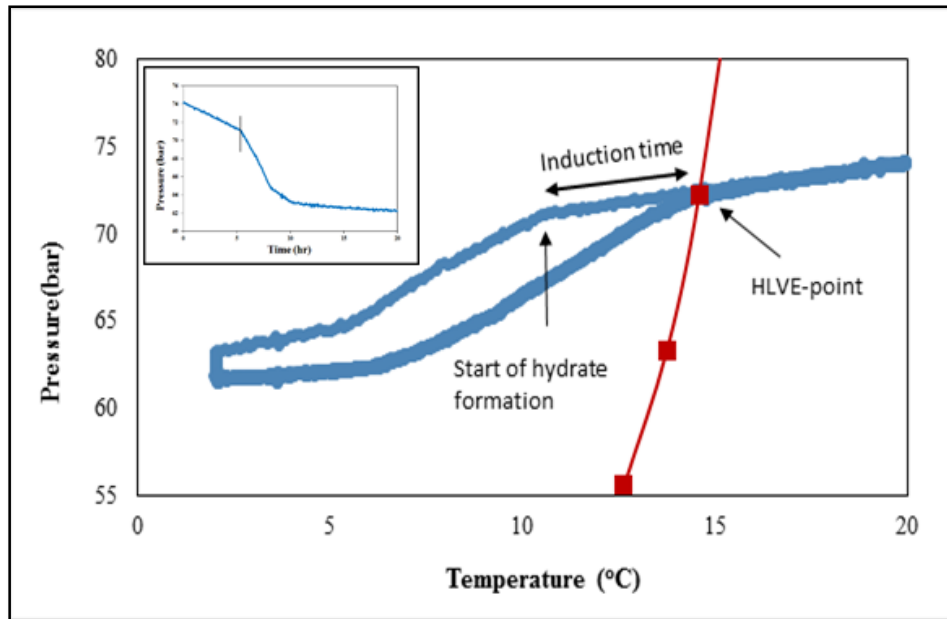


Figure 46: Pressure-temperature and pressure-time in the upper left corner used to obtain induction time.

4.3. MICRO BENCH TOP REACTOR

The first goal of this study was to calibrate the micro bench top reactor using gases with known HLVE data to check its performance. In this work, calibration was performed using pure methane and carbon dioxide. Then, QNG-S1 was tested and its HLVE data were obtained.

4.3.1. Methane

The accuracy of the HLVE points obtained using the micro reactor as described previously was verified by comparing them with published experimental data and model prediction. The results (Table 13) show a good agreement with Sloan's experimental data and the gas gravity method's (SG method) result as presented in in Figure 47 [5]. The gas gravity method is developed by Katz and it is widely used to predict hydrate equilibrium conditions [5]. Moreover, the equilibrium points recorded by this experimental work were compared with those obtained using HydraFLASH® software. There is a deviation of less than 2 °C between the obtain HLVE points and those from these three different sources. However, this deviation falls within the range of the expected system accuracy. Additionally, HydraFLASH® predicts that the type of hydrate structure formed is cubic structure (sI).

Table 13: Measured hydrate liquid vapor equilibrium points for pure methane using micro bench top reactor.

Experiment No.	Initial Pressure at 20°C (bar)	HLVE-Temperature (°C)	HLVE-Pressure (bar)
I.1	115.82	15.74	113.48
I.2	107.31	15.21	105.34
I.3	96.71	13.56	95.04

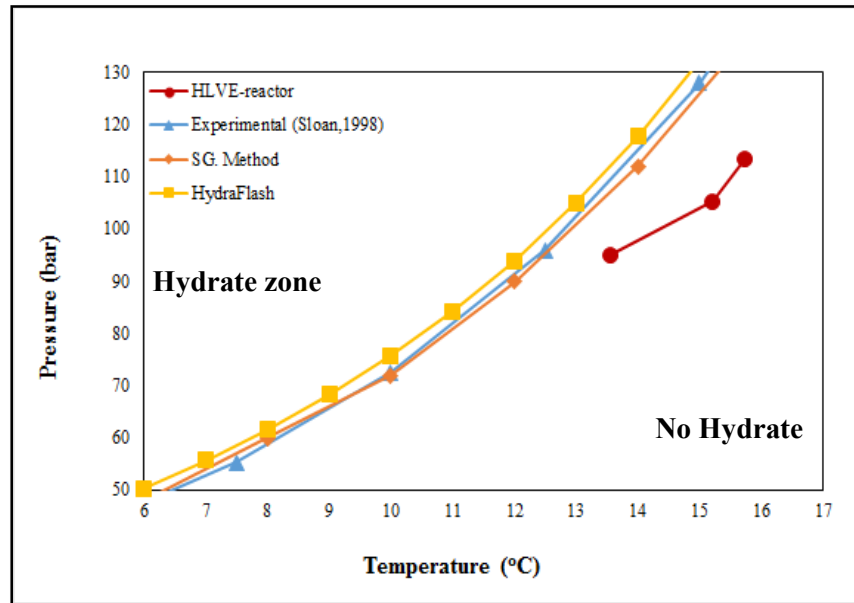


Figure 47: HLVE curve for pure CH₄ using Micro reactor compared with those obtained by Sloan (1998), gas gravity method and HydraFLASH®.

4.3.2. Carbon dioxide

Carbon dioxide was used as a second calibration step to validate the micro bench top reactor performance by repeating the experimental procedure used for methane. The measurement's accuracy was again detected by comparing the obtained data with those published by Sloan and calculated by K-factor method within the same temperature/pressure range [5]. Carbon dioxide data were compared with those obtained using K-factor method rather than gas gravity method because the latter cannot be used for gases with specific gravity greater than 1 (CO₂ specific gravity is 1.5). Carbon dioxide structure (cubic structure sI) and hydrate equilibrium points were calculated using the HydraFLASH® software. In this case, the measured deviation compared with all above

mentioned methods was around 1 °C. The experimental data is listed in Table 14 and plotted in Figure 48.

Table 14: Measured hydrate liquid vapor equilibrium points for pure CO₂ using the micro bench top reactor.

Experiment No.	Initial Pressure at 20°C (bar)	HLVE-Temperature (°C)	HLVE-Pressure (bar)
II.1	41.77	10.23	41.18
II.2	33.96	8.420	30.39

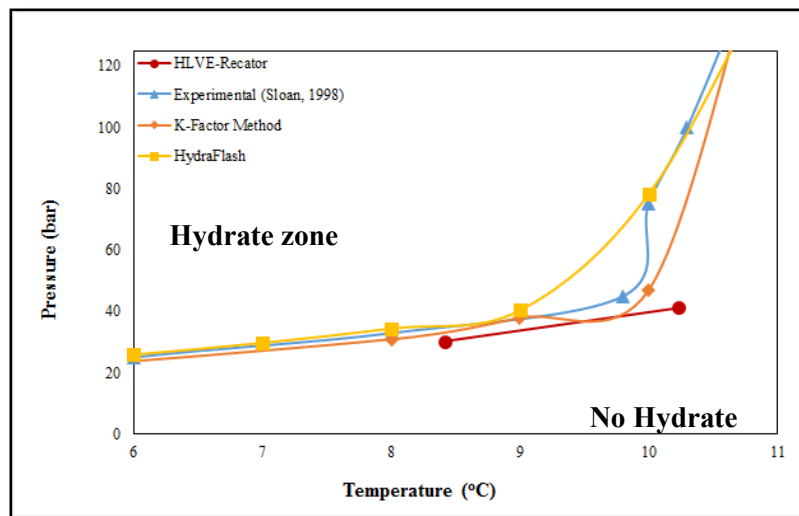


Figure 48: HLVE curve for pure CO₂ using Micro reactor compared with those obtained by Sloan (1998), K-factor method and HydraFLASH®.

4.3.3. Plain QNG-S1

Experiments with Qatar natural gas started after the reactor was calibrated with CH₄ and CO₂. These measurements are a novelty of the current study since QNG-S1 HLVE curves

were obtained for the first time. Accordingly, the obtained figures were compared with the calculated HLVE points using gas gravity method and HydraFLASH® software as presented in Table 15 and Figure 49. The deviation was again within the expected system accuracy (around 2 °C) compared with the theoretical prediction. For this type of natural gas, the hydrate structure, predicted by the software is cubic structure sII. The total uncertainty of these measurements is +/-0.5%.

Table 15: Measured hydrate liquid vapor equilibrium points for plain QNG-S1 system using micro bench top reactor.

Experiment No.	Initial Pressure at 20°C (bar)	HLVE-Temperature (°C)	HLVE-Pressure (bar)
III.1	102.61	21.91	102.55
III.2	93.71	21.08	93.51

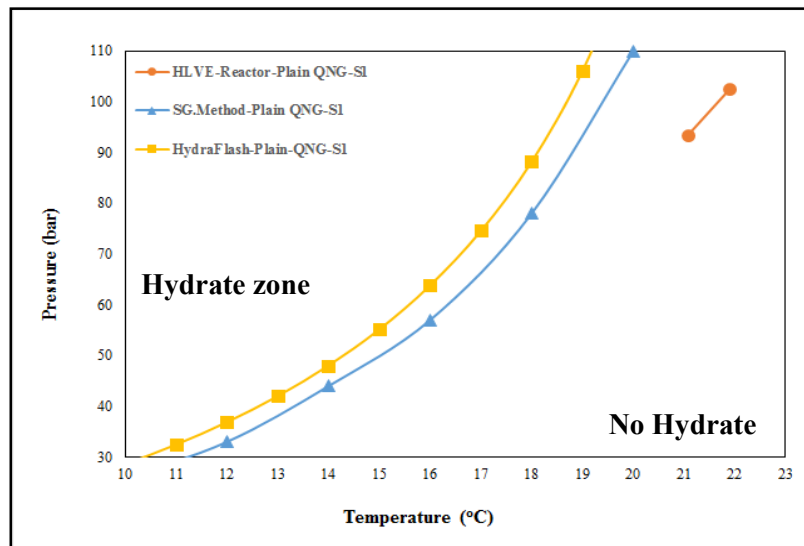


Figure 49: HLVE curve for plain QNG-S1 system using micro reactor compared with those obtained by specific gravity method and HydraFLASH®.

Considering the above mentioned results, micro bench top reactor could be used as a typical hydrate cell once the modifications, mentioned in section 3.2.1, were applied to it. The obtained HLVE curves of CH₄, CO₂ and plain QNG-S1 show a deviation of around 2°C in comparison with past literature and the HydraFLASH® software. Accordingly, this study proves that this reactor can be used as an economical hydrate cell for preliminary studies.

4.4. HIGH PRESSURE AUTOCLAVE

After presenting HLVE points and curves obtained using the modified non hydrate cell (micro bench top reactor), data acquisition using typical hydrate cells started. A high pressure autoclave is one of these typical hydrate cells, which is usually used to visualize the whole hydrate formation/dissociation processes. Figure 50 shows some captured photographs taken with a boroscope-camera.

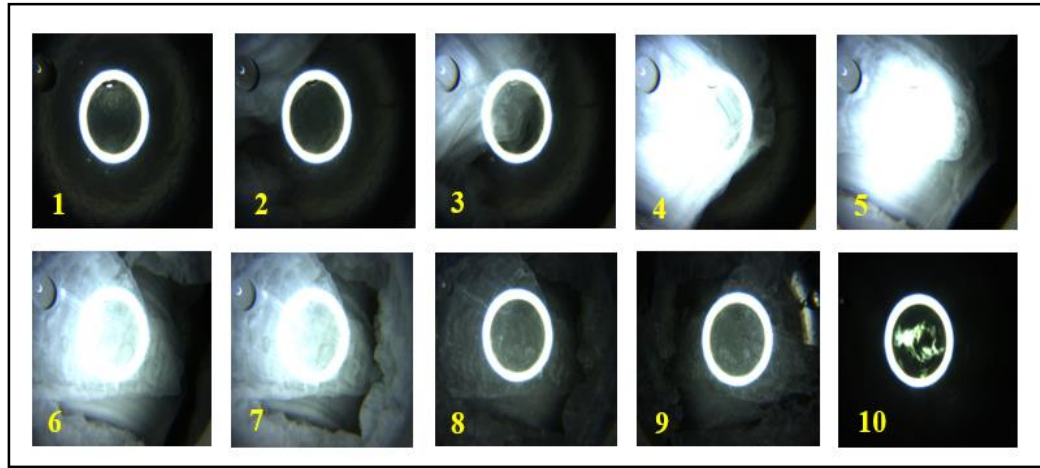


Figure 50: Image of the hydrate formation/dissociation process in high pressure autoclave. Picture 1: start of the experiment; Picture 2 beginning hydrate formation; picture 7: completion of hydrate formation; picture 8: start of hydrate dissociation; and picture 10: end of the experiment.

Since this apparatus was already pre-calibrated by the manufacture company, the measurements were started directly with plain QNG-S1. The obtained HLVE points of structure (sII) were compared with theoretical data and HydraFLASH® software as explained in micro bench top reactor section. The comparison shows very small deviation of less than 1.5 °C. These measurements are tabulated in Table 16 and plotted in Figure 51. The total uncertainty of these measurements is +/-0.3%.

Table 16: Measured HLVE points for plain QNG-S1 system using autoclave.

Experiment No.	Initial Pressure at 20°C (bar)	HLVE-Temperature (°C)	HLVE-Pressure (bar)
IV.1	91.78	20.2	91.00
IV.2	71.10	18.68	70.37
IV.3	58.48	17.61	57.65
IV.4	50.34	16.55	49.39

The high pressure autoclave, as a typical hydrate cell, shows a better performance in acquiring HLVE points compared with the micro bench top reactor as shown in Figure 51. However, the deviation is less than 1 °C, which confirms the accuracy of the measurements obtained using the newly commissioned micro bench top reactor. The main advantage of using autoclave is the possibility to visualize the entire hydrate formation and dissociation processes.

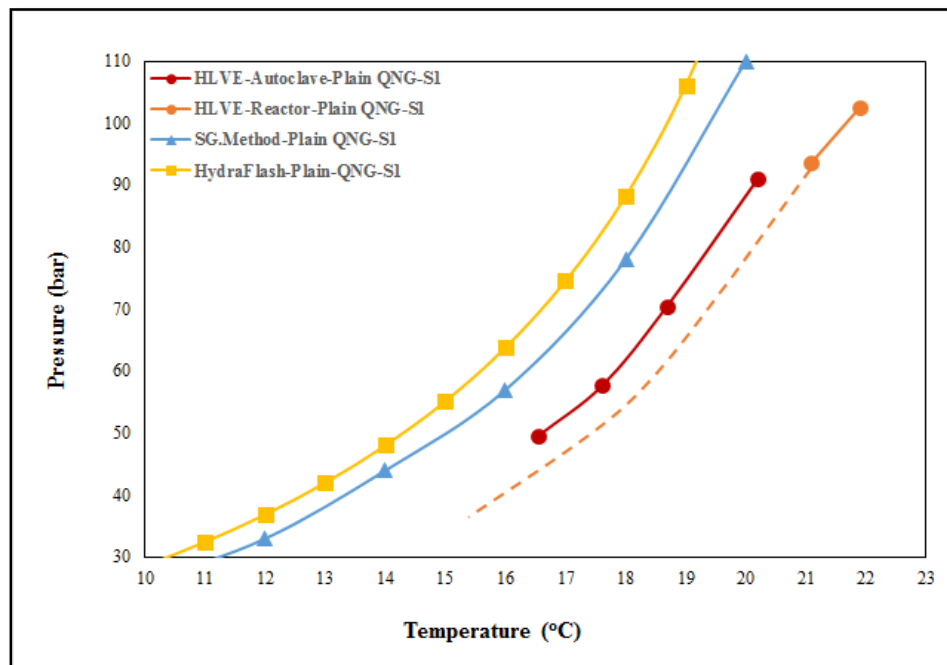


Figure 51: HLVE curve for QNG-S1 system using autoclave compared with those obtained by gas gravity method and HydraFLASH® and the data obtained in micro reactor. The dashed lines present the expected HLVE data for micro bench top reactor.

4.5. ROCKING CELL

Another typical hydrate cell is the rocking cell (RC-5 in this project), which is used to study the effect of ionic liquid inhibitors on QNG-S1 from the thermodynamics and kinetics inhibition points of view. In this section, two types of QNG-S1 mixtures are discussed: Nitrogen Rich Qatar Natural Gas (NR-QNG-S1), and plain QNG-S1.

4.5.1. NR-QNG-S1

Hydrate measurement of NR-QNG-S1 was the first experiment performed using RC-5. This type of mixture is also called low quality natural gas in which nitrogen constitutes almost 50 mol. % of the mixture. The importance of preventing hydrate formation in this type of gas mixture arises from the fact that this mixture has huge impact on environment and human beings, as one of the main byproducts that could be formed during the combustion of nitrogen rich natural gas is nitrogen oxide (NO_x). The emission of this byproduct at high concentrations can be detrimental to the environment.

Specific gravity method is used as “gold standard” to predict NR-QNG-S1 HLVE points due to the absence of experimental equilibrium conditions for this mixture. This was due to time constrain since measuring HLVE points is a very slow process. The performance of HydraFLASH® is highly unpredictable for such a complex mixture and that is why it is neglected in this subsection.

Furthermore, when comparing plain QNG-S1 with NR-QNG-S1 based on SG method, the presence of nitrogen in large amount increases the hydrate risk region as illustrated in Figure 52.

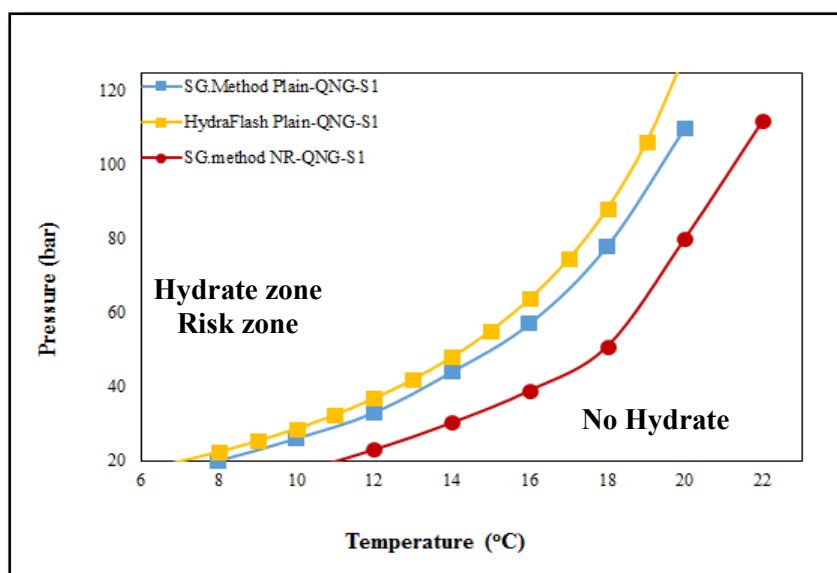


Figure 52: HLVE curves for both plain and nitrogen rich QNG-S1 obtained by SG method and HydraFLASH® for plain QNG-S1.

The hydrate equilibrium curve for NR-QNG-S1 was shifted up to 5.6 °C and up to 5.8 °C using 1 wt. % and 5 wt. % of choline chloride respectively. The inhibition effect depends on the starting pressure in this experiment. Two main concerns arise: firstly, the inhibition effect is decreased at a high pressure; secondly, increasing the mass percentage of the inhibitor has little effect on hydrate formation. This means that increasing the mass percentage of choline chloride by 5 times added less than 1 °C to the inhibition effect when

using 1wt. % of the same type of inhibitor. These data are summarized in Table 17 and Figure 53.

Table 17: Measured HLVE points for NR-QNG-S1 system using rocking cell.

Experiment No.	Initial Pressure at 20°C (bar)	HLVE-Temperature (°C)	HLVE-Pressure (bar)	Inhibitor performance (°C)	Induction Time (h)
NR-QNG-S1 with 1 wt. % ChCl					
V.1	117.76	17.56	116.63	4.80	2.13
V.2	74.12	14.59	72.22	5.00	2.00
V.3	65.29	13.75	63.35	5.30	1.55
V.4	57.21	12.64	55.58	5.60	1.25
NR-QNG-S1 with 5 wt. % ChCl					
V.5	123.76	16.91	121.97	5.20	2.10
V.6	105.35	16.21	103.33	5.30	2.50
V.7	79.41	13.95	77.22	5.80	1.65

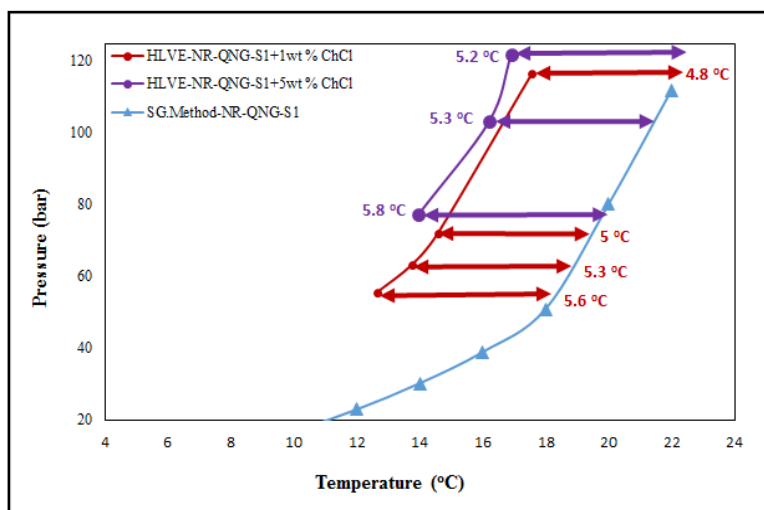


Figure 53: Inhibition effect of 1 wt % and 5 wt% choline chloride on NR-QNG-S1 using RC-5 compared with that obtained using SG method

From the kinetic point of view, the influence of memory-effect phenomenon on the induction time was studied on NR-QNG-S1. This was achieved using the same hydrate test cell (Cell-2) without applying the constant isothermal step and heating stage up to 30 °C in order not to destroy the residual hydrate crystals. In NR-QNG-S1 with 1 wt. % of choline chloride experiments (V.1, V.2, V.3 and V.4), induction time was decreased from 2.13 h in V.1 to 1.25 h in V.4 as illustrated in Table 17. This rapid hydrate growth can be explained due to the presence of tiny hydrate crystals. However, no conclusion can be drawn regarding the effect of ionic liquid inhibition performance on induction time for different concentrations due the above mentioned phenomenon.

4.5.2. Plain QNG-S1

After testing the effect of choline chloride on NR-QNG-S1, the experiments with plain-QNG-S1 started. In these experimental tests, the additional isothermal step and heating stage were applied to eliminate the memory effect by allowing the system to destroy the residual hydrate crystals. By doing so, the effect of using different ionic liquid concentrations on induction time can be examined. Hydrate measurements were performed to study the inhibition performance of ionic liquid with the presence of 1% and 5% on a mass basis. The obtained HLVE data for both concentrations were compared with the result of the HydraFLASH® software and gas gravity method [5]. According to predictions of these methods and comparing them with the experimental results, there was no inhibition effect of choline chloride. There may be two main reasons for this:

1. It might be due to inaccuracy of theoretical calculations via HydraFLASH® and gas gravity method for the complex mixture used to predicting HLVE curves. Moreover, both methods deviate about 5% from the obtained HLVE curve using autoclave.
2. Mixture preparation inaccuracy, mainly because of uncertainties in the manufacturing process as mentioned in Table 8.

However, comparing plain QNG-S1 data obtained using autoclave and micro bench top reactor with those obtained in the presence of choline chloride using RC-5 show an inhibition effect as presented in Figure 54. The inhibition effect obtained using 1 wt. % of choline chloride was 0.7 – 1.1 °C and 1.5 – 1.8 °C compared with autoclave and micro bench top reactor respectively. Choline chloride inhibition performance was even better with 5 wt. % as it was able to shift HLVE curve up to 2.0 °C for autoclave and 2.6 °C for micro bench top reactor as shown in Figure 54 and Table 18. This effect of inhibition was also observed by Xiao in 2009 using 10 wt.% of different ionic liquid [50]. The total uncertainty of these measurements is +/-0.4%.

Table 18: Measured HLVE points for plain-QNG-S1 system using rocking cell compared with autoclave.

Experiment No.	Initial Pressure at 20°C (bar)	HLVE-Temperature (°C)	HLVE-Pressure (bar)	Inhibitor performance (°C)	Induction Time (h)
Plain-QNG-S1 with 1 wt. % ChCl					
V.1	79.55	18.64	78.73	0.70	2.35
V.2	66.85	17.69	66.14	0.80	2.15
V.3	58.83	16.69	57.80	0.91	1.80
V.4	49.25	15.46	8.35	1.10	1.90
Plain-QNG-S1 with 5 wt. % ChCl					
V.5	94.39	18.94	93.84	1.30	2.30
V.6	78.67	17.93	77.94	1.40	2.80
V.7	60.58	15.78	59.33	2.00	2.15

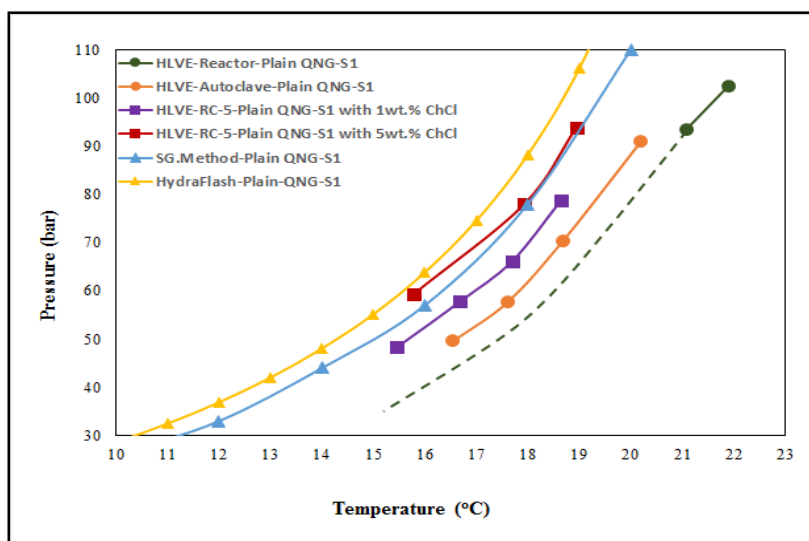


Figure 54: Inhibition effect of 1 wt % and 5 wt% choline chloride on plain QNG-S1 using RC-5 compared with those data obtained using autoclave, micro bench top reactor SG method and HydraFLASH®. The dashed lines present the expected HLVE data for micro bench top reactor.

Additionally, the inhibition effect of choline chloride was compared with classical inhibitors such as methanol (MEOH) obtained using HydraFLASH® software as illustrated in Figure 55. The inhibition effect of 1% and 5 % on mass basis of MEOH are 2.8 °C and 4.4 °C, respectively, compared with 1.1 °C and 2.0 °C for 1 wt. % and 5 wt. % of choline chloride obtained using autoclave high pressure cell.

When only comparing the inhibition performance of these two class of inhibitors, one could argue that classical inhibitors are preferred in preventing hydrate formation in industrial application. Yet, classical inhibitors have many environmental and economic concerns for being toxic, corrosive especially in sweet system as oxygen diffuses to the metal surface and increases the corrosion rate, and expensive due to the high concentration required to prevent hydrate formation (> 50% by weight) and recovery unit which is necessary because of its high toxicity. On the other hand, ionic liquid inhibitors can be nontoxic, noncorrosive, green, and environmentally friendly with a proper tuning of cation/anion combination. In addition, using ionic liquid as inhibitors might be cheaper and more practical to be implemented especially in Qatar industry because of its desert climate (average temperature > 37 °C in summer and > 14 °C in winter) and only small shifting in HLVE curve is required.

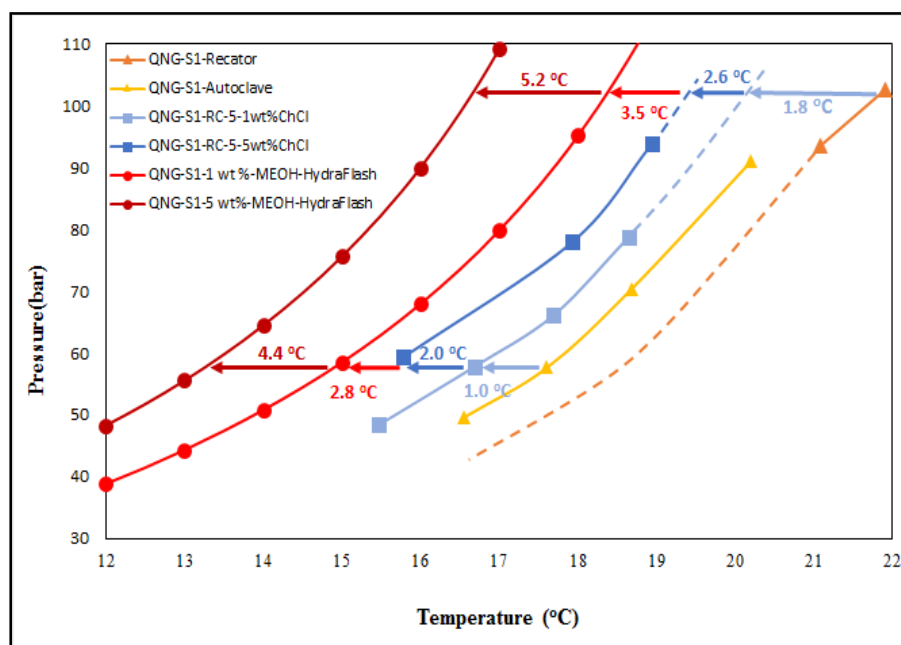


Figure 55: Comparing the inhibition effect of classical inhibitor and ionic liquid. The dashed lines present the expected inhibition effects.

From the kinetic point of view, by comparing 1 wt. % with 5 wt. % of choline chloride, the measured induction time increased for higher concentration. For instance, at starting pressure of around 60 bar and 79 bar, the induction time was 1.80 h and 2.35 h. for 1 wt. % vs. 2.15 h. and 2.80 h for 5 wt. %, respectively as tabulated in Table 18 and plotted in Figure 56. In this figure the two arrows illustrate the catastrophic pressure drop that indicates the start of hydrate formation.

The above mentioned data show that the ionic liquid was able to shift the HLVE curve and delay hydrate formation by increasing induction time. This confirms the dual inhibition effect of choline chloride.

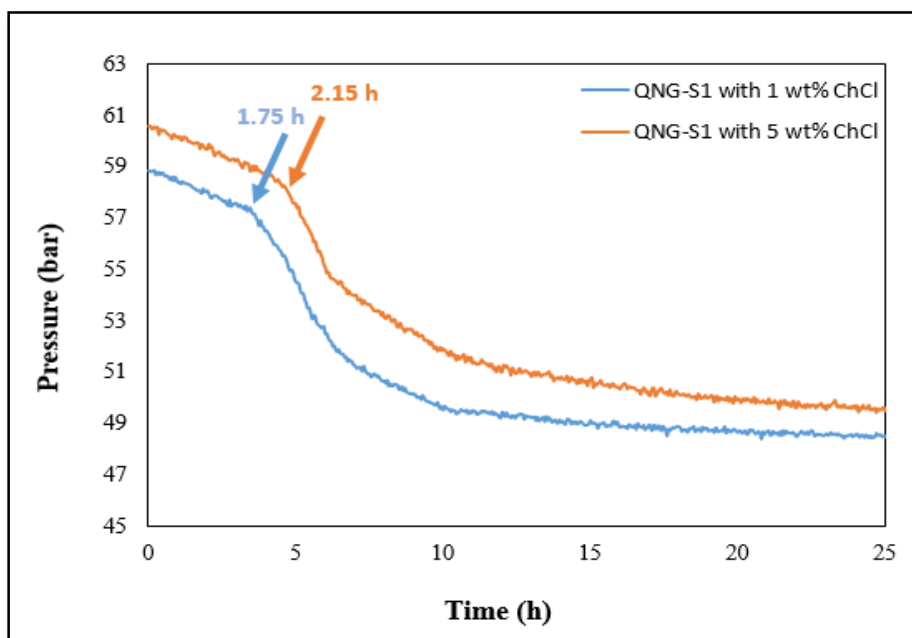


Figure 56: Induction time measurement for 1 wt. % and 5 wt. % of choline chloride applied on plain QNG-S1 using RC-5 at starting pressure of 60 bar. The two arrows illustrate the induction time which increase with higher ionic liquid concentration.

4.6. DISCUSSION

4.6.1. Scientific point of view

Current state of the art for gas inhibition is similar to CO₂ capture routine in industry, where conventional type of inhibitors (or absorbents) are still used. For example MEA (monoethanolamine) is a substance well known for its CO₂ affinity and absorption. For gas hydrate inhibition, MEG (monoethylene glycol), and methanol (so-called classical thermodynamic inhibitors), and PVCAP (a kinetic inhibitor) are industry favorites. However all of these chemicals, although their performances are appreciable, bring several serious environmental and processing problems along with them, which increase cost remarkably and reduce the pipe and equipment life time. Due to their toxicity and corrosive nature, researchers are seeking for more healthy, green, environmentally friendly, degradable, and, at the same time, better performance materials. That is why ionic liquids are important. These are recent-developed materials and fascinating solvents with tunable chemical and physical properties. In theory, an ionic liquid solvents can be designed with all desired physical properties. However, it needs some fundamental thermodynamic experiments to prove the concept. This is what the current work tried to achieve by testing the ILs performances. The next stage of this study is to investigate how much of KIs effect comes from the cation and THIs effect comes from the anion part of the ionic liquid.

4.6.2. Engineering point of view

More experimental runs are needed on multi-component Qatar natural gas mixture to compare the efficacy and efficiency of classical thermodynamic inhibitors with respect to ionic liquid from different perspectives such as the inhibition performance and environmental impact. In addition, a better ionic liquid inhibitor can be designed with a better inhibition performance, where cation size and chain length is considered from fundamental scientific perspective. A systematic study is required to identify the effects of the above mentioned chain effect and the molecular size in order to bring forward the current study. In order to achieve this, a fundamental molecular dynamics study is essential to minimize the required experimental study in the laboratory.

On the other hand, equation validation is equally important and essential for HydraFLASH® software predictions for QNG-S1 complex mixture. This might be achieved by comparing the HydraFLASH® software data output for simple binary or ternary gas mixtures that are rich in methane content with respect to the empirical data obtained using high pressure autoclave and rocking cell. Furthermore, the development (or optimizing existing models) of equilibrium model is necessary for hydrate equilibrium line prediction similar to the development of equation of state for density predictions, especially for the complex mixture compositions similar to the one presented in this work.

5. CONCLUSION

In this thesis, the following tasks were completed successfully:

- 1) Know-how establishment for gas hydrate research in Qatar.
- 2) Commissioning micro bench top reactor to a typical hydrate cell.
- 3) Obtaining the hydrate equilibrium curve of a mixture that represents a typical Qatar North Field natural gas mixture.
- 4) Testing the performance of novel inhibitors, ionic liquids, on Qatar natural gas mixture in laboratory conditions.

Upon successful commissioning of the experimental apparatus, data were measured with and without inhibitor. These data were analyzed and the following conclusions were drawn:

1. Commissioning of micro bench top reactor as a typical hydrate cell resulted with deviation of 2 °C from theoretical predictions and less than 1 °C compared with a high-pressure autoclave cell, also implemented in this study. This piece of equipment can be improved by using better quality thermocouples and if direct heat transfer is used. With better temperature control, it might be converted into a reference quality equipment. It is quite economical when compared with off-the-shelf specific hydrate autoclaves and can be used for preliminary studies. It was quite important to use this cell at the initial stages of the work in order to establish the know-how part of the hands-on hydrate equilibrium experiments.

2. Thermodynamics point of view: when inhibition of gas hydrates is considered, choline chloride resulted in a moderate shift of the hydrate equilibrium curve on QNG-S1 sample up to (0.7 to 1.1) °C and (1.5 to 1.8) °C compared with autoclave and micro bench top reactor respectively for 1 wt. %. The performance is even better with 5 wt. % as it was able to shift HLVE curve up to 2 °C for the autoclave and 2.6 °C for the micro bench top reactor.
3. The tested ionic liquid inhibitor was efficient but not as good as the current conventional thermodynamic inhibitors such as methanol and monoethylene glycol. Nevertheless, when the amount of inhibitor used, toxicity levels, and corrosion effects are considered ionic liquids still are good candidates for future alternative inhibitors. In this project, a common ionic liquid was used, however, a tailor-made ionic liquid may have better performance.
4. From kinetics point of view: choline chloride was able to delay hydrate formation as the induction time was increased from 2.35 h to 2.80 h for 1 % and 5 % on weight basis of choline chloride at starting pressure of 79 bar, respectively.
5. Eliminating the memory effect at the end of loop experiments: heating step of up to 30 °C after the isothermal heating step is found to be necessary in order to prevent a quicker hydrate formation in subsequent experiments. This step helps to

eliminate any residual hydrate crystal that can act as a seed and accelerate hydrate nucleation and growth in subsequent experiments and cause the loop not to close.

6. HydraFLASH® software: this excellent software provides an initial estimate of the hydrate equilibrium region of multi-component gas mixtures and makes it possible to identify the starting conditions of hydrate formation experiments. Yet, after comparing these predictions with the data from a typical hydrate cell, deviations of up to 5% were observed for multi-component gas mixtures. This suggests that the underlying mathematical model is not accurate enough to model multi-component gas mixtures as the Qatar natural gas studied in this work.

REFERENCES

- [1] I.M. Fund, World Economic Outlook Database-2012, October 2013.
- [2] E.D. Sloan, Nature 426 (2003) 353-363.
- [3] C.A. Koh, Chemical Society Reviews 31 (2002) 157-167.
- [4] E. Berez, M. Ballâanâe Achs, Gas hydrates, Elsevier ; Distribution for the U.S.A. and Canada, Elsevier Sciene Pub. Co., Amsterdam ; New York, N.Y., 1983.
- [5] J.J. Carroll, Natural gas hydrates : a guide for engineers, Gulf Professional Pub., Amsterdam ; Boston, 2002.
- [6] Y.F. Makogon, Formation of hydrates in shut-down pipelines in offshore conditions, Offshore Technology Conference, Richardson, TX, USA, , 1996, pp. 749-756.
- [7] C.A. Koh, R.E. Westacott, W. Zhang, K. Hirachand, J.L. Creek, A.K. Soper, Fluid Phase Equilibria 194 (2002) 143-151.
- [8] Y.F. Makogon, Hydrates of hydrocarbons, PennWell Books, Tulsa, Okla., 1997.
- [9] Y.F. Makogon, Journal of Natural Gas Science and Engineering 2 (2010) 49-59.
- [10] C. Giavarini, K.C. Hester, Gas hydrates immense energy potential and environmental challenges, Green energy and technology, Springer,, London ; New York, 2011, pp. 1 online resource.
- [11] Personal communication with Qatar gas industry, 2011.
- [12] U.S.E.I. Administration, Oil & Gas Journal (2014).
- [13] K. Momma, T. Ikeda, K. Nishikubo, N. Takahashi, C. Honma, M. Takada, Y. Furukawa, T. Nagase, Y. Kudoh, Nature Communications 2 (2011).

- [14] J.P. Henriot, J. Mienert, Gas hydrates : relevance to world margin stability and climate change, Geological Society, London, 1998.
- [15] D.L. Katz, Trans. A.I.M.E., 160 (1945) 140-149.
- [16] E.D. Sloan, Koh, C. A., Clathrate hydrates of natural gases, 3rd ed., CRC Press, Boca Raton, FL, 2008.
- [17] N.O.C. webpage, Methane hydrates. <http://noc.ac.uk/science-technology/marine-resources/energy/methane-hydrates>. Retained (2013).
- [18] E.D. Sloan, J.B. Bloys, Society of Petroleum Engineers, Hydrate engineering, Society of Petroleum Engineers, Richardson, TX, USA., 2000.
- [19] S. Changyu, L. Wenzhi, Y. Xin, L. Fengguang, Y. Qing, M. Liang, C. Jun, L. Bei, C. Guangjin, Chinese Journal of Chemical Engineering 19 (2011) 151-162.
- [20] M. Atilhan, S. Aparicio, F. Benyahia, E. Deniz, Advances in Natural Gas Technology, Natural Gas Hydrates., 2012.
- [21] H. Davy, Phil., Trans., Roy., Soc., Royal Society of London 101 (1811) 1.
- [22] E.G. Hammerschmidt, Ind. Eng. Chem., 26 (1934) 851-855.
- [23] P. Gayet, C. Dicharry, G. Marion, A. Graciaa, J. Lachaise, A. Nesterov, , Chemical Engineering Science 60 (2005) 5751-5758.
- [24] Y.S. Kim, S.K. Ryu, S.O. Yang, C.S. Lee, Industrial & Engineering Chemistry Research 42 (2003) 2409-2414.
- [25] H.O. Sakaguchi, R.; Mori, Y. H., Journal of Crystal Growth 247 (2003) 631-641.
- [26] S.P. Kang, Y.T. Seo, H. Lee, B.J. Ryu, Journal of Chemical Thermodynamics 31 (1999) 763-772.

- [27] F. Fleyfel, K.Y. Song, A. Kook, R. Martin, R. Kobayashi, *Journal of Physical Chemistry* 97 (1993) 6722-6725.
- [28] C. Gaillard, J.P. Monfort, J.L. Peytavy, *Oil & Gas Science and Technology-Revue De L Institut Francais Du Petrole* 54 (1999) 365-374.
- [29] J.H. Lee, Y.S. Baek, W.M. Sung, *Journal of Industrial and Engineering Chemistry* 8 (2002) 493-498.
- [30] L. Del Villano, M.A. Kelland, *Chemical Engineering Science* 65 (2010) 5366-5372.
- [31] H. Davy, *Philosophical Transactions of the Royal Society* 101 (1811) 155-162.
- [32] M. von Stackelberg, Meinhold, W., *Z. Elektrochem.*, 58 (1954) 40.
- [33] H.R. Muller, von Stackelberg, M., *Naturwissenschaften* 39 (1952) 20.
- [34] M. von Stackelberg, Muller, H.R., *Naturwissenschaften* 38 (1951) 456.
- [35] C.A. Koh, Savidge, J.L., Tang, C.C., Motie, R.E., Wu, X.P., Nooney, R.I., Westacott, R., *Materials Science Forum* 228-231 (1996) 239-246.
- [36] J.L. Cox, *Natural gas hydrates: properties, occurrence and recovery.*, Butterworth, Boston, 1983.
- [37] C. Tang, e. al, *Science China Chemistry* 53 (2010) 2622-2627.
- [38] B. Kvamme, T. Kuznetsova, K. Aasoldsen, *Journal of molecular graphics & modelling* 23 (2005) 524-536.
- [39] R.L.a.S. Christiansen, E.D., *Annals of the New York Academy of Sciences*, 715 (1994) 283-305.

- [40] M.A. Kelland, Production chemicals for the oil and gas industry, CRC Press, Boca Raton, Fla., 2009.
- [41] M.A. Kelland, Energy & Fuels, 20 (2006) 825-847.
- [42] J.J. Carroll, Knovel (Firm), Natural gas hydrates a guide for engineers, Gulf Professional Pub./Elsevier,, Amsterdam ; Boston, 2009, pp. xvii, 276 p.
- [43] U.P. Igboanusi, Opara, A.C., International Journal of Chemical and Environmental Engineering, 2 (2011) 131-134.
- [44] H. Guan, SPE, M-I SWACO Production Technologies, The Inhibition of Gas Hydrates and Synergy of the Inhibiting Molecules, International Oil and Gas Conference and Exhibition in China, , Beijing, China, 2010.
- [45] J. Zheng, O.M. Musa, C. Lei, Y. Zhang, Innovative KHI Polymers for Gas Hydrate Control, , Offshore Technology Conference, Houston, Texas, USA. , 2011.
- [46] M. Wu, Wang, S., Liu, H., Journal of Natural Gas Chemistry 16 (2007) 81-85.
- [47] S. Mokhatab, Wilkens, R.J., Leontaritis, K.J., Energy Sources, Part A: Recovery, Utilization and Environmental Effects 29 (2007) 39-45.
- [48] L.M. Frostman, Baker Petrolite,, In Anti-agglomerant hydrate inhibitors for prevention of hydrate plugs in deepwater systems, Society of Petroleum Engineers(SPE) Annual Technical Conference and Exhibition, Dallas, Texas, USA., 2000, pp. 573-579.
- [49] L.M. Frostman, Przybylinski, J.L., In Successful Applications of Anti-Agglomerant Hydrate Inhibitors, SPE International Symposium on Oilfield Chemistry, Houston, Texas, USA, 2001, pp. 259-268.

- [50] C. Xiao, H. Adidharma, Dual function inhibitors for methane hydrate, AICHE Annual Meeting, Philadelphia, PA, 2009, pp. 16–21.
- [51] P. Wasserscheid, T. Welton, Ionic Liquids in synthesis, 2 ed., WILEY-VCH Verlag GmbH & Co., Weinheim, 2008.
- [52] Z. Suojiang, L. Xingmei, Z. Qing, L. Xiaohua, Z. Xiang ping, L. Shucaai, Ionic Liquids Physicochemical Properties, Amsterdam, The Netherlands, 2009.
- [53] A. Rasoolzadeh, J. Javanmardi, Experimental Study and Modeling of Methane Hydrate Formation Induction Time in the Presence of Ionic Liquids, 2nd National Iranian Conference on Gas Hydrate (NICGH), Iran, 2013.
- [54] L. Del Villano, M.A. Kelland, Chemical Engineering Science 66 (2011) 1973-1985.
- [55] PSL-Systemtechnik, Research of Gas Hydrates with the Sapphire Rocking Cell, 2011.
- [56] U.C. Klomp, A.P. Mehta, Validation of Kinetic Inhibitors for Sour Gas Fields, International Petroleum Technology Conference, Dubai, U.A.E., 2007.
- [57] J. Tian, Low Dosage Hydrate Inhibitors (LDHI): Advances and Developments in Flow Assurance Technology for Offshore Oil and Gas Productions,, Offshore Technology Conference, Houston, Texas, USA., 2011.
- [58] J.K. Fink, Petroleum engineer's guide to oil field chemicals and fluids, Gulf Professional Pub., Waltham, MA, 2011, pp. 1 online resource (xxii, 785 p.).
- [59] Y. Rojas, X. Los, Asia-Pacific Journal of Chemical Engineering (2009).
- [60] D. Dalmazzone, C. Dalmazzone, H. B., SPE 7 (2002) 196–202.

- [61] D. Dalmazzone, M. Kharrat, V. Lachet, B. Fouconnier, C. D., *Therm. Anal. Cal.* 70 (2002) 493–505.
- [62] D. Dalmazzone, D. Clause, C. Dalmazzone, H. B., *American Mineralogist* 89 (2004) 1183–1191.
- [63] M. Kharrat, D. D., *Journal of Chemical Thermodynamics* 35 (2003) 1489–1505.
- [64] P. Le Parlouer, C. Dalmazzone, B. Herzhaft, L. Rousseau, C. Mathonat, *Journal of Thermal Analysis and Calorimetry* 78 (2004) 165-172.
- [65] T.M. Svartaas, M.A. Kelland, L. Dybvik, 1 912 (2000) 744-752.
- [66] M.A. Kelland, T.M. Svartaas, L. Dybvik, Control of hydrate formation by surfactants and polymers,, SPE Annual Technical Conference and Exhibition,, New Orleans, LA, USA,, 1994, pp. 431-438.
- [67] T. Balson, performance in a challenging environment, Chemistry in the oil industry VII, The Society, London, 2002.
- [68] L. Ballard, E.D. Sloan, *Fluid Phase Equilibria* 216 (2004) 257-270.
- [69] Y.T. Seo, S.P. Kang, J. Lee, J. Seol, H. Lee, *Journal of Chemical and Engineering Data* 56 (2011) 2316–2321.
- [70] L. Jensen, K. Thomsen, N. Von Solms, *Chemical Engineering Science* 63 (2008) 3069-3080.